Max-Planck-Institut
für Meteorologie

MAX-PLANCK-GESELLSCHAFT

International Max Planck Research School
on Earth System Modelling

Rethinking the relationship between the observed, simulated and real Arctic sea-ice evolution

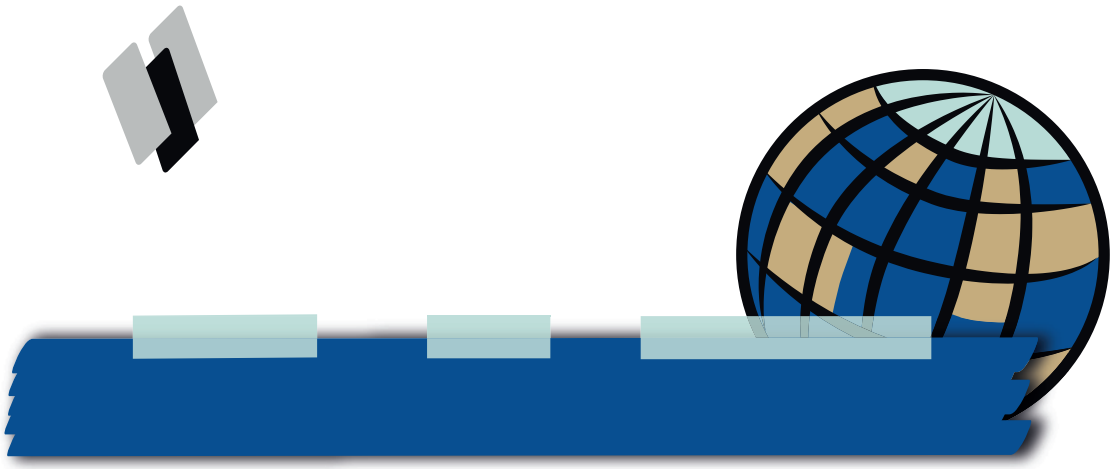

Clara Elisabeth Burgard

Hamburg 2019

Berichte zur Erdsystemforschung
Reports on Earth System Science

220
2019

Hinweis

Die Berichte zur Erdsystemforschung werden vom Max-Planck-Institut für Meteorologie in Hamburg in unregelmäßiger Abfolge herausgegeben.

Sie enthalten wissenschaftliche und technische Beiträge, inklusive Dissertationen.

Die Beiträge geben nicht notwendigerweise die Auffassung des Instituts wieder.

Die "Berichte zur Erdsystemforschung" führen die vorherigen Reihen "Reports" und "Examensarbeiten" weiter.

Notice

The Reports on Earth System Science are published by the Max Planck Institute for Meteorology in Hamburg. They appear in irregular intervals.

They contain scientific and technical contributions, including Ph. D. theses.

The Reports do not necessarily reflect the opinion of the Institute.

The "Reports on Earth System Science" continue the former "Reports" and "Examensarbeiten" of the Max Planck Institute.

Anschrift / Address

Max-Planck-Institut für Meteorologie
Bundesstrasse 53
20146 Hamburg
Deutschland

Tel./Phone: +49 (0)40 4 11 73 - 0
Fax: +49 (0)40 4 11 73 - 298

name.surname@mpimet.mpg.de
www.mpimet.mpg.de

Layout

Bettina Diallo and Norbert P. Noreiks
Communication

Copyright

Rethinking the relationship between the observed, simulated and real Arctic sea-ice evolution

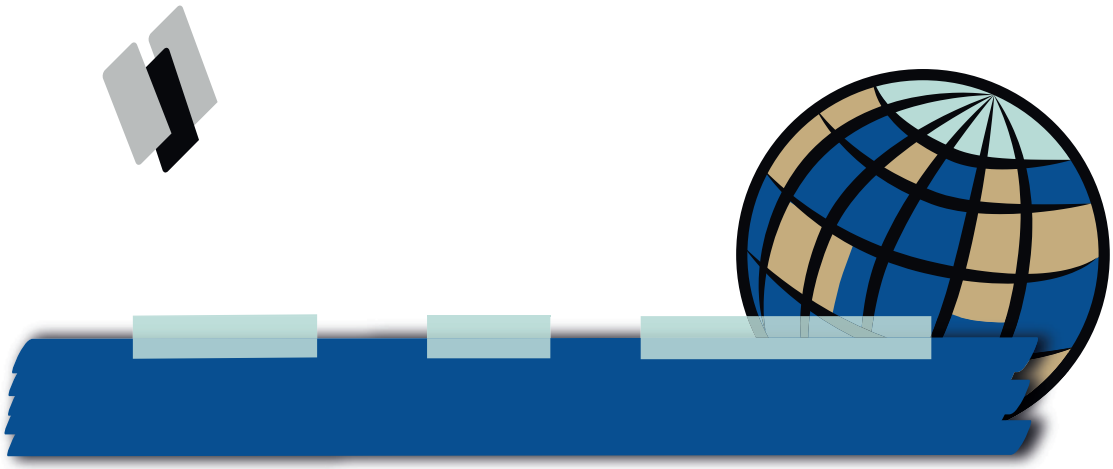

Clara Elisabeth Burgard

Hamburg 2019

Clara Elisabeth Burgard
from Strasbourg, France

Max-Planck-Institut für Meteorologie
The International Max Planck Research School on Earth System Modelling
(IMPRS-ESM)
Bundesstrasse 53
20146 Hamburg

Universität Hamburg
Geowissenschaften
Meteorologisches Institut
Bundesstr. 55
20146 Hamburg

Tag der Disputation: 25. Juni 2019

Folgende Gutachter empfehlen die Annahme der Dissertation:
Dr. Dirk Notz
Prof. Dr. Johanna Baehr

Vorsitzender des Promotionsausschusses:
Prof. Dr. Dirk Gajewski

Dekan der MIN-Fakultät:
Prof. Dr. Heinrich Graener

Typeset using a modified version of the mimosis template developed by Bastian Rieck, available at: https://github.com/Pseudomanifold/latex-mimosis/

Berichte zur Erdsystemforschung / Max-Planck-Institut für Meteorologie 220
Reports on Earth System Science / Max Planck Institute for Meteorology 2019

ISSN 1614-1199

ABSTRACT

In this dissertation, I explore the large differences in Arctic sea-ice evolution between climate models and observations, and among individual climate models.

First, I investigate the drivers of the long-term Arctic Ocean warming in a multi-model ensemble. I find that there is no consensus between the models about whether the excess energy is gained by the ocean through the net atmospheric surface flux or through the meridional oceanic heat flux. However, all models agree on the magnitude of the projected warming. The warming is small compared to the anomalies in the energy fluxes. This is because most of the energy gained through one energy flux is lost through the other energy flux due to a relationship between the magnitude of the increase in oceanic heat inflow and the increase in turbulent heat loss to the atmosphere.

Second, I explore the feasibility of an observation operator for the Arctic Ocean. An observation operator translates the Arctic Ocean climate simulated by a climate model into a brightness temperature. The brightness temperature is the quantity directly measured by satellites from space. Hence, an observation operator enables us to circumvent the observational uncertainty currently inhibiting reliable climate model evaluation. Sea-ice brightness temperatures at 6.9 GHz are driven by the liquid water fraction profile inside the ice and snow, which is not resolved in most climate models. I show that in winter this profile can be described reasonably well by a linear temperature profile and a salinity profile prescribed as a self-similar function of depth. In summer, the melt-pond fraction is more important for the simulation of the brightness temperature than the internal structure of the ice.

Third, I develop an Arctic Ocean Observation Operator for 6.9 GHz based on these findings. I compare brightness temperatures simulated from the output of an Earth System Model to brightness temperatures measured by satellites. The differences between simulated and measured brightness temperatures can mainly be explained by the uncertainty in the simulated state of the sea-ice concentration, the assimilation process, and the melt-pond parametrization. Differences attributable to biases in the observation operator itself are small. The operator is therefore a suitable method for climate model evaluation.

In summary, I show different perspectives on the large differences in Arctic sea-ice evolution. On the one hand, I point out that the multi-model ensemble mean is not always representative for the simulated Arctic climate and should be interpreted with care. On the other hand, I introduce and develop an unconventional tool providing new opportunities for future climate model evaluation.

ZUSAMMENFASSUNG

In dieser Dissertation untersuche ich die großen Unterschiede in der zeitlichen Entwicklung des arktischen Meereises, zum einen zwischen verschiedenen Klimamodellen und Beobachtungen und zum anderen zwischen einzelnen Klimamodellen.

Im ersten Teil der Dissertation untersuche ich die Faktoren, die innerhalb der verschiedenen Klimamodellen die langfristige Erwärmung des Arktischen Ozeans vorantreiben. Ich finde heraus, dass es zwischen den Modellen keinen Konsens darüber gibt, ob die überschüssige Energie vom Ozean durch den atmosphärischen Oberflächenfluss oder durch den meridionalen ozeanischen Wärmefluss gewonnen wird. Einig sind sich die Modelle jedoch alle in der Größenordnung der Erwärmung. Im Vergleich zu den Anomalien in den Energieflüssen ist diese Erwärmung gering, da die meiste Energie, die durch einen der Energieflüsse gewonnen wird, durch den anderen Energiefluss wieder verloren geht. Das liegt am Zusammenhang zwischen dem Ausmaß der Zunahme im ozeanischen Wärmeeinfluss und der Zunahme im turbulenten Energieverlust an die Atmosphäre.

Im zweiten Teil der Dissertation untersuche ich die Realisierbarkeit eines Beobachtungsoperatoren für den Arktischen Ozean. Ein Beobachtungsoperator übersetzt das von einem Klimamodell simulierte Klima des Arktischen Ozeans in eine Helligkeitstemperatur. Die Helligkeitstemperatur ist die Größe, die direkt von Satelliten vom All aus gemessen wird. Deshalb kann mit einem solchen Beobachtungsoperator die Beobachtungsunsicherheit umgangen werden, die derzeit einer zuverlässigen Klimamodellevaluierung im Weg steht. Meereishelligkeitstemperaturen bei 6.9 GHz werden von dem Profil des Flüssigwasseranteils im Eis und Schnee getrieben. Dieses Profil ist in den meisten Klimamodellen nicht aufgelöst. Ich zeige auf, dass der Flüssigwasseranteil im Winter durch ein lineares Temperaturprofil und ein Salzgehaltsprofil, das als selbstähnliche Funktion der Tiefe vorgeschrieben ist, vernünftig beschrieben werden kann. Im Sommer ist der Schmelztümpelanteil an der Eisoberfläche wichtiger für die Simulation von Helligkeitstemperaturen als die Struktur des Eisinneren.

Im dritten Teil der Dissertation baue ich auf diesen Ergebnissen auf und entwickle den "Arctic Ocean Observation Operator", einen Beobachtungsoperatoren für den Arktischen Ozean bei 6.9 GHz. Ich vergleiche Helligkeitstemperaturen, die basierend auf Erdsystemmodellergebnissen simuliert werden, mit Helligkeitstemperaturen, die von Satelliten gemessen wurden. Die

Unterschiede zwischen simulierten und gemessenen Helligkeitstemperaturen können hauptsächlich durch die Unsicherheit in der simulierten Meereiskonzentration, dem Assimilierungsprozess und der Schmelztümpelparametrisierung erklärt werden. Unterschiede, die auf Fehler des Beobachtungsoperators selbst zurückzuführen sind, sind gering.

Insgesamt blicke ich aus verschiedenen Perspektiven auf die großen Unterschiede in der zeitlichen Entwicklung des arktischen Meereises. Einerseits finde ich heraus, dass der Mittelwert über verschiedene Klimamodelle nicht immer repräsentativ für das simulierte arktische Klima ist, und deshalb mit Vorsicht interpretiert werden sollte. Andererseits führe ich ein unkonventionelles Instrument ein, das neue Möglichkeiten für die zukünftige Evaluierung von Klimamodellen bietet.

PARTS OF THIS DISSERTATION PRE-PUBLISHED OR INTENDED FOR PUBLICATION

Appendix A
Burgard, C. and D. Notz (2017): "Drivers of Arctic Ocean warming in CMIP5 models". *Geophysical Research Letters*, 44, 4263-4271, doi: 10.1002/2016GL072342.

Appendix B
Burgard, C., D. Notz, L.T. Pedersen and R.T. Tonboe. "How to obtain sea-ice brightness temperatures at 6.9 GHz from climate model output". *To be submitted to The Cryosphere.*

Appendix C
Burgard, C., D. Notz, L.T. Pedersen and R.T. Tonboe. "ARC3O: The Arctic Ocean Observation Operator for 6.9 GHz". *To be submitted to The Cryosphere.*

CONTENTS

LIST OF FIGURES

LIST OF TABLES

ACRONYMS

ARC3O Arctic Ocean Observation Operator for 6.9 GHz

AMJ April/May/June

AMSR-E Advanced Microwave Scanning Radiometer Earth Observing System

AMSR2 Advanced Microwave Scanning Radiometer 2

CMIP3 Coupled Model Intercomparison Project Phase 3

CMIP5 Coupled Model Intercomparison Project Phase 5

ECHAM Atmospheric component of the Max Planck Institute Earth System Model

FYI First-year ice

GCM General Circulation Model

JFM January/February/March

JAS July/August/September

MEaSUREs Making Earth System Data Records for Use in Research Environments

MEMLS Microwave Emission Model for Layered Snowpacks

MPI-ESM Max Planck Institute Earth System Model

MPIOM Ocean component of the Max Planck Institute Earth System Model

MYI Multiyear ice

OND October/November/December

RCP Representative Concentration Pathway

RRDP Round Robin Data Package

SAMSIM Semi-Adaptive Multi-phase Sea-Ice Model

SIC Sea-ice concentration

SICCI Sea-Ice Climate Change Initiative

TB Brightness temperature

THE BIASED SIMULATION OF THE ARCTIC SEA-ICE RETREAT IN CLIMATE MODELS: A COLD CASE

"In a dark place we find ourselves...
a little more knowledge might light our way."
Yoda

1 INTRODUCTION

As already suggested by the term "scientific research", science is about searching. Searching for the explanation of processes governing the universe around us on various scales. But also searching for new methods to get these explanations if they cannot be accessed with current ones. In other words, scientists can be compared to detectives. Different sources of information are available to solve a crime: hard evidence from the crime scene, testimonies from witnesses, and common knowledge about human psychology. Combining these informations, the detective tries to find the culprit, the motive, and the progression of events that have led to the current state. If these sources of information are not enough, the detective has to extend their methods to more unconventional ones.

In this dissertation, the case I investigate is the biased simulation of the historical and projected retreat of the Arctic sea-ice cover. The simulated melting of the Arctic sea-ice cover is slower than the observed melting and the spread between climate model simulations is large (Stroeve et al., 2007, 2012). Some studies suggested that natural variability is a possible culprit for the differences between the simulated and observed sea-ice melting rate (e.g. IPCC, 2013; Notz, 2014; Swart et al., 2015). Other studies suggested that possible culprits for these differences are a too low sensitivity of simulated sea ice to global warming (Rosenblum and Eisenman, 2017) or the treatment of atmospheric and oceanic properties and dynamics in climate models (Overland and Wang, 2013). I follow the latter line of thought, implying that there are biases in the simulation of the sea-ice retreat by the climate models. To uncover the main culprit driving the simulated melting and the progression of events possibly leading to the bias, my sources of information are in-situ

observations, observational estimates retrieved from satellite measurements from space, and climate models.

Before I dive into the case, let me give you some information about its setting. The Arctic Ocean represents a unique climate system, especially because of its extensive sea-ice cover, which affects both regional and global climate. Sea ice is at the interface of atmosphere and ocean. While the ice forms an insulating layer which strongly dampens the exchange of energy, moisture and momentum between the two spheres, it also interacts with them. On the one hand, due to its high albedo, the sea-ice cover reflects a large part of the incoming solar radiation from spring to fall, keeping the energy gain of the surface low (Nakamura and Oort, 1988). On the other hand, the release of brine during the freezing process leads to a densification of the oceanic water underneath the ice and therefore enhances vertical mixing, contributing to the global thermohaline circulation (Aagaard et al., 1985). Finally, sea ice is also the basis of a unique ecosystem, providing habitat for the biosphere above it, inside it, and underneath it.

The sea-ice cover is also the main reason why human activity has remained low in the Arctic Ocean until recently. The Central Arctic, but also the Northern Sea Route north of Russia and the Northwest passage north of Canada, are covered by ice most of the year, inhibiting commercial and touristic shipping in the region. Additionally, sea ice hinders drilling activities carried out to exploit the large amounts of oil and gas expected under the Arctic Ocean floor.

This unique Arctic Ocean landscape has changed at a rapid pace in past decades due to climate change. Rising anthropogenic CO_2 emissions since the end of the 19th century have led to an increase in the global mean temperature by nearly 1 °C (Hawkins et al., 2017; IPCC, 2013). This global warming is currently drastically changing global climate and has not spared the Arctic Ocean. On the contrary, the increase in surface air temperature is even enhanced in the Arctic through Arctic Amplification, a synergy between several feedbacks involving sea-ice loss, energy exchange, and moisture and clouds. As a consequence, the rate of warming is on average 1.9 times higher in the Arctic than in the global mean (Serreze and Barry, 2011). The most prominent indicator of this warming in both atmosphere and ocean is the dramatic retreat of the Arctic sea-ice cover (Stroeve et al., 2012; Stroeve and Notz, 2015; Notz and Stroeve, 2016). And that is where my case begins: the sea-ice is retreating at different paces depending on the source of information.

As mentioned before, I have three sources of information available to solve the case: in-situ observations, observational estimates retrieved from satellite measurements from space, and climate models. From the detective's view, in-situ observations are the equivalent of the hard evidence found on the crime scene.

In-situ observations were the main source of knowledge in early Arctic Ocean research and are still the representation closest to reality that we currently can have. The Arctic Ocean long remained untouched and unexplored due to its sea-ice cover, its remoteness, and its harsh climatic conditions. It was not until the late 19th century that the Arctic Ocean and its ice cover became of serious interest to explorers, the military, and the scientific community (e.g., Nansen, 1911; Weeks, 2010). In-situ observations therefore only date back to the first half of the 20th century. Since then, the number and size of observational campaigns has increased. This increase in sample size is for example reflected in the evolution of coordinated international interdisciplinary observational campaigns organised approximately every twenty years (Untersteiner, 1980; Uttal et al., 2002; Barber et al., 2016). Although a precious source of information, the spatial and temporal coverage of in-situ observations are not sufficient for a comprehensive investigation of the Arctic Ocean climate on large time and spatial scales, especially for large-scale metrics such as the sea-ice area.

The launch of various Earth-observing satellites starting in the second half of the 20th century has been a game-changer for the observation of the remote polar regions. Especially the use of passive microwave sensors since 1972 has been very beneficial for the monitoring of the Arctic Ocean surface as microwave radiation is emitted during both polar day and polar night and is not stopped by clouds (e.g. Swift and Cavalieri, 1985). While some of these Earth-orbiting satellites do not cover the high latitudes, the ones that reach the high latitudes fly over the Arctic at each revolution, so that their temporal and spatial coverage of the Arctic is particularly large. The microwave radiation is measured in the form of brightness temperatures. Observational estimates of geophysical variables of interest, e.g. sea-ice concentration, are then retrieved by applying an algorithm to these brightness temperature. From the detective's view, observational estimates retrieved from satellite measurements are the equivalent of testimonies from witnesses. They are a comprehensive source of information but do not necessarily describe the sequence of events objectively and might be biased due to an incomplete knowledge of the situation. For microwave measurements of the Arctic Ocean surface, an unambiguous interpretation of the measured brightness temperature is not possible due to the variety of physical drivers which cannot be quantified individually. This uncertainty results in a variety of retrieved sea-ice concentration estimates depending on the algorithm used (Fig. 1, red and orange line) (see e.g., Ivanova et al., 2014), which makes observational estimates a source of information to be handled with care.

Finally, the steady development of global climate models, starting in the middle of the 20th century (Edwards, 2011), has provided a third representation of the Arctic

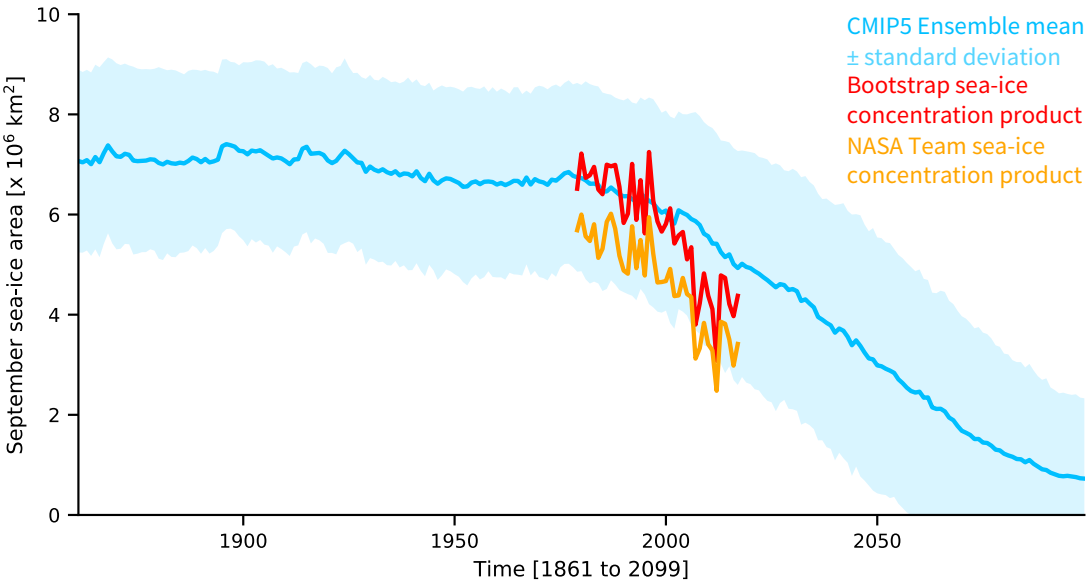

Figure 1: September sea-ice area as simulated by CMIP5 models, the latest generation of climate models, (Ensemble mean, blue) for the historical period [1861-2005] and the 21st century under the RCP8.5 forcing scenario [2006-2099] and as retrieved by the Bootstrap (red) and NASA Team algorithms (orange) [1979-2017]. The shading represents the CMIP5 ensemble standard deviation.

Ocean climate, which complements in-situ and observational estimates from satellites. From the detective's view, climate models are the equivalent of the common knowledge of human psychology. They simulate the climate system in a comprehensive and consistent manner in time and space following the basic physical principles. Hence, climate models allow us to deepen the understanding of physical processes and relationships at work in the coupled Arctic Ocean climate. Additionally, they provide the possibility of projecting future climate evolution. However, climate models are only approximations of the real physical processes at work as we do not know all processes playing a role in climate and cannot necessarily represent all processes we know. For example, many of the processes are active on subgrid scales and therefore need to be parametrized in the model. Like the common knowledge about human psychology, they might lead the investigation in an uncertain direction by giving generalized solutions possibly not fit for this case. Due to different prioritizations of processes to include and to different parametrizations, different climate models differ in their representation of the climate, e.g. for the sea-ice evolution (Fig. 1, blue shading). Climate models therefore need to be seen as a complementary tool to in-situ observations and observational estimates and cannot replace them.

The lack of in-situ observations on large spatial and temporal scales leaves my investigation with two main sources of information: the observational estimates of sea-ice concentration derived from satellites and sea ice simulated by climate models. The disagreement within and between these two sources are a sign that we still lack a proper understanding of the mechanisms governing the sea-ice evolution. The goal of this dissertation is to gain new insights into the main drivers of the retreat of the Arctic sea-ice cover despite these disagreements. To do so, I use conventional and less conventional methods, which shed light on the Arctic Ocean climate system from different perspectives:

- The melting of the sea-ice cover is a consequence of excess energy gained by the Arctic Ocean through energy exchange with the polar atmosphere and with oceans from lower latitudes. In a first step, my goal is to find the main mechanism driving the melting by examining the Arctic Ocean warming through an energy budget analysis. **In Appendix A**, I investigate the different representations of the Arctic Ocean energy budget in an ensemble of climate models. In this multi-model framework, I identify mechanisms explaining agreement and disagreement between climate models on the Arctic Ocean warming and its drivers but I do not find a robust progression of events resolving the case of the biased simulation of the sea-ice melting. Ultimately, the disagreement between climate models shows that we still need to learn about the current Arctic Ocean climate from observations.

- Reliably evaluating simulated sea ice is however a challenge due to the spread in sea-ice observational estimates induced by the use of different retrieval algorithms. In a second step, I explore a less conventional approach for climate model evaluation by developing a new tool: the ARCtic Ocean Observation Operator (ARC3O). My goal is to introduce a new perspective on the case, situated between the too little amount of hard evidence and the large spread in witness testimonies, and therefore to gain a new source of information to our investigation. An observation operator translates the simulated climate state into an observable quantity, in this case a brightness temperature. This simulated brightness temperature can be compared directly to the brightness temperature measured by satellites, so that we circumvent the uncertainty introduced by retrieval algorithms in the climate model evaluation. **In Appendix B**, I explore the feasibility of simulating brightness temperatures from a simple sea-ice representation as simulated in most climate models. **In Appendix C**, I develop the observation operator, simulate brightness temperatures from a climate model, and present the potential of ARC3O for both the evaluation of climate models and the evaluation of observational estimates against satellite measurements.

2 Drivers of the Arctic Ocean warming in a multi-model ensemble

The retreat of the sea-ice cover is a symptom of the increase in Arctic Ocean heat content, which has been taking place in past decades, both in sensible and latent heat content (Polyakov et al., 2010; Zhang, 2005; Steele et al., 2008; Serreze et al., 2007b). This increase in heat content is projected to continue throughout the century if no drastic measures are taken to reduce the CO_2 concentration present in the atmosphere (Vavrus et al., 2011; Koenigk and Brodeau, 2013; Stroeve et al., 2007, 2012). Excess heat can be gained by the Arctic Ocean either through vertical exchange with the atmosphere in the form of the net atmospheric surface flux or through lateral exchange with oceans from lower latitudes in the form of the meridional oceanic heat flux. It remains however unclear which of these two fluxes drive the long-term Arctic Ocean warming. This is the question I address in the following.

For the historical period, the Arctic Ocean energy budget was investigated based on reanalyses, as we lack the necessary in-situ observations. The annual mean state from 1979 to 2001 shows that nearly as much energy was gained by the ocean through the meridional oceanic heat flux as was lost to the atmosphere through the net atmospheric surface flux (Serreze et al., 2007a). Only a small amount of the energy inflow was taken up by the ocean in the form of latent heat to melt sea ice, while the sensible heat uptake was near to zero. In contrast, from 2000 to 2015, both latent and sensible heat uptake by the ocean were observed. These changes were mainly driven by the meridional oceanic heat flux up to 2007 and by the atmospheric radiative fluxes from 2007 onwards (Mayer et al., 2016).

For longer time scales and for a more comprehensive overview of the processes at work, climate models are needed to understand changes in the Arctic Ocean climate system. As different climate models are based on slightly different assumptions and parametrizations, one single climate model does not give a robust representation of the climate evolution (see Sec. 1). To counteract this limitation, the Coupled Model Intercomparison Project (CMIP) was launched in the 1990s. The CMIP allows a structured comparison framework of different climate models following a common simulation protocol. Hence, the robustness of the simulated climate evolution can be assessed across a variety of models. It is also assumed that the mean over all models represents the consensus between models on the climate evolution as it averages out individual model biases. Most research institutions developing a climate model participate in this exercise, which takes place once every five years (Meehl et al., 2007; Taylor et al., 2012; Eyring et al., 2016).

In the climate models of the CMIP Phase 3 (CMIP3), the net atmospheric surface flux was found to increase until the end of the 21st century (Sorteberg et al., 2007). In an individual climate model, the meridional oceanic heat flux was also found to increase over that period (Koenigk and Brodeau, 2013). However, these long-term changes in the different fluxes have not been compared to each other and to the increase in ocean heat content. In Appendix A, I consider the long-term evolution of the full Arctic Ocean energy budget during the late 20th and the 21st century to find out if the simulated Arctic Ocean warming is mainly driven by the net atmospheric surface flux or by the meridional oceanic heat flux.

To this purpose, I use 26 GCMs from the CMIP Phase 5 (CMIP5) framework and investigate the Arctic Ocean energy budget as a whole over the time period between 1961 and 2099. I choose 26 GCMs following the availability of the variables needed for the computation of the net atmospheric surface flux and of the Arctic Ocean sensible and latent heat content (Sec. A.2). The meridional oceanic heat flux is computed as a residual from the net atmospheric surface flux and the Arctic Ocean total heat content. The positive direction for the fluxes is defined towards the Arctic Ocean interior. We consider the period from 1861 to 2099, which is represented by historical simulations from 1861 to 2005 and by Representative Concentration Pathway (RCP) 4.5 simulations from 2006 to 2099. In the following, we discuss the anomalies in the Arctic Ocean energy budget from 1961 to 2099 with respect to 1861 to 1960.

Comparing cumulative changes in the energy exchange through the fluxes and in the heat content of the ocean, I show that the CMIP5 models disagree on the main driver of the Arctic Ocean warming (Sec. A.3). While the multi-model ensemble mean suggests that the long-term warming is driven by positive anomalies in both the meridional oceanic heat flux and the net atmospheric surface flux, the individual models disagree on the main driver. The models can be divided into three categories. In 11 of the models, positive anomalies in the meridional oceanic heat flux dominate, while they are slightly counteracted by negative anomalies in the net atmospheric surface flux. In 11 other models, the opposite is true. Finally, the four remaining models depict a similar picture as the multi-model ensemble mean, where the ocean warming is driven by positive anomalies in both the net atmospheric surface flux and the meridional oceanic heat flux. In a next step, I investigate the drivers of these different behaviours.

I investigate the relationship between changes in the net atmospheric surface flux, changes in the meridional oceanic heat flux and changes in radiative fluxes, turbulent fluxes, oceanic heat inflow, oceanic heat outflow, sea-ice properties and ocean surface properties (Sec. A.4). Doing so, I show that the different behaviours

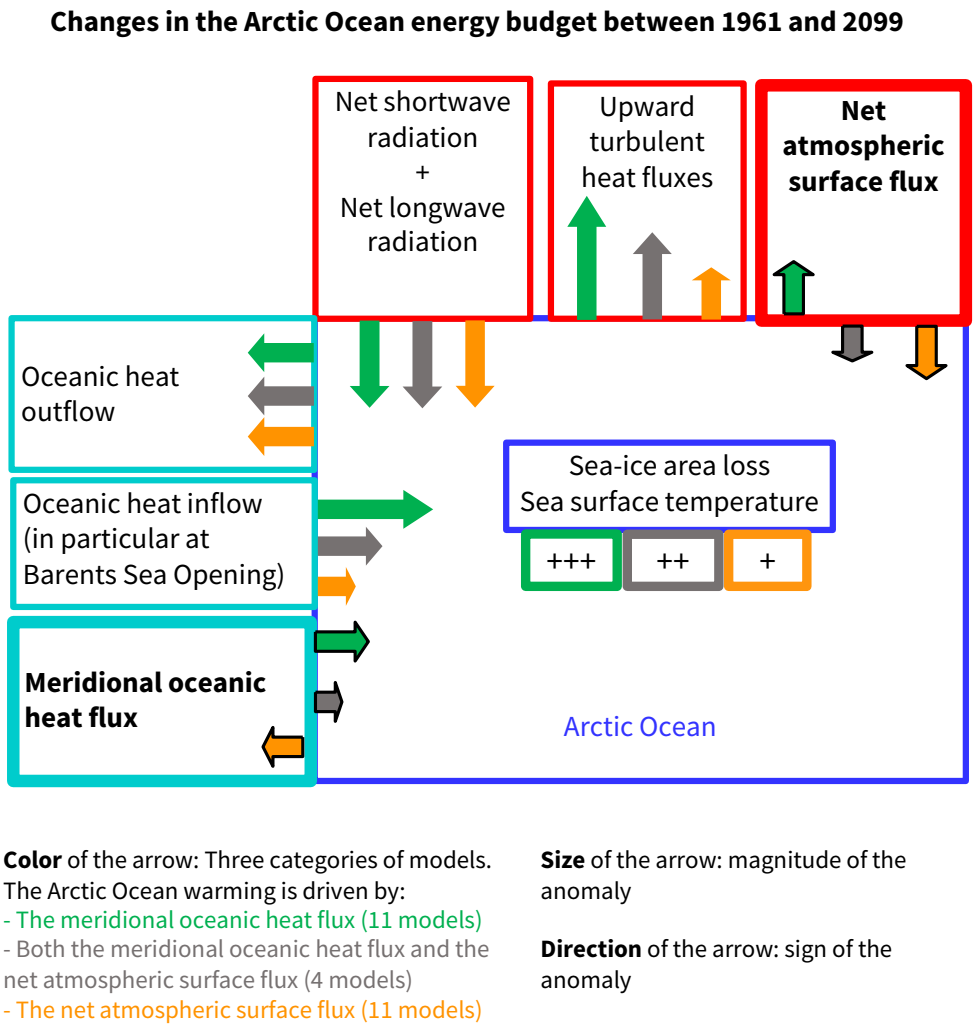

Figure 2: Summary of changes in the Arctic Ocean energy budget between 1961 and 2099 as simulated by CMIP5 models. The different colors represent the different model categories. The direction of the arrow shows if the cumulated energy anomaly leads to an energy gain or loss by the Arctic Ocean. The size of the arrow is the magnitude in the cumulated energy gain or loss.

are linked through a mechanism in which the magnitude of the increase in oceanic heat inflow through the mass transport through the Barents Sea Opening modulates the magnitude of the increase in sea-ice area loss and in sea surface temperature, which in turn modulates the magnitude of the increase in turbulent heat loss through upward turbulent fluxes (Fig. 2).

This mechanism works as follows. A large increase in oceanic heat inflow ultimately leads to a large increase in turbulent heat loss (green arrows in Fig. 2). The increase in oceanic heat inflow counteracts the increase in the oceanic heat outflow, while the increase in turbulent heat loss counteracts the increase in the net radiative fluxes. This leads to positive anomalies in the meridional oceanic heat flux and to negative anomalies in the net atmospheric surface flux. In models showing negative anomalies in the meridional oceanic heat flux and positive anomalies in the net atmospheric surface flux, the increase in oceanic heat inflow and turbulent heat loss is not large enough to fully counteract the increase in heat outflow on the one hand, and the increase in radiative fluxes on the other hand (orange arrows in Fig. 2). Finally, in the last model category, the moderate increase in oceanic heat inflow is large enough to counteract the increase in oceanic heat outflow but its effect on the turbulent heat loss is not large enough to counteract the increase in radiative fluxes (grey arrows in Fig. 2). These models therefore show positive anomalies in both meridional oceanic heat flux and net atmospheric surface flux.

Despite the disagreement about the drivers of the warming, the models agree well on the amount of energy gained by the Arctic Ocean in the period between 1961 and 2099 (Sec. A.4.3). In an equilibrium climate, changes in the meridional oceanic heat flux and changes in the net atmospheric surface flux are strongly correlated due to the Bjerknes compensation, a process in which changes in the oceanic meridional heat flux are compensated by changes in the atmospheric meridional heat flux. The mechanism described in Fig. 2 and the agreement on the magnitude of the ocean warming suggest that Bjerknes compensation is at work in the simulated transient climate as well and confirm that differences in the Arctic Ocean energy budget evolution are ultimately driven by changes in the oceanic meridional heat flux.

The investigation of the Arctic Ocean energy budget did not clearly solve the case of the bias in the simulation of the sea-ice retreat. The results of the investigation show that the sea-ice area loss is slightly higher in models where the increase in oceanic inflow through the Barents Sea Opening will be large until the end of the 21st century than in models where it will be small. However, the magnitude of the projected increase in oceanic inflow through the Barents Sea Opening could not be linked to current climate conditions and is therefore rather a diagnostic, which can be discussed at the end of the 21st century, than a prognostic, which can be estimated from the current state.

Another investigation approach to gain insight into the spread or disagreement between climate models is to focus on the time period covered by observations. Better understanding of processes which are currently at work can be reached by

combining or comparing simulations with observations. This is however not straightforward in our case. While there is a spread between climate models on the current sea-ice evolution, there is also a large spread in observational estimates, inhibiting reliable climate model evaluation over the historical period. In the following, I develop an Arctic Ocean observation operator as an alternative tool to evaluate the simulated and estimated Arctic Ocean climate directly against satellite measurements, a source of information largely omitted up to now.

3 Development of an Arctic Ocean Observation Operator at 6.9 GHz

Currently, the sea-ice concentration estimates used for long-term monitoring of the Arctic sea-ice evolution rely on measurements from passive microwave sensors on satellites (see Sec. 1). The sensors measure the thermal microwave radiation emitted by the Earth's surface and atmosphere in the form of brightness temperatures at different frequency bands. Retrieving sea-ice concentration from these brightness temperatures comes with uncertainty as it is not trivial to disentangle the effect of sea-ice concentration, other sea-ice properties, snow properties, atmospheric properties, and ocean surface properties, on the brightness temperatures. To circumvent this ambiguous interpretation process, I suggest the use of an observational operator, which translates the simulated climate state from a climate model into brightness temperatures. In the following, I motivate this approach, explore the feasibility of an Arctic Ocean observation operator, construct one, and evaluate it.

Sea-ice concentration estimates from brightness temperature measurements are currently retrieved by a range of algorithms differing slightly in four points: the frequency and polarization they use, the tie-points they use, their sensitivities to the physical surface temperature, and their weather filters (Ivanova et al., 2014). The resulting sea-ice concentration estimates therefore also differ and this difference can result in an uncertainty in the total sea-ice area of up to 25% in summer and up to 10% in winter (Ivanova et al., 2014). The uncertainty is largest in summer, where melt ponds cannot be distinguished from open water in the microwave brightness temperatures. The different algorithms attempt to counteract this effect by diverse correction approaches (Stroeve and Notz, 2015; Ivanova et al., 2014, 2015), resulting in a large spread in the retrieved sea-ice concentration estimates.

The disagreement between the sea-ice concentration estimates and not knowing how they relate to the real sea-ice concentration are a serious challenge for climate model evaluation, initialization, and the use of observations to constrain future projections. If observational estimates do not agree on the real state, the choice of observation estimate used for model evaluation and initialization strongly affects the results of the procedure (Notz et al., 2013; Bunzel et al., 2016). Finally, relationships about the future evolution of the sea-ice cover can be inferred from observations, based on the relationship e.g. between sea-ice area and CO_2 emissions (Notz and Stroeve, 2016) or between sea-ice area and global-mean surface air temperature (Niederdrenk and Notz, 2018). However, projections about future states of the sea-ice cover inferred from these relationships are strongly dependent on the observational dataset used to infer these projections (Niederdrenk and Notz, 2018).

The use of an observation operator provides an opportunity to circumvent the observational uncertainty. An observation operator simulates the observable quantity, here the microwave brightness temperature, from the sea ice, ocean and atmosphere simulated by a climate model. This simulated brightness temperature can be compared to the brightness temperature measured from space, which is the closest measure we have to the real climate state on a large temporal and spatial scale. This approach has been introduced for several climate variables, such as clouds and atmospheric moisture (an overview can be found in Flato et al., 2013), and is a promising perspective for climate model evaluation (Eyring et al., 2019), also for the Arctic Ocean climate system. First results of an Arctic Ocean observation operator at 1.4 GHz based on an ocean reanalysis showed good potential for this approach (Richter et al., 2018). However, the feasibility and limitations of an Arctic Ocean observation operator applied to coupled climate model output have not been investigated yet.

An ideal Arctic Ocean observation operator would simulate brightness temperatures at all operational microwave frequency bands used for the retrieval of sea-ice concentration estimates, i.e. between 1.4 and 91 GHz (Ivanova et al., 2014; Gabarro et al., 2017). The brightness temperature is a result of emission, absorption, and scattering inside the sea ice, the snow cover, and the atmosphere, and the relative influence of the individual media on the brightness temperature measured from space depends on the frequency. At rather low frequencies, the radiation is little disturbed by scattering in the snow and atmosphere, and therefore the brightness temperature is mainly a result of emission, absorption and scattering inside the ice. With increasing frequency, the snow and atmosphere have a larger impact and the importance of the ice properties decreases. My study is a first step towards a more general development of sea-ice observation operators

applied to climate model output. For this first step, I choose to concentrate on the simulation of brightness temperatures mainly driven by the ice properties and focus therefore on the frequency of 6.9 GHz, vertical polarization.

At 6.9 GHz, the main difficulty of an observation operator is the translation of the simulated sea ice into a sea-ice surface brightness temperature. Sea-ice brightness temperatures mainly depend on the liquid water fraction inside the ice and snow, which is driven by temperature and salinity profiles. However, in most climate models, such as the Max Planck Institute Earth System Model (MPI-ESM), the vertical profiles of the ice properties are not computed explicitly. I therefore first investigate, in a one-dimensional idealized setup, the feasibility of the sea-ice brightness temperature simulation based on the limited output provided by a climate model (Appendix B).

Second, I develop the Arctic Ocean Observation Operator for 6.9 GHz (ARC3O), using the results from Appendix B. Then, I investigate the brightness temperatures simulated from the output of three different assimilation experiments and compare them to brightness temperatures observed by satellites to evaluate the performance of ARC3O (Appendix C).

3.1 Simulating sea-ice brightness temperatures in an idealized 1D setup

In a first step, I investigate the simulation of sea-ice surface brightness temperatures at 6.9 GHz, vertical polarization, in an idealized one-dimensional setup (Sec. B.3). I force the one-dimensional thermodynamic Semi-Adaptive Multi-phase Sea-Ice Model (SAMSIM, Griewank and Notz, 2013, 2015) with atmospheric reanalysis data over a period of 4.5 years. The resulting temperature and salinity profiles for ice and snow are then used as input for a slightly modified version of the one-dimensional Microwave Emission Model for Layered Snowpacks (MEMLS) extended to sea ice (Tonboe et al., 2006). MEMLS computes the brightness temperature emitted at the surface resulting from these sea-ice properties.

I find that the effect of vertical sea-ice temperature and salinity profiles on simulated brightness temperatures depends on the surface liquid water fraction of the ice (Sec. B.4.1). For surface liquid water fractions above 0.2, mainly occurring in summer, the brightness temperature is closely tied to the surface liquid water fraction, decreasing from ≈260 K, a typical sea-ice brightness temperature, at a

surface liquid water fraction of 0.2 to ≈160 K, a typical open water brightness temperature, at a surface liquid water fraction of 1. These high surface liquid water fractions above 0.2 occur when the temperature is near 0°C but the salinity is above zero, i.e. mainly in summer. In these conditions, information about the inner properties of the ice are not necessary as the simulated brightness temperature only depends on the surface. However, such high surface liquid water fractions are not realistic. I therefore suggest to interpret the surface liquid water fractions above 0.2 as a measure for the fraction of melt ponds covering the ice in summer.

At surface liquid water fractions below 0.2, the brightness temperature does not depend on the surface only but also on the liquid water fraction distribution inside the ice. Unfortunately, I cannot constrain a given layer or a given liquid water fraction driving it specifically. I therefore investigate if very simple assumptions about the temperature and salinity profile can be made to simulate reasonable sea-ice surface brightness temperatures. I investigate different simplifications for the temperature and salinity profiles and find that reasonable winter sea-ice brightness temperatures can be simulated based on a linear temperature profile and a salinity profile defined as a function of depth (Fig. 3, Sec. B.4.3). These profiles can have as little layers as seven without increasing the uncertainty in the brightness temperature simulation substantially (Sec. B.5).

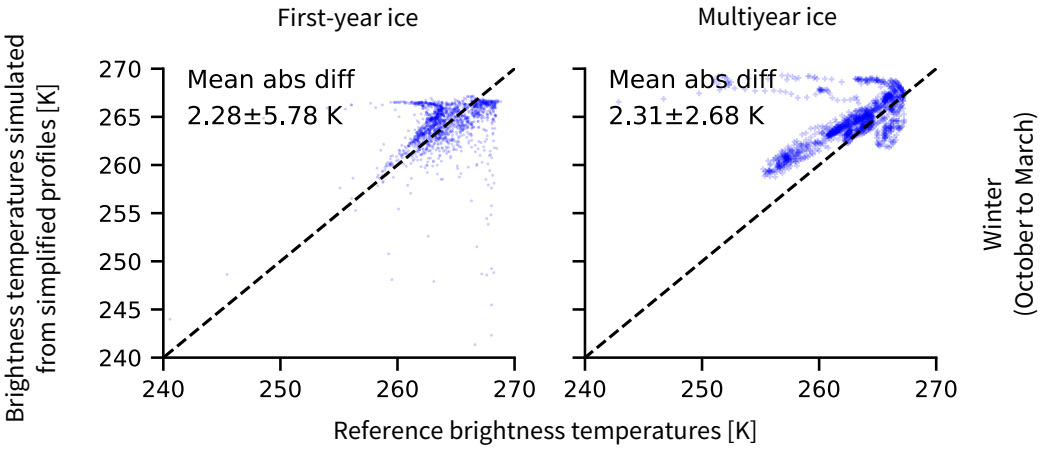

Figure 3: Simulated brightness temperature based on a linear temperature profile and a salinity profile as a function of depth against the reference brightness temperature, for first-year and multiyear ice in winter (October to March). The mean absolute difference and standard deviation of the difference between the two is shown.

Based on these results, I suggest that an observation operator at 6.9 GHz, vertical polarization, for the Arctic Ocean should follow the guidelines below:

For periods of cold conditions:

1. Use the temperature profile provided by the climate model if existing. Otherwise, use the simulated ice surface temperature to interpolate a linear temperature profile.
2. Use the salinity profile provided by the climate model if existing. Otherwise, interpolate the salinity profile as a function of depth, for example following the functions given by Griewank and Notz (2015).
3. Apply an emission model, e.g. MEMLS, to these profiles, combined with information about scatterer size, sea-ice type, etc.
4. Apply a simple atmospheric radiative transfer model, e.g. Wentz and Meissner (2000), to account for the effect of open water when the sea-ice concentration is below 100% and for the effect of the atmosphere.

For periods of bare ice near 0 °C:

1. Use a constant brightness temperature for the ice surface.
2. Weight this constant brightness temperature with the melt pond fraction.
3. Apply a simple atmospheric radiative transfer model, e.g. Wentz and Meissner (2000), to account for the effect of open water when the sea-ice concentration is below 100% and for the effect of the atmosphere.

For periods of melting snow:

Ignore these points in the analysis. The climate model output does not provide enough information about the snow properties and wet snow strongly affects the brightness temperature.

3.2 Simulating Arctic Ocean brightness temperatures from 2D climate model output

In a next step, I construct the ARCtic Ocean Observation Operator for 6.9 GHz (ARC3O) following the guidelines presented in Appendix B to be applied on simple output of a climate model. I apply it to output from the Max Planck Institute Earth System Model (MPI-ESM). In this more realistic setup, I investigate the simulated brightness temperatures and compare them to brightness temperatures observed by satellites.

The structure of ARC3O is based on five steps (Sec. C.3). First, the dataset is divided into different seasons and different ice types. Second, the profiles describing sea-ice properties are prepared for the cold season based on sea-ice thickness, snow thickness and surface temperature output from the climate model. Third, the sea-ice surface brightness temperature is computed for cold conditions by using the sea-ice profiles as input for MEMLS. Fourth, the sea-ice surface brightness temperature is computed for all seasons. Fifth, the effect of open water and atmosphere is added through the use of a simple radiative transfer model by Wentz and Meissner (2000).

The simulated Arctic Ocean brightness temperatures I compare to satellite observations are based on assimilation runs conducted with MPI-ESM (Sec. C.4). These assimilation runs are close to the observed climate state as the model is regularly nudged towards observations. In this setup, I compare simulated and observed brightness temperatures which should be close to each other. I use three model runs assimilated with three different sea-ice concentration estimates to account for the spread in the retrieved sea-ice concentration product. For all three assimilation experiments, the simulated brightness temperatures compare well in autumn to spring, the differences locally ranging from 0 K to 10 K, with most differences being in the range of 0 K to 5 K.

I show that, from autumn to spring, most of the differences between simulated and observed brightness temperatures are small compared to the spread between the observational estimates used in the assimilation (Sec. C.4.3). If the uncertainty introduced by the choice of observational estimate and the uncertainty introduced by the data assimilation are removed, the minimal uncertainty attributable to biases in ARC3O is below 5 K over most of the region (Fig. 4).

In summer, the discrepancies between simulated and observed brightness temperatures locally reach between 15 and 20 K and simulated brightness temperatures differ substantially between the different assimilation runs (Sec. C.4.4). This is because the melt ponds covering the sea ice in summer cannot be distinguished from open water at microwave frequencies. They are therefore a challenge for retrieval algorithms. To account for this difficulty, retrieval algorithms apply differently correction methods. As MPI-ESM provides a melt pond fraction, we assess the uncertainty introduced in the retrieved sea-ice concentration by these correction methods.

In summary, ARC3O allows us to simulate realistic brightness temperature from climate model output. Using assimilation runs, I show that biases introduced by ARC3O itself remain small. ARC3O can therefore be used as a new tool for climate model evaluation, comparing the full simulated climate state represented in the

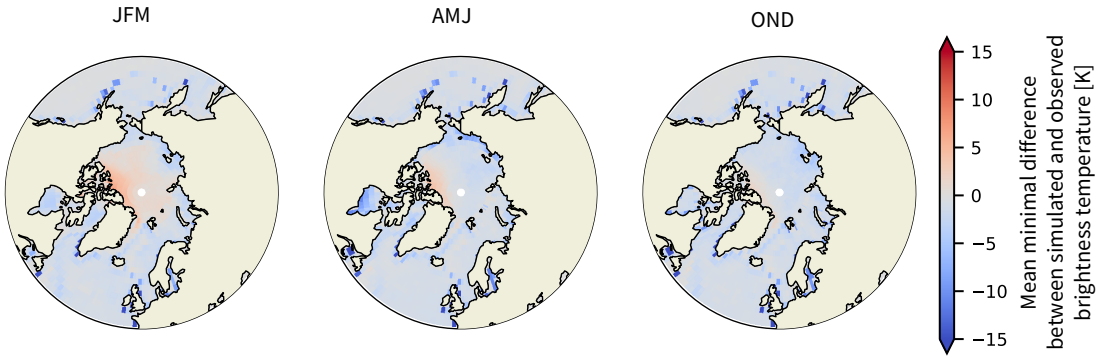

Figure 4: Mean minimal estimate of bias introduced by ARC3O. JFM stands for January/February/March, AMJ for April/May/June, JAS for July/August/September and for OND for October/November/December. See Sec. C.4.3 for more information on the estimation of the bias.

brightness temperature to the observed brightness temperature, allowing us to circumvent observational uncertainty. Additionally, due to its simple structure, ARC3O can be applied to a variety of climate models.

4 Conclusions

In my dissertation, I set out to resolve the case of the biased simulation of the Arctic sea-ice retreat. While I cannot resolve it, I advance it and pave the way for the further continuation of this investigation by providing a new source of information.

Using a multi-model ensemble to investigate the Arctic Ocean energy budget, I show the following:

- The use of the multi-model ensemble mean does not only average out individual model biases but can be a serious misrepresentation of the model ensemble. In my example, the multi-model ensemble mean represents a consensus representation on the magnitude of the Arctic Ocean warming. However, taking a step back and looking at the individual models, it appears that the multi-model ensemble mean does not represent a consensus between the models on the driver of this warming. In 11 of 26 models the Arctic Ocean warming is driven by the meridional oceanic heat flux, and, in 11 other models it is driven by the net atmospheric surface flux. Only four of the 26 models show a warming driven by both fluxes, as suggested by the multi-model ensemble mean.

- Model disagreement is not necessarily inhibiting our understanding of the climate system. The spread between climate models can be turned to our advantage as it provides an opportunity to identify processes and relationships that hold across all models. I show that the different behaviours between disagreeing models can be explained by a mechanism involving the heat inflow through the Barents Sea Opening, the sea-ice area loss and the the ocean surface warming, and the atmospheric turbulent fluxes.

A multi-model ensemble mean is therefore a useful tool to identify differences between climate models and consistent relationships across models.

Further understanding of model biases can come through reliable model evaluation, which is however inhibited by observational uncertainty in the case of sea ice. To tackle this issue, I develop the Arctic Ocean Observation Operator ARC3O for the frequency of 6.9 GHz, which provides the possibility to evaluate both climate models and observational estimates, if assimilated into the climate model, against direct satellite measurements. In this context, I show the following:

- Realistic brightness temperatures at 6.9 GHz can be simulated based on low-complexity output of a climate model, using simple assumptions. The simulation of winter sea-ice brightness temperatures relies on sea-ice temperature and salinity within the ice. Summer sea-ice brightness temperatures are mainly driven by the surface and reliable information about melt ponds is more important than properties inside the ice.

- Differences in the simulated sea-ice concentration account for most of the differences between simulated and observed brightness temperatures. Discrepancies between simulated and observed brightness temperatures possibly attributable to ARC3O itself remain smaller than discrepancies attributable to the spread in sea-ice concentration estimates used in the simulation. This means that the observation operator reduces the uncertainty in the model evaluation process.

ARC3O has proven to be a useful tool to identify variables driving the brightness temperature and therefore driving the uncertainty in the conventional model evaluation procedure. Also, as it circumvents observational uncertainty, the observation operator provides a new possibility to explain model biases in sea ice by possible biases in the surrounding climate conditions.

5 OUTLOOK

Generally, biases in sea-ice simulations have been investigated on the climate-model level, based on the disagreement between simulated and so-called "observed" sea ice, i.e. sea-ice estimates retrieved from satellites. In this dissertation, I investigate different approaches, looking at the sea-ice melting problem from different perspectives, in a multi-model framework on the one hand, and in an observation operator framework on the other hand. In the following, I discuss the implications of my results for a possible continuation of the case investigation about the bias in the simulation of the Arctic sea-ice retreat.

Differences in sea-ice representations, both in observational estimates and climate model simulations are a strong indicator that we do not yet grasp the finer mechanisms at work in the Arctic climate system. This is not surprising, as the Arctic Ocean climate is very heterogeneous and in-situ observations remain sparse. In-situ observations are needed to interpret satellite measurements, and the observational estimates retrieved from these satellite measurements are used to evaluate climate models. While the coverage of in-situ observations has increased in many areas of the world reaching even remote oceanic regions through large-scale networks such as the Argo floats (Gould et al., 2004), the sea-ice cover has strongly inhibited such progress in the Arctic. Observational campaigns to the Arctic Ocean are costly due to the remoteness and the harsh climatic conditions and sea-ice buoys are often lost during the melting season. There is therefore a limit to the amount of in-situ observations that can be collected.

Satellite measurements are difficult to interpret due to the ambiguous origin of the radiation signal, which is influenced by sea-ice properties, snow properties, atmospheric properties, and ocean surface properties. The effect of these variables on the brightness temperature is not straightforward to disentangle. The small number of in-situ observations makes the evaluation of observational estimates retrieved from satellite measurements difficult. Here, I concentrate on the example of sea-ice concentration as this is the longest large-scale record available of a sea-ice property but large uncertainties can also be found in the retrieval of sea-ice thickness from altimeter data (e.g. Bunzel et al., 2018) for example.

Due to the sparsity of in-situ observations and the ambiguous interpretation of satellite measurements, Arctic climate scientists have gotten used to rely on models, be it in the form of reanalyses, regional climate models, or global climate models. These gridded products are easy to use and available over long time periods. In particular, reanalyses are often used as the true "observational" data although, especially in the Arctic, they rely only on a small number of observational

information and are therefore not necessarily close to reality (Lindsay et al., 2014; Boisvert et al., 2018). While I show that the intercomparison of climate models can bring new insights into relationships and processes holding across models, new methods are needed to come closer to the real climate.

An observation operator is a promising alternative to reduce the gap between models and reality. Translating the model simulation results into observation space, i.e. into a quantity that can be measured by satellites directly, opens up new possibilities for Arctic climate research. With this approach the climate model evaluation circumvents most of the observational uncertainty and the simulated climate can be compared to a quantity closer to reality than observational estimates. Additionally, in combination with the assimilation of observational estimates into the model, the simulated brightness temperature can help to identify shortcomings in observational estimates and, eventually, support the improvement of retrieval algorithms.

Besides the evaluation of models and observational estimates, the observation operator offers an opportunity for more reliable data assimilation to initialize climate model hindcasts and forecasts. Especially data assimilation techniques relying on a first guess, such as variational data assimilation (Talagrand and Courtier, 1987; Andersson et al., 1994) and ensemble Kalman filters (Evensen, 1994; Hunt et al., 2007), benefit from having the simulated state in the form of a brightness temperature. These brightness temperatures are directly comparable to the satellite measurements and therefore minimize the observational uncertainty.

The full potential of an observation operator can ultimately be unfolded by including a large range of frequency bands. If only one frequency band is used, differences between simulated and observed brightness temperature cannot be clearly attributed to biases in the brightness temperature simulation or to biases in single climate variables. This can be seen in my example, where the differences between simulated and observed brightness temperatures can potentially be attributed to a biased simulated state of the sea-ice concentration or the surface temperature, or a biased brightness temperature simulation. Different climate properties, such as the sea-ice thickness, snow properties, atmospheric properties, or ocean surface properties, affect the brightness temperature differently at different frequency bands. Using the combination of frequency bands gives the possibility to disentangle the effects and attribute more clearly differences between simulated and observed brightness temperatures to given individual variables or to biases in the operator.

Further development of the Arctic observation operator for higher frequency bands faces the challenge of understanding and parametrizing the snow properties realistically, which are not well represented in climate models and relatively unexplored in in-situ observations. This calls for expertise between different fields, underlining the importance of collaboration in Arctic science as the components of the Arctic Ocean climate system are highly interactive.

Although climate change does not leave us much time to unravel the secrets of an Arctic Ocean covered by ice throughout the year, the sea-ice cover is projected to endure in winter on a much longer time horizon. There is therefore still high potential for "scientific detectives" to continue the investigation, applying unconventional methods for climate model evaluation, and to improve our understanding of the Arctic Ocean climate. As human activity in the region is projected to increase, the prediction of sea ice is becoming increasingly important and therefore a better understanding of biases in both climate models and observational estimates is crucial. While observational uncertainty and model spread inhibit reliable model evaluation, the observational operator I developed here is a promising first step into a novel perspective on the evaluation of simulated Arctic climate against observations.

APPENDICES

Appendix A
Burgard, C. and D. Notz (2017): "Drivers of Arctic Ocean warming in CMIP5 models". *Geophysical Research Letters*, 44, 4263-4271, doi: 10.1002/2016GL072342.

C.B. carried out all analyses of this manuscript, including harmonising, processing and synthesizing the data, interpreting the results, and preparing the manuscript including all text and figures. D.N. provided the original idea and provided guidance at all stages.

Appendix B
Burgard, C., D. Notz, L.T. Pedersen and R.T. Tonboe. "How to obtain sea-ice brightness temperatures at 6.9 GHz from climate model output". *To be submitted to The Cryosphere.*

C.B. carried out all analyses of this manuscript, including the setup of all simulations, re-writing the MEMLS model for the requirements of this study, processing and synthesizing the model output, interpreting the results, and preparing the manuscript including all text and figures. D.N. and L.T.P. developed the original idea. D.N., L.T.P. and R.T.T. provided guidance at all stages.

Appendix C
Burgard, C., D. Notz, L.T. Pedersen and R.T. Tonboe. "ARC3O: The Arctic Ocean Observation Operator for 6.9 GHz". *To be submitted to The Cryosphere.*

C.B. carried out all analyses of this manuscript, including the development of the Arctic Ocean Observation Operator framework, setup of all simulations, processing and synthesizing the model output, interpreting the results, and preparing the manuscript including all text and figures. C.B., D.N. and L.T.P. developed the original idea. D.N., L.T.P. and R.T.T. provided guidance at all stages.

A

DRIVERS OF ARCTIC OCEAN WARMING IN CMIP5 MODELS

CLARA BURGARD AND DIRK NOTZ

Abstract

We investigate changes in the Arctic Ocean energy budget simulated by 26 general circulation models in the CMIP5 framework. Our goal is to understand whether the Arctic Ocean warming between 1961 and 2099 is primarily driven by changes in the net atmospheric surface flux or by changes in the meridional oceanic heat flux. We find that the simulated Arctic Ocean warming is driven by positive anomalies in the net atmospheric surface flux in 11 models, by positive anomalies in the meridional oceanic heat flux in 11 models and by positive anomalies in both energy fluxes in four models. The different behaviors are mainly characterized by the different changes in meridional oceanic heat flux that lead to different changes in the turbulent heat loss to the atmosphere. The multi-model ensemble mean is hence not representative of a consensus across the models in Arctic climate projections.

A.1 INTRODUCTION

The heat content of the Arctic Ocean is regulated by its lateral energy exchange through the meridional oceanic heat flux and its vertical energy exchange through the net atmospheric surface flux. It remains, however, unclear which of these two energy fluxes is primarily driving the observed (Polyakov et al., 2010; Zhang, 2005; Steele et al., 2008; Serreze et al., 2007b) and projected (Vavrus et al., 2011; Koenigk and Brodeau, 2013; Stroeve et al., 2007, 2012) long-term Arctic Ocean warming. This is the question we address here.

For the historical period, the topic has been investigated using reanalyses. During the period from 1979 to 2001, in the annual mean state, nearly as much energy was gained by the ocean through the meridional oceanic heat flux as was lost to the atmosphere through the net atmospheric surface flux (Serreze et al., 2007a). Only a small amount of the energy inflow was taken up by the ocean in form of latent heat to melt sea ice, the sensible heat uptake being near to zero. From 2000 to 2015, however, both latent and sensible heat uptake by the ocean were observed and were found to be mainly driven by the meridional oceanic heat flux up to 2007 and mainly driven by the radiative fluxes from 2007 onwards (Mayer et al., 2016).

For a more extensive analysis on longer timescales, including future projections, general circulation models (GCMs) are needed. Up to now, the future evolution of the different components of the Arctic Ocean energy budget have only been investigated separately. On the one hand, the net atmospheric surface flux was found to increase over the whole Arctic domain (land and ocean) until the end of the 21st century, using the CMIP3 model ensemble (Sorteberg et al., 2007). On the other hand, the northward oceanic heat transport was found to increase as well until the end of the 21st century, using the EC-EARTH model (Koenigk and Brodeau, 2013). These results suggest that both the net atmospheric surface flux and the meridional oceanic heat flux could in principal provide the necessary energy for Arctic Ocean warming. However, as the energy fluxes were investigated separately without direct comparison to each other and to changes in the ocean heat storage, the main driver of the long-term warming cannot clearly be inferred from these studies.

We investigate the Arctic Ocean energy budget as a whole to understand if the simulated long-term Arctic Ocean warming during the late 20th and the 21st century is mainly driven by changes in the net atmospheric surface flux or by changes in the meridional oceanic heat flux. To this purpose, we examine the evolution of the different components of the Arctic Ocean energy budget in data from 26 GCMs from the fifth phase of the Coupled Model Intercomparison Project (CMIP5). By studying the energy budget in a closed framework, we can directly attribute changes in the energy storage of the Arctic Ocean to changes in the two energy fluxes.

A.2 METHODS AND DATA

A.2.1 ARCTIC OCEAN ENERGY BUDGET

The total Arctic Ocean heat content H_{tot}, defined here for the ocean north of 66°N, can be decomposed as follows :

$$H_{\text{tot}} = H_{\text{sens}} + H_{\text{lat}} \tag{A.1}$$

where H_{sens} is the sensible heat content of the ocean water and H_{lat} the latent heat content of the sea ice and snow on sea ice. As shown in both observational studies from Serreze et al. (2007a) and Mayer et al. (2016), the change in latent heat content of snow can be neglected, and we will do so in this study as well.

The change in total ocean heat content in a given period, called hereafter total ocean heat storage ΔH_{tot}, is regulated by the energy fluxes at its boundaries integrated over the given time period and domain. These fluxes are the net atmospheric surface flux F_{sfc} and the meridional oceanic heat flux F_{mer} :

$$\Delta H_{\text{tot}} = \Delta H_{\text{sens}} + \Delta H_{\text{lat}} = \Delta H_{\text{sfc}} + \Delta H_{\text{mer}} \tag{A.2}$$

$$\Delta H_{\text{sfc}} = \int\int F_{\text{sfc}}\,\mathrm{dA}\,\mathrm{dt} = \int_{1\text{ year}}\int_{66°N}^{90°N} (F_{\text{SW}\downarrow} - F_{\text{SW}\uparrow} + F_{\text{LW}\downarrow} - F_{\text{LW}\uparrow} + F_{\text{S}} + F_{\text{L}})\,\mathrm{dA}\,\mathrm{dt} \tag{A.3}$$

where $F_{\text{SW}\downarrow}$ and $F_{\text{SW}\uparrow}$ are the incoming and outgoing shortwave radiation, $F_{\text{LW}\downarrow}$ and $F_{\text{LW}\uparrow}$ are the incoming and outgoing longwave radiation and F_{S} and F_{L} are the sensible and latent heat flux. All fluxes are defined as positive into the Arctic Ocean domain, except $\text{F}_{\text{SW}\uparrow}$ and $\text{F}_{\text{LW}\uparrow}$.

Due to energy conservation, the energy exchanged through the meridional oceanic heat flux can be computed as a residual from the two other components :

$$\Delta H_{\text{mer}} = \int\int F_{\text{mer}}\,\mathrm{dA}\,\mathrm{dt} = \Delta H_{\text{tot}} - \Delta H_{\text{sfc}} \tag{A.4}$$

We investigate changes in the three components of the energy budget presented in Eq. (A.2), (A.3) and (A.4) compared to a reference period defined here from 1861 to 1960. To this purpose, we compute anomalies of each of the components by subtracting their mean state during this reference period. Cumulated over 1961 to 2099, the resulting anomalies yield the total anomalous energy gained or lost by or through the different components over the late 20th and 21st century.

A.2.2 DATA

We use data from 26 GCMs run in the CMIP5 framework (see Tab. S1). The models used in this study were chosen following the availability of the following variables: incoming/outgoing longwave radiation, incoming/outgoing shortwave radiation, sensible/latent heat flux, sea-ice concentration, sea-ice thickness, and ocean potential temperature. Note that the more terms we include in our analysis, the fewer models can be used as not all institutes provide all the variables of interest to the CMIP5 archive. For example, we further use the water mass transport across the Barents Sea Opening, the Fram Strait, the Canadian Archipelago and the Bering Strait from those seven models where these values appear reasonable (see Fig. S1). The sea-ice export across Fram Strait is available for 10 models and can easily be computed for 2 additional models. The mass transport and sea-ice export across the Fram Strait are used as proxies for the mass transport and sea-ice export across the Denmark Strait, as changes in these variables are comparable in those two regions.

We conduct our analysis on data covering the period 1861 to 2099, using historical simulations for the period between 1861 and 2005 and RCP4.5 simulations for the period between 2006 and 2099. If several realizations or ensemble members are available for a model, the ensemble mean is used.

A.2.3 METHOD EVALUATION

We use one of the GCMs that provides all the components of the Arctic Ocean energy budget (MPI-ESM-LR), including snow on sea ice and the oceanic heat flux, to evaluate our method. We use Eq. (A.4) to compute the annual mean meridional oceanic heat flux F_{mer} and compare it to direct model output from the model for F_{mer}. This yields reasonable results (see Fig. A.1), with an average difference between the two values of F_{mer} of 0.192±0.429 W/m^2, i.e. around 1% of the flux value. If the latent energy of snow is included in the computation of ΔH_{tot}, the difference changes by 0.001 W/m^2, confirming that the changes in snow cover can be neglected from an energetic point of view.

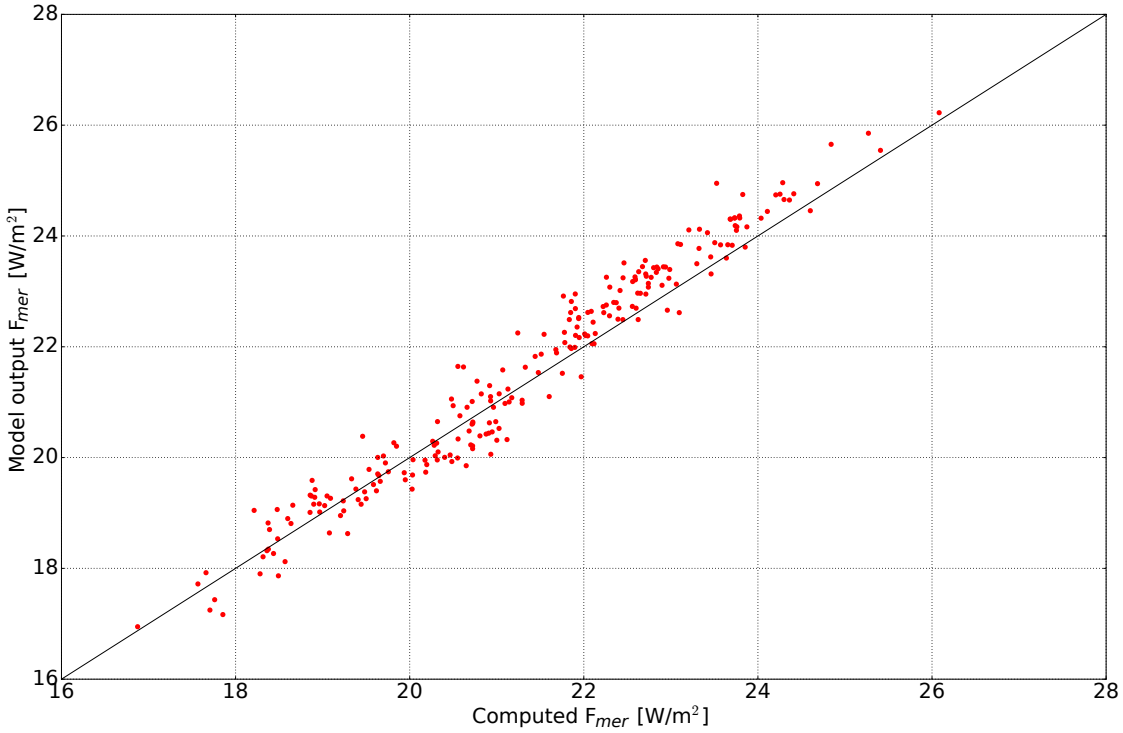

Figure A.1: Annual mean meridional oceanic heat flux given by the model against annual mean meridional oceanic heat flux computed as a residual (in W/m^2) with Eq. (A.4) for MPI-ESM-LR.

A.3 Drivers of the Arctic Ocean warming

As a first step, we examine the relative roles of changes in the net atmospheric surface flux and meridional oceanic heat flux on the Arctic Ocean warming. The multi-model ensemble mean suggests that the ocean warming is mainly driven by positive anomalies in the meridional oceanic heat flux (see Fig. A.2, first panel). However, this does not represent a consensus across the individual models.

Although the total cumulated energy resulting from anomalies in the total ocean heat storage is positive in all models, the models disagree on the evolution of the net atmospheric surface flux and the meridional oceanic heat flux. In 11 models (model names in red in Fig. A.2, called M_{atm} hereafter), energy is gained by the ocean due to positive anomalies in the net atmospheric surface flux, while this gain is compensated partly by negative anomalies in the meridional oceanic heat flux. In 11 other models (model names in light blue in Fig. A.2, called M_{oc} hereafter), the opposite is true. In the four remaining models (model names in grey in Fig. A.2, called M_{both} hereafter), energy is gained by positive anomalies in both the net atmospheric surface flux and the meridional oceanic heat flux.

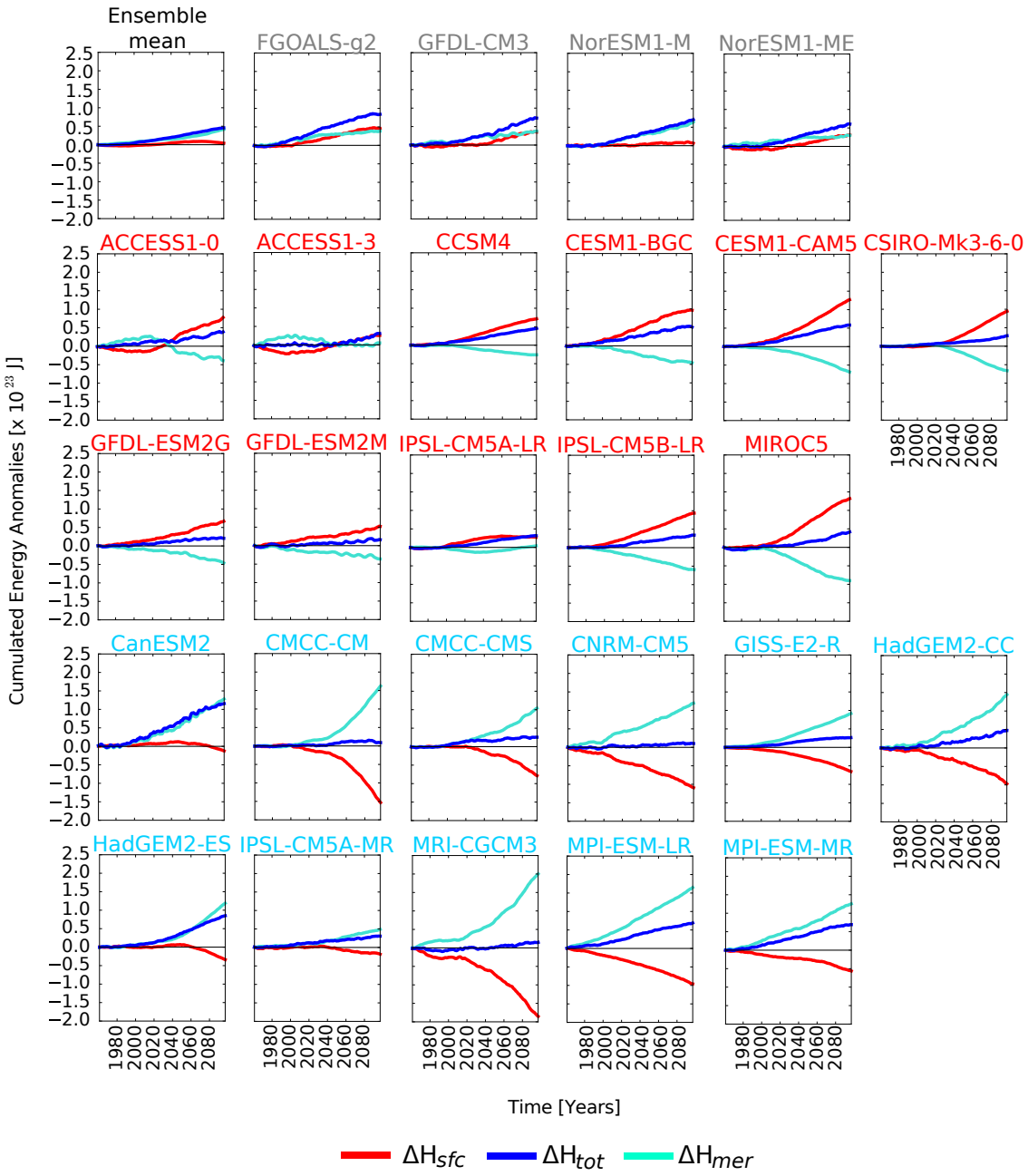

Figure A.2: Cumulated anomalies relative to the reference period (1861-1960) for ΔH_{tot} (dark blue line), ΔH_{sfc} (red line) and ΔH_{mer} (light blue line) (in 10^{23} J). The models are divided into three categories: $\mathrm{M_{atm}}$ (red font), $\mathrm{M_{oc}}$ (light blue font) and $\mathrm{M_{both}}$ (grey font).

As a consequence, although we have used several models with the goal of inferring a robust conclusion, there is no consensus across the models about whether the ocean warming is mainly driven by changes in the vertical energy exchange with the atmosphere or in the lateral energy exchange with the ocean from lower latitudes. We therefore turn to the changes in the drivers of the net atmospheric

surface flux and meridional oceanic heat flux to understand the processes steering the different evolution of the energy fluxes in the models.

A.4 Drivers of changes in the energy fluxes

We examine differences between the end of the 21st century (2079-2099) and the reference period (1861-1960) in variables influencing the net atmospheric surface flux and the meridional oceanic heat flux (see Fig. A.3). Our goal is to understand the different behaviours between the three model categories defined in section A.3. We compute the correlation coefficient between the change in the variables and the change in both the net atmospheric surface flux (upper values in Fig. A.3) and the meridional oceanic heat flux (lower values in Fig. A.3). The net atmospheric surface flux and meridional oceanic heat flux are strongly negatively correlated (r=-0.97). In addition, we find significant correlations ($p<0.05$, bold in Fig. A.3) with the net atmospheric surface flux for seven variables and with the meridional oceanic heat flux for 12 variables. Note that the values of the correlation coefficients might be biased slightly high because of model interdependence (Knutti et al., 2013). In the following, we present changes influencing the net atmospheric surface flux and the meridional oceanic heat flux, then we suggest processes linking changes in the two energy fluxes.

A.4.1 Changes in the net atmospheric surface flux

Changes in the net atmospheric surface flux are driven by changes in the shortwave radiation, longwave radiation and turbulent (sensible and latent) heat fluxes. All models show an increase in net shortwave radiation linked to the decrease in outgoing shortwave radiation. Also, they all show an increase in both incoming and outgoing longwave radiation but disagree on which of the two longwave fluxes increases more. Hence, the models disagree on the sign of the change in the net longwave radiation. Still, all models agree on an increase in the sum of the net radiative fluxes, i.e. an increase in radiative heat gain by the ocean. However, changes in shortwave radiation, longwave radiation, and the sum of the two are not significantly correlated with the changes in the net atmospheric surface flux.

In contrast, the changes in turbulent heat fluxes are significantly correlated with the change in the net atmospheric surface flux (r=0.68). The net atmospheric surface flux decreases with increasing turbulent heat loss to the atmosphere.
The changes in the different atmospheric surface fluxes suggest that the negative

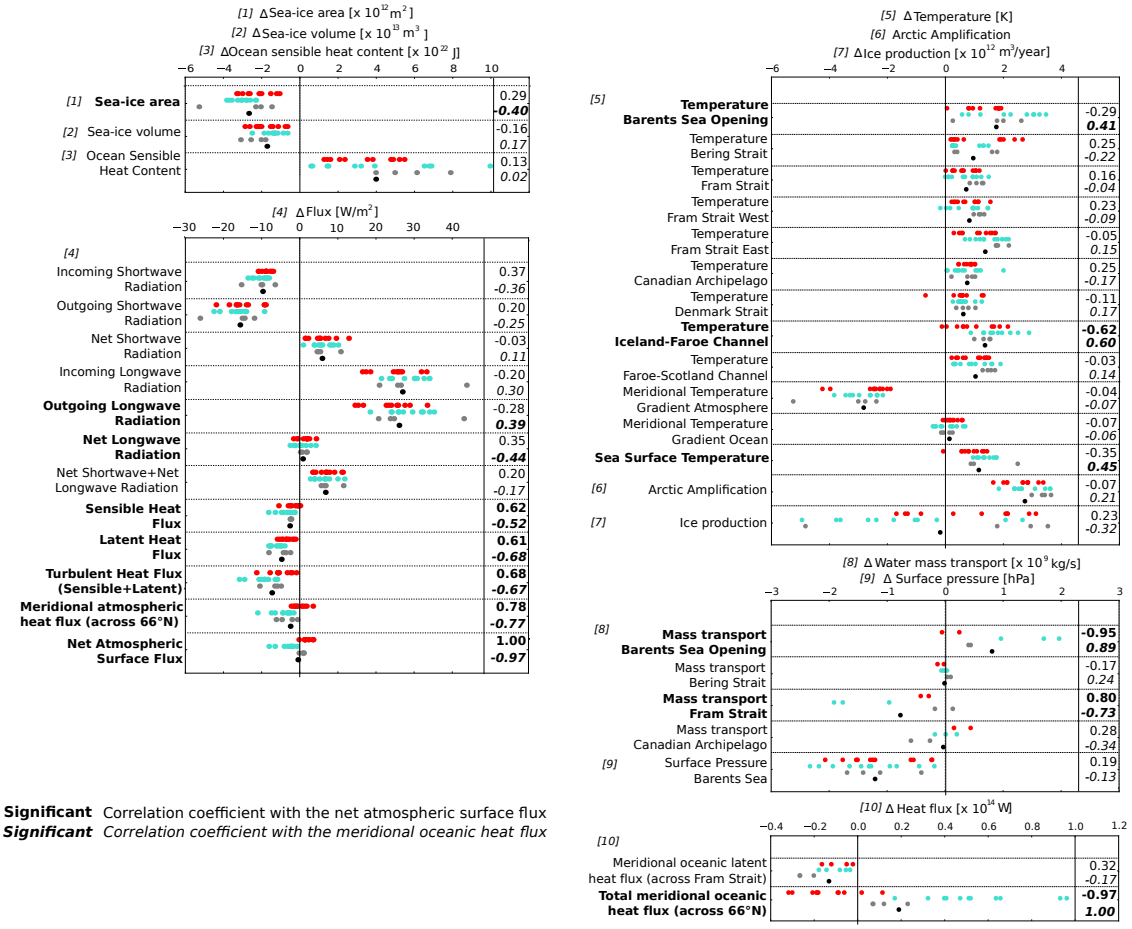

Significant Correlation coefficient with the net atmospheric surface flux
Significant *Correlation coefficient with the meridional oceanic heat flux*

Figure A.3: Change in variables having an influence on the Arctic Ocean net atmospheric surface flux and meridional oceanic heat flux between end of the 21st century (2079 to 2099) and the reference period (1861 to 1960) for each model. Colors stand for the model categories (red: M_{atm}, light blue: M_{oc}, grey: M_{both}, black: multi-model ensemble mean). Coefficients and variables in bold show a significant correlation between the change in the given variable and the change in the net atmospheric surface flux and/or the change in meridional oceanic heat flux. Numbers in brackets represent which units describe the given variable(s). The positive direction for the mass transports is into the domain.

anomalies in net atmospheric surface flux in M_{oc} models are primarily driven by an increase in turbulent heat loss from the ocean to the atmosphere which is larger than the increase in radiative heat gain by the ocean. The positive anomalies in net atmospheric surface flux in M_{atm} and M_{both} models are primarily driven by an increase in radiative heat gain by the ocean which is larger than the increase in turbulent heat loss from the ocean to the atmosphere.

A.4.2 CHANGES IN THE MERIDIONAL OCEANIC HEAT FLUX

The available variables do not allow us to accurately compute the heat transports at the different Arctic Ocean lateral boundaries. This is because the meridional mass transport in different depths is not provided. We therefore use changes in mass transport, temperature and sea-ice export averaged at the different boundary regions as proxies to understand changes in oceanic heat inflow and outflow.

For the inflow, we examine the inflow regions of our domain (Bering Strait, Iceland-Faroe Channel and Faroe-Scotland Channel) and, additionally, the Barents Sea Opening inside the domain. We find the strongest correlation between the meridional oceanic heat flux and the mass transport at the Barents Sea Opening (r=*0.89*). Additionally, the water temperature increases in all inflow regions, significantly correlated with the change in meridional oceanic heat flux in the Iceland-Faroe Channel (r=*0.60*) and at the Barents Sea Opening (r=*0.41*). Changes in the meridional oceanic heat inflow are therefore strongly linked to changes in mass transport and water temperature on the Atlantic side.

For the outflow, we examine the outflow regions of our domain (Denmark Strait and Canadian Archipelago) and, additionally, the Fram Strait inside the domain. We find that the water temperature increases and the sea-ice export decreases in all models in these regions, which both lead to an increase in the energy outflow. We also find a strong negative correlation between the meridional oceanic heat flux and the mass transport at the Fram Strait (r=*-0.73*). We suggest that this is a consequence of the increased mass transport through the Barents Sea Opening owing to mass conservation.

The Fram Strait is both inflow (Eastern part) and outflow region (Western part) concurrently. We attempt to examine the two parts separately by dividing the Atlantic Water layer (upper 1000 m) within the Fram Strait meridionally. Doing so, we do not find any significant correlation between temperature changes in either of the two regions and changes in the meridional oceanic heat flux or changes in the net atmospheric surface flux. As the mass transport is only given across a horizontal line through the whole width of the Fram Strait and cannot be divided similarly, we cannot draw any conclusion in regard to differences in the mass transport changes.

We infer from the changes in temperature and mass transport in the inflow and outflow regions that positive anomalies in the net meridional oceanic heat flux in M_{oc} and M_{both} models are primarily driven by an increase in both the water mass transport and the water temperature at the inflow, especially the Barents Sea Opening. Negative anomalies in the net meridional oceanic heat flux in M_{atm}

models seem to be primarily driven by an increase in the water temperature at the outflow and decrease in sea-ice export which both lead to an increase in energy outflow that compensates the small increase in energy inflow in these models.

A.4.3 PROCESSES LINKING CHANGES IN THE ENERGY FLUXES

We now turn to analyzing the interrelationship between the net atmospheric surface flux and the meridional oceanic heat flux to identify the main driver for the differences between the model categories. In doing so, it is instructive to first briefly consider the linkages between the oceanic and atmospheric meridional heat fluxes. In a steady climate, these two fluxes are linked because of Bjerknes compensation, a process in which changes in the oceanic meridional heat flux are compensated by changes in the atmospheric meridional heat flux (Bjerknes, 1964; Van der Swaluw et al., 2007; Jungclaus and Koenigk, 2010).

In the model simulations considered here, the climate is not in steady state. Nevertheless, we find a strong negative correlation between the two different meridional heat fluxes (r=*-0.77*). Hence, we conjecture that Bjerknes compensation is at work also in the simulated transient climate, which implies that differences in the Arctic Ocean energy budget evolution are ultimately driven by changes in the oceanic meridional heat flux.

This also applies to the explanation for the different model categories that we identified. In all models, increasing net radiative fluxes provide a surplus of energy to the ocean, leading to an increase in sea surface temperature and sea-ice area loss. These effects in turn lead in all models to an increase in turbulent heat loss to the atmosphere, counteracting the increase in radiative heat gain. In M_{oc} models, the sea surface warming, sea-ice loss and consequent increase in turbulent heat loss are amplified by the additional heat gain through the increased meridional oceanic heat flux, leading to a negative change in the net atmospheric surface flux. The ocean loses additional heat to the atmosphere. In contrast, in M_{atm} models, the additional turbulent heat loss is decreased because of the decrease in the meridional oceanic heat flux. Hence, in these models, the change in net atmospheric surface flux is positive, the ocean gains additional heat from the atmosphere.

Although the models disagree on the source of energy for the ocean warming, they agree that changes in the meridional oceanic heat flux are largely compensated by respective changes in the net atmospheric surface flux (Fig. A.4). The resulting change in ocean heat storage is comparably small (ΔH_{tot}=+4.6±2.6x10^{22} J between

1961 and 2099) but very similar across the models, with a regression fit being close to a one-to-one fit (Fig. A.4, r=-0.95).

Hence, under the same forcing, the models agree on the order of magnitude of the surplus energy stored by the Arctic Ocean. However, because of differences in meridional oceanic heat flux, they disagree on the dominating mode of transport for the surplus energy from low to high latitudes.

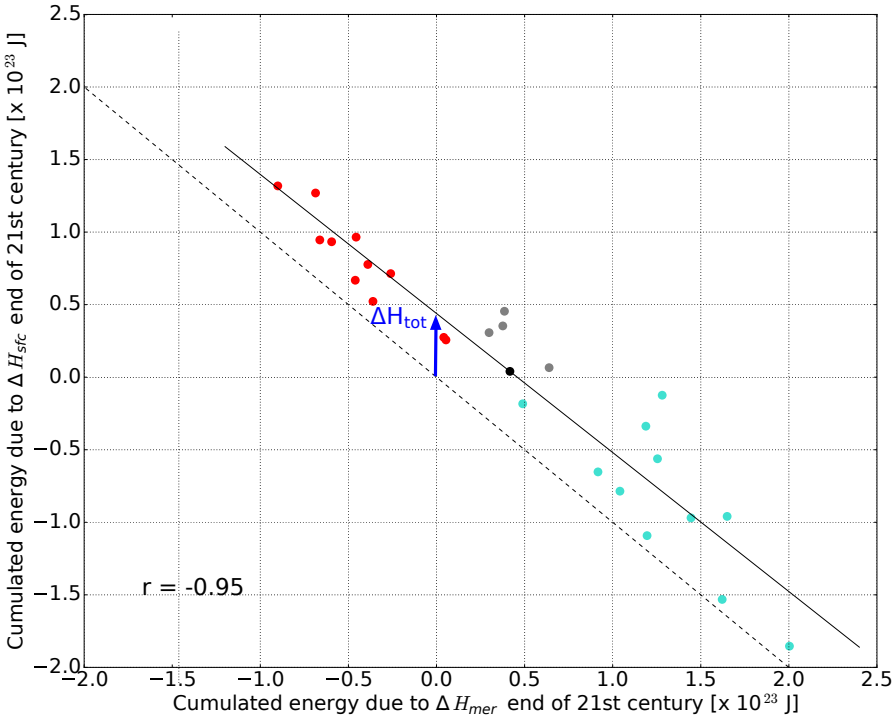

Figure A.4: Sum of the anomalies to the reference period in ΔH_{sfc} as a function of the sum of the anomalies to the reference period in ΔH_{mer} (in 10^{23} J) from 1961 to 2099 for each model. The plain line is a linear regression fit. The dashed line represents the one-to-one fit. Colors represent the model categories, see Fig. A.3. The blue arrow shows the intercept of the linear regression, which represents the total ocean heat gain, if all models would lie on the regression line.

A.4.4 Additional remarks

Additionally to relationships between the three main components of the Arctic Ocean energy budget, the evolution of the other variables (see Fig. A.3) allows us to briefly investigate further relationships discussed in previous literature. First, the chain of effects between meridional oceanic heat flux, sea surface temperature, sea-ice area and turbulent heat fluxes has been observed in the Barents Sea (Ikeda,

1990; Ådlandsvik and Loeng, 1991; Årthun et al., 2012; Smedsrud et al., 2013). However, in addition, the formation of a low pressure system in the Barents Sea as a consequence of the increased turbulent heat loss to the atmosphere was observed in these studies. In CMIP5 atmospheric pressure data, there is no indication of a significant correlation between the surface pressure in the Barents Sea and the change in meridional oceanic heat flux (see Fig. A.3).

Second, the change in meridional oceanic heat flux is significantly correlated with sea-ice area loss rather than sea-ice volume loss. In regions with seasonal ice cover (e.g. Barents Sea), the warming of the ocean water leads to a reduction in the mean annual sea-ice cover due to delayed freezing, as discussed by Bathiany et al. (2016). This results in a pronounced loss of sea-ice area instead of a pronounced loss of sea-ice volume.

Third, we cannot find a significant correlation between the magnitude of simulated Arctic Amplification and the change in meridional oceanic heat flux in the models. This is in contrast with previous studies. An increase in the meridional oceanic heat transport was found to lead to a higher surface warming through the resulting increase in turbulent heat loss to the atmosphere (Holland and Bitz, 2003; Mahlstein and Knutti, 2011; Marshall et al., 2014, 2015; Nummelin et al., 2017). Still, the lack of significant correlation is not necessary at odds with these studies because they examined correlations between Arctic Amplification and meridional oceanic heat flux at latitudes different than 66°N. On the opposite, it would be plausible that Arctic Amplification reduces the water temperature gradient between lower and higher latitudes which would lead, in isolation, to a decrease in the meridional oceanic heat flux. However, although all models agree on a decrease in the atmospheric meridional temperature gradient, we find that only nine models show a decrease in the oceanic meridional temperature gradient. In the remaining 17 models, the oceanic meridional temperature gradient increases (see Fig. A.3).

Finally, an increase in the temperature of the meridional oceanic inflow, as seen in our results, could be explained by weaker heat loss from the ocean to the atmosphere in subpolar latitudes due to a faster atmospheric warming than oceanic warming (Nummelin et al., 2017). A similar mechanism was shown to drive the delayed ocean warming in the Southern Ocean as well (Armour et al., 2016). Additionally, our results also show an increase in mass transport at the inflow. One explanation for this increase would be that a thinner ice cover would lead to an increase in the sea-ice production (Bitz et al., 2006). This would lead to a strengthening in the oceanic ventilation, leading to a higher ocean heat content. However, we do not find any correlation between the change in ice production and the change in meridional oceanic heat flux. This might be a consequence of our

method, as we only look at changes in ice production on a large scale while the explanation by Bitz et al. (2006) relies on regional changes in ice production.

A.5 Summary and conclusions

We show that the CMIP5 models agree on a positive trend in ocean sensible heat content and a negative trend in sea-ice area and volume in the Arctic Ocean from 1961 to 2099. They disagree, however, on the main driver for this overall warming. Ocean warming and decrease in sea-ice cover are driven by positive anomalies in the net atmospheric surface flux in 11 models, by positive anomalies in the meridional oceanic heat flux in 11 models and by positive anomalies in both energy fluxes in four models.

The net atmospheric surface flux exhibits positive anomalies when the increase in radiative heat gain by the ocean is larger than the increase in turbulent heat loss to the atmosphere. When the increase in turbulent heat loss to the atmosphere is larger than the increase in radiative heat gain by the ocean, the net atmospheric surface flux exhibits negative anomalies. The disagreement in the sign of the change in the net atmospheric surface flux stands in opposition to Sorteberg et al. (2007), who found a robust positive twentieth century trend in the net atmospheric surface flux in CMIP3 models. As they considered land surfaces as well, this points to the difference in the evolution of the surface energy budget between land and ocean surfaces (Laîné et al., 2016).

Positive anomalies in the meridional oceanic heat flux are driven by an increase in the water mass transport and water temperature of the oceanic inflow, mainly through the Barents Sea Opening. Negative anomalies are driven by an increase in the water temperature of the oceanic outflow, that overcompensates the small increase in energy inflow. This is in agreement with studies based on observations (Schauer et al., 2004; Spielhagen et al., 2011) and model simulations (Koenigk and Brodeau, 2013), which point towards an increase in both mass transport and temperature as a driver for an increase in the meridional oceanic heat flux.

We also find that changes in net atmospheric surface flux and meridional oceanic heat flux are strongly linked. The magnitude of the increase in turbulent heat loss, driven by the change in meridional oceanic heat flux, is responsible for the sign of the change in the net atmospheric surface flux. Our results therefore underline the importance of the meridional oceanic heat flux for the evolution of the Arctic Ocean energy budget as a whole. This result is in agreement with Mahlstein and Knutti (2011), who found that the meridional oceanic heat flux is responsible for the large

spread in the future warming of the Arctic atmosphere in CMIP3 models, although it contributes only a small amount to the total energy budget.

However, the influence of the meridional atmospheric heat flux is not negligible. Changes in the ocean-atmosphere exchange in the subpolar ocean were shown to be a source for differences in the meridional oceanic heat flux between models (Nummelin et al., 2017). Both components of the meridional heat flux and their interactions before reaching the Arctic region are therefore important to explain the different behaviors of the models.

Unfortunately, the observational record of ocean heat transport is only about 15 years long (Onarheim et al., 2015; Mayer et al., 2016). Hence, we cannot infer robustly which of the models are evolving closest to the "real" world behavior. More observations on longer timescales are needed to better understand the meridional oceanic heat flux and to improve its representation in climate models.
Finally, the disagreement of the simulated changes in the components of the Arctic Ocean energy budget highlights a high uncertainty in future projections for the Arctic. The multi-model ensemble mean is not a good proxy for the future evolution of the Arctic climate system.

ACKNOWLEDGMENTS
We thank two anonymous reviewers for their very insightful suggestions and comments. We also thank Johann Jungclaus, Helmuth Haak and Steffen Tietsche for helpful discussions and comments. We acknowledge the World Climate Research Programme's Working Group on Coupled Modelling, which is responsible for CMIP, and we thank the climate modeling groups (listed in Table S1 of the Supplementary Information) for producing and making available their model output. For CMIP the U.S. Department of Energy's Program for Climate Model Diagnosis and Intercomparison provides coordinating support and led development of software infrastructure in partnership with the Global Organization for Earth System Science Portals. Thanks to the Earth System Grid Federation (ESGF) portal and especially to the Centre for Environmental Data Analysis (CEDA) for providing all the CMIP5 data on their ftp server
(ftp://ftp.ceda.ac.uk/../badc/cmip5/data/cmip5/output1/), while the ESGF website was in maintenance. Funding for this work was provided through a Max-Planck Research Fellowship. Scripts used in the analysis and other supporting information that may be useful in reproducing the authors work are archived by the Max Planck Institute for Meteorology and can be obtained by contacting publications@mpimet.mpg.de.

A.6 Supporting Information to Appendix A

A.6.1 CMIP5 models used.

Table A.1: CMIP5 climate models used and their ensemble size. Models with a (*/+/x) provide a (reasonable) sea water transport across lines/sea-ice transport across Fram Strait/easily computable sea-ice transport across Fram Strait.

Modeling Center/Group	**Model Name**	**Ensemble size**
Commonwealth Scientific and Industrial Research Organization (CSIRO) and Bureau of Meteorology (BOM) *Australia*	ACCESS1.0*+	1
	ACCESS1.3*+	1
Canadian Centre for Climate Modelling and Analysis *Canada*	CanESM2*	5
National Center for Atmospheric Research *USA*	CCSM4	6
Community Earth System Model Contributors *USA*	CESM1-BGC	1
	CESM1-CAM5	3
Centro Euro-Mediterraneo per I Cambiamenti Climatici *Italy*	CMCC-CM	1
	CMCC-CMS	1
Centre National de Recherches Météorologiques / Centre Européen de Recherche et Formation Avancée en Calcul Scientifique *France*	CNRM-CM5+	1
Commonwealth Scientific and Industrial Research Organization in collaboration with Queensland Climate Change Centre of Excellence *Australia*	CSIRO-Mk3.6.0	10
LASG, Institute of Atmospheric Physics, Chinese Academy of Sciences and CESS, Tsinghua University *China*	FGOALS-g2x	1
NOAA Geophysical Fluid Dynamics Laboratory *USA*	GFDL-CM3	1
	GFDL-ESM2G+	1
	GFDL-ESM2M+	1
NASA Goddard Institute for Space Studies *USA*	GISS-E2-Rx	6
Met Office Hadley Centre (additional HadGEM2-ES realizations contributed by Instituto Nacional de Pesquisas Espaciais) *UK*	HadGEM2-CC*	1
	HadGEM2-ES	4
Institut Pierre-Simon Laplace *France*	IPSL-CM5A-LR	4
	IPSL-CM5A-MR	1
	IPSL-CM5B-LR	1
Japan Agency for Marine-Earth Science and Technology, Atmosphere and Ocean Research Institute (The University of Tokyo) and National Institute for Environmental Studies *Japan*	MIROC5	3
Max Planck Institute for Meteorology *Germany*	MPI-ESM-LR+	3
	MPI-ESM-MR*+	3
Meteorological Research Institute *Japan*	MRI-CGCM3+	1
Norwegian Climate Centre *Norway*	NorESM1-M*+	1
	NorESM1-ME*+	1

A.6.2 Definition of the regions

The regions for the temperature calculations in Sec. A.4 are defined as follows:

- Barents Sea Opening: 16.5 to 19°E, 70 to 76.5°N
- Bering Strait: 171 to 166°W, 65 to 66°N
- Fram Strait: 11.5°W to 10.5°E, 79.5 to 81.5°N
- Canadian Archipelago: 128.5 to 59.5°W, 70.5 to 82°N
- Denmark Strait: 37 to 22.5°W, 65.5 to 66.5°N
- Iceland-Faroe Channel: 13.6 to 7.4°W, 62.2 to 64.9°N
- Faroe-Scotland Channel: 6.9 to 5°W, 58.7 to 62°N
- Fram Strait East: 0 to 15°E, 77 to 80°N
- Fram Strait West: 30 to 0°W, 77 to 80°N
- Barents Sea: 17.5 to 60°E, 66 to 80°N

A.6.3 Calculation of the oceanic heat content

For the calculation of the oceanic heat content, the following formulas were used:

$$H_{\text{tot}} = H_{\text{sens}} + H_{\text{lat}} \tag{A.5}$$

$$H_{\text{sens}} = \rho_w \, c_{pw} \int_{66°N}^{90°N} \int_{z_{\max}}^{0} T \; \text{dz dA} \tag{A.6}$$

with ρ_w the density of the water (taken as constant $\rho_w = 1025$ kg/m^3), c_{pw} the heat capacity of the water ($3902 \leq c_{pw} \leq 4186$ J kg^{-1} K^{-1}, depending on the model - see https://search.es-doc.org/), T the potential water temperature in K, $z_{\max}$ the depth of the water column in m and dA the area of the Arctic Ocean domain in the individual models.
Using a constant density between 1015 and 1035 kg/m^3 yields an error of up to ±1% compared to using 1025 kg/m^3. We therefore assume that the error induced by

assuming a constant density of 1025 kg/m^3 is negligible.

$$H_{\text{lat}} = -\rho_i L_i \int_{66°N}^{90°N} SIV \text{ dA} \tag{A.7}$$

with ρ_i the density of the ice (ρ_i = 910 kg/m^3), L_i the latent heat of fusion of fresh ice (L_i=334774 J/kg) and SIV the sea-ice volume in each grid cell.

A.6.4 Mass transport in and out of the Arctic Ocean

The sum of the mass transport at the Arctic Ocean boundaries is shown in Fig. A.5. This is the sum of the mass transport through the Fram Strait, the Barents Sea Opening, the Canadian Archipelago and the Bering Strait. We set the threshold for a 'reasonable value' to a net mass gain or loss of below 0.25x10^9 kg/s. We do not consider *GFDL-ESM2M*, *MRI-CGCM3* and *MPI-ESM-LR* further in our study, as their mass budget is not closed properly.

A.6.5 Calculation of the meridional temperature gradients

The meridional temperature gradients were calculated as the difference of the mean temperature between the Arctic (66°N to 90°N) and the region south of the Arctic (50°N to 66°N). For the atmospheric gradient, the surface air temperature was used. For the oceanic gradient, the sea surface temperature was used.

A.6.6 Calculation of the Arctic Amplification

The Arctic Amplification was computed as the ratio between the surface air temperature increase in the Arctic (66°N to 90°N) and the surface air temperature increase in the tropics (30°S to 30°N) between 1961 and 2099.

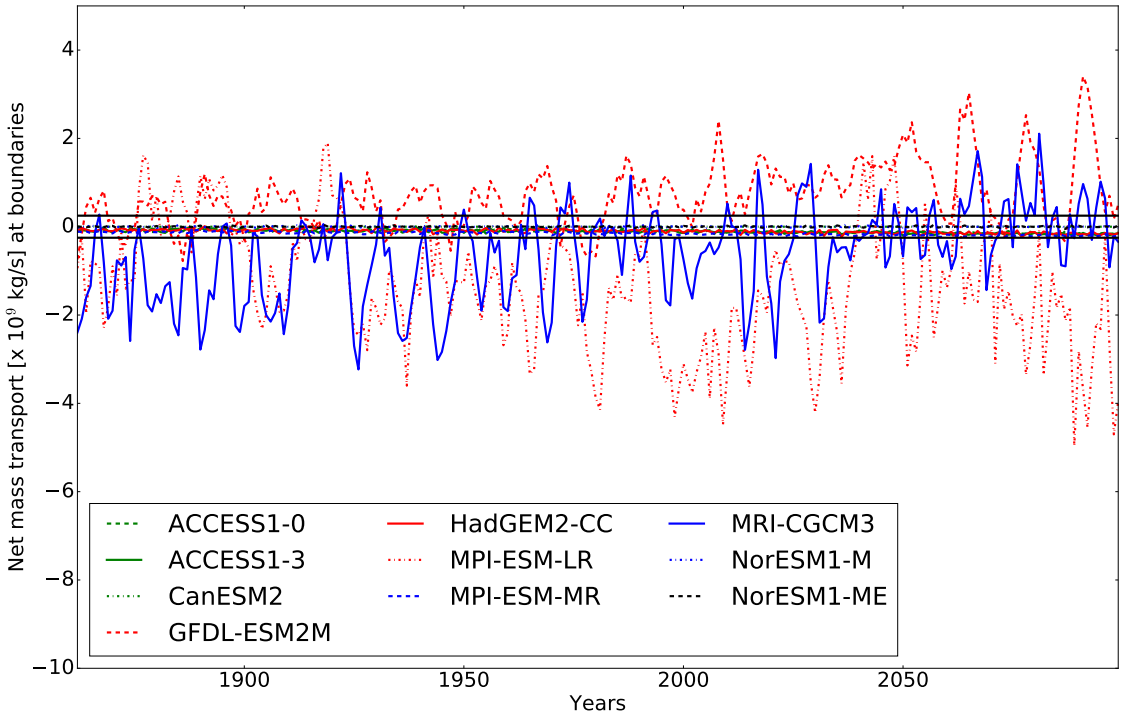

Figure A.5: Mass budget for the Arctic Ocean boundaries for the models providing mass transport across lines. The thick black lines represent our chosen threshold for the variability of the mass budget.

B

How to obtain sea-ice brightness temperatures at 6.9 GHz from climate model output

Clara Burgard, Dirk Notz, Leif T. Pedersen
and Rasmus T. Tonboe

Abstract

The observational uncertainty in sea-ice concentration products is a challenge for climate model evaluation, initialization and climate analysis. One approach to circumvent observational uncertainty relies on the use of observation operators applied to climate model output. Observation operators translate the simulated climate state into the quantity measured by satellites, e.g. the brightness temperature. We explore the feasibility of an observation operator to obtain passive microwave brightness temperatures for sea ice at a frequency of 6.9 GHz. We investigate the influence of simplifying assumptions for the representation of sea-ice vertical properties on the simulation of microwave brightness temperatures. We do so in a one-dimensional setup, using a complex 1D thermodynamic sea-ice model and a 1D microwave emission model. We find that realistic brightness temperatures can be simulated in winter from a simplified linear temperature profile and a self-similar salinity profile in the ice. These realistic brightness temperatures can be obtained based on profiles interpolated to as few as seven layers. Most of the uncertainty resulting from the simplifications is introduced by the simplification of the salinity profiles. In summer, the simplified salinity profile leads to too high liquid water fractions at the surface. To overcome this limitation, we suggest to use a constant brightness temperature for the ice during summer and to treat melt ponds as water surfaces. Finally, during periods of melting snow, microwave brightness temperatures can currently not realistically be estimated as wet snow properties cannot be simplified yet. As periods of melting snow typically last for less than a month, our approach allows one to estimate realistic brightness temperatures at 6.9 GHz from climate model output for about 11 months throughout the year.

B.1 Introduction

Sea-ice concentration products are retrieved from passive microwave brightness temperatures measured by satellites and come with a non-negligible uncertainty (Ivanova et al., 2015; Tonboe et al., 2016; Lavergne et al., 2019). This observational uncertainty hinders reliable climate model initialization (Bunzel et al., 2016) and model evaluation (Notz et al., 2013). Additionally, it hinders a robust extrapolation of the future sea-ice evolution based on current observations. For example, sea-ice area is strongly coupled to changes in the global-mean air temperature (Gregory et al., 2002; Winton, 2011; Mahlstein and Knutti, 2012; Ridley et al., 2012; Li et al., 2013) and thus to CO_2 emissions (Notz and Stroeve, 2016). The relationship between CO_2 emissions, global-mean air temperature and sea ice provides the possibility to project the future Arctic sea-ice evolution under different forcing scenarios. However, Niederdrenk and Notz (2018) showed that the observational uncertainty in sea-ice concentration translates into uncertainty in the sensitivity of sea ice to changes in global-mean air temperature and therefore leads to uncertainty in the temperature at which an ice-free Arctic in summer can be expected.

Observation operators are a current approach in climate science to circumvent observational uncertainty and the spread introduced by the use of retrieval algorithms on satellite measurements (Flato et al., 2013; Eyring et al., 2019). They simulate directly the observable quantity, in our case the brightness temperature, from the climate model output instead of retrieving the simulated quantity, in our case the sea-ice concentration, from the satellite observations. A sea-ice observation operator reduces the uncertainty introduced by assumptions used in retrieval algorithms about the state of other climatic variables besides the sea-ice concentration. It takes advantage of knowing the consistent climate state in time and space simulated by the climate model alongside the sea ice. The feasibility and limitations of an observation operator applied to sea ice simulated by a climate model have not been investigated yet. This is the question we address here.

We investigate how important the complexity of the representation of sea-ice properties is for the simulation of sea-ice surface brightness temperatures emitted by different ice types. Experiments using a model accounting for part of the processes at work inside the sea ice combined with an emission model have shown that knowing the vertical sea-ice properties are sufficient to generate realistic microwave brightness temperatures (Tonboe, 2010; Tonboe et al., 2011). We mainly concentrate on the vertical representation of temperature and salinity inside the ice and snow, as they are the main drivers of the liquid brine fraction in the ice and

liquid water fraction in the snow and thus of sea-ice brightness temperatures, especially at low microwave frequencies (Ulaby et al., 1986). As most general circulation models (GCMs) do not explicitly represent the time evolution of vertical profiles of temperature and salinity in the ice and snow, we investigate the effect of simplified temperature and salinity profiles on the simulation of brightness temperatures. We do so by comparing reference profiles representing an estimate of reality on the one hand and simplified profiles, representing GCM output on the other hand in an idealized one-dimensional setup, using a complex thermodynamic sea-ice model and a microwave emission model.

We focus on the simulation of sea-ice brightness temperatures at 6.9 GHz at vertical polarization as a first step. At this frequency, the main driver of brightness temperatures are the sea-ice properties, and the contribution of the snow emission and scattering and of the atmospheric absorption and scattering due to water vapor, cloud liquid water and temperature are small compared to the surface contribution. The framework can, however, be extended to other frequencies and polarizations in the future, if the increasing importance of the snow and atmospheric contribution with increasing frequency is taken into account.

In Sec. B.2, we provide the theoretical background about drivers of sea-ice brightness temperatures and in Sec. B.3 we present our method and the sea-ice and emission models used. In Sec. B.4, we explore the influence of simplifications in the temperature and salinity profiles on the simulation of sea-ice brightness temperatures to then explore the effect of a reduced number of layers in Sec. B.5. To complete the study, we quantify the uncertainty introduced by a snow cover and the atmosphere in Sec. B.6. Finally, we discuss our findings in Sec. B.7 and conclude with suggestions for a functional observation operator for sea ice in Sec. B.8.

B.2 THEORETICAL BACKGROUND

The brightness temperature TB is a measure for the microwave radiation emitted at the surface of a given medium and represents the temperature of a blackbody emitting the observed radiation. It is defined as:

$$\mathrm{TB} = \epsilon_{\mathrm{eff}} \cdot T_{\mathrm{eff}} \tag{B.1}$$

where ϵ_{eff} is the emissivity of the emitting part of the medium, i.e. the layers influencing the resulting radiation emitted at the surface and T_{eff} the integrated temperature over this same emitting part (Hallikainen and Winebrenner, 1992;

Shokr and Sinha, 2015a). The thickness of the emitting part and its emissivity depend on the permittivity and scattering properties of the medium, which in turn depend on the medium and on the frequency of the radiation.

In the case of sea ice, the permittivity is mainly a function of the fraction and distribution of liquid water in the form of brine inside the ice as the permittivity of water is an order of magnitude higher than the permittivity of pure ice (Ulaby et al., 1986; Shokr and Sinha, 2015b). This means that water is a stronger absorber than pure ice in the microwave range. The liquid water fraction is a function of temperature and bulk salinity. Liquid water can be present within the ice throughout the year in the form of brine. If the ice becomes multiyear ice, most of its brine will have drained and the liquid water fraction decreases substantially compared to first-year ice. In snow, liquid water is mainly present during melting periods. Also, the lowest layer of the snow can be saline, especially above first-year ice (Barber et al., 1998; Shokr and Sinha, 2015a), enabling the presence of liquid water at the base of the snow. We do not investigate saline snow in this study.

The scattering of the microwave radiation in sea ice is a function of the permittivity and the size of scatterers inside the ice, snow, and atmosphere. In first-year ice, the main scatterers are brine pockets, while in multiyear ice the main scatterers are air bubbles, as most of the brine will have drained out (Winebrenner et al., 1992; Nghiem et al., 1995; Tonboe et al., 2006). While a dry atmosphere and dry snow cover have a low permittivity, they can still influence scattering for frequencies higher than 10 GHz (Barber et al., 1998). In ice, snow, and atmosphere, the scattering becomes increasingly important with increasing frequency (Tonboe et al., 2006) as the wavelength successively approaches the size of brine pockets, snow grains and atmospheric aerosols and droplets.

Sea-ice concentration retrievals are based on satellite measurements at frequencies ranging from 1.4 GHz to 91 GHz (Ivanova et al., 2014; Gabarro et al., 2017). In the following, we concentrate on radiation at 6.9 GHz and vertical polarization. This frequency is advantageous as, with a wavelength of approx. 4.3 cm, it is only slightly affected by scattering inside the ice, the snow, and the atmosphere. The brightness temperature at 6.9 GHz therefore mainly depends on the emission and absorption properties inside the ice rather than on the scattering properties. This is why our focus lies on the properties of the sea-ice column, rather than on the snow structure or the state of the atmosphere. The emitting part of the ice can be around 20 cm thick for first-year ice and around 50 cm thick for multiyear ice (Tonboe et al., 2006).

B.3 Method and Data

B.3.1 Method

Although a few GCMs use detailed sea-ice modules (Vancoppenolle et al., 2009; Bailey et al., 2018), most GCMs use very simple sea-ice models that do not resolve the properties driving absorption and scattering inside the ice and snow. The Max Planck Institute Earth System Model (MPI-ESM, Wetzel et al., 2012) is such a GCM. To describe the evolution of its sea-ice properties, MPI-ESM provides a sea-ice (bare ice) or snow (snow-covered ice) surface temperature, a constant sea-ice bottom temperature at -1.8 °C, and a constant salinity of 5 g/kg regardless of sea-ice type or age (Notz et al., 2013). It is not clear yet how these simple assumptions affect a brightness temperature simulated based on these properties.

To explore the importance of the vertical distribution of sea-ice properties on the simulation of brightness temperatures, we use an idealized one-dimensional setup. This one-dimensional setup works as follows. On the one hand, we use a one-dimensional thermodynamic sea-ice model to simulate our reference (see Sec. B.3.2). It computes highly resolved vertical sea-ice profiles under a given atmospheric forcing. On the other hand, we simplify these reference profiles to emulate profiles that could be inferred from information given by MPI-ESM for the same conditions. These two sets of profiles can be used to simulate two sets of brightness temperatures with a microwave emission model (see Sec. B.3.3). The two sets of resulting brightness temperatures can then be used to quantify the effect of the GCM simplification on the brightness temperature simulation, compared to our reference (Fig. B.1).

In this setup, we can quantify the influence of each parameter separately on the simulated brightness temperature. We could have compared brightness temperatures simulated on the basis of MPI-ESM output directly to brightness temperatures measured by satellites. However, we would then have not been able to infer the contribution to the difference in brightness temperatures of fundamental differences between model and observations on the one hand, and the contribution of the differences in the resolution of the ice properties on the other hand.

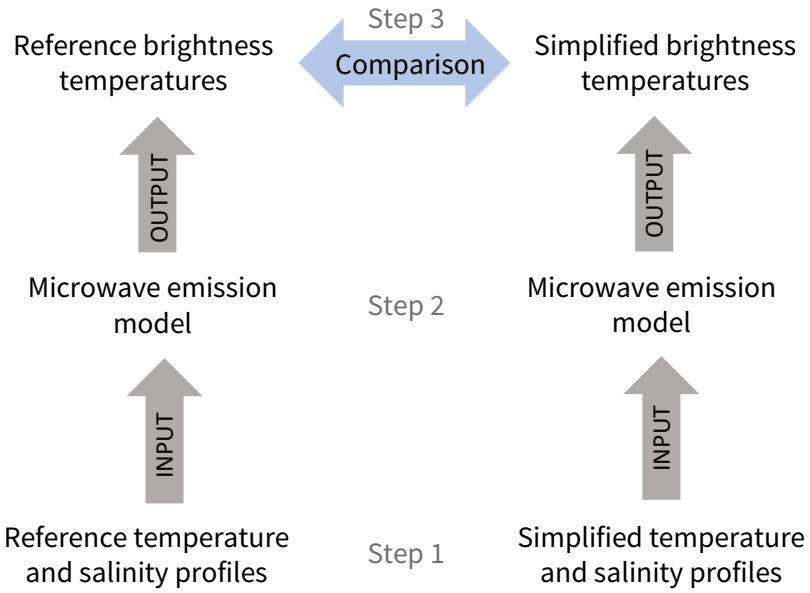

Figure B.1: Schematic of the steps of our simulation and comparison method.

B.3.2 SAMSIM

Our reference profiles are simulated by the 1D Semi-Adaptive Multi-phase Sea-Ice Model (SAMSIM, Griewank and Notz, 2013, 2015). This is a complex thermodynamical model simulating the evolution of a 1D sea-ice column under given surface forcing. It computes sea-ice temperature, salinity, and liquid water fraction profiles on a semi-adaptive grid, with a number of layers varying between 0 and 100. It includes most of the processes governing sea-ice growth and melt, and interactions between the ice and, if existent, its snow cover. It was developed to investigate the brine dynamics inside the ice. A detailed description of underlying equations and represented processes can be found in Griewank and Notz (2013) and Griewank and Notz (2015).

We force SAMSIM with 2 m air temperature, surface downward longwave radiation, surface downward shortwave radiation, and precipitation from the ERA-Interim reanalysis (Dee et al., 2011) in the time period from July 2005 to December 2009. This gives us insight into 4.5 annual cycles, so that we can assess the interannual variability of the growth and melt of sea ice and the evolution of its properties. The ocean salinity is kept at 34 g/kg and the oceanic heat flux at the bottom of the ice is derived from SHEBA measurements, varying between 0 W/m^2 in spring and 14 W/m^2 in autumn (Huwald et al., 2005; Griewank and Notz, 2015).

To gain insight into differences in microwave emission between first-year ice and multiyear ice, we focus on two points in the Arctic Ocean (Fig. B.2). The first point represents first-year ice at 75°N00°W, where the ice always melts completely in summer. The second point is at 90°N, where the ice survives the melt season and becomes multiyear ice from the second simulation year onwards. Note that in our setup the simulated sea-ice evolution is not necessarily representative for the real sea-ice evolution at that location. For example, sea ice seldom exists at 75°N00°W in reality. The presence of ice in this idealized simulation is likely linked to the oceanic heat flux used. This oceanic flux was measured in the SHEBA site north of Alaska and is very different than in the North Atlantic. However, this does not affect our study because we work in an idealized setup.

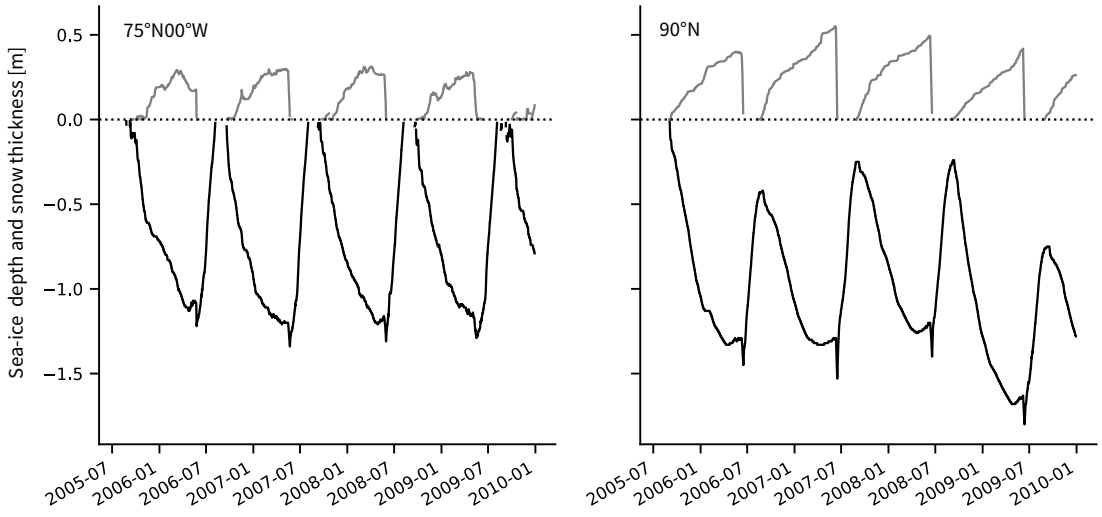

Figure B.2: Evolution of sea-ice (black line) and snow (grey line) thickness as simulated by SAMSIM under ERA-Interim forcing between July 2005 and December 2009.

B.3.3 MEMLS

The simulation of sea-ice brightness temperatures is conducted with a slightly modified version of the Microwave Emission Model for Layered Snowpacks (MEMLS) extended to sea ice (Tonboe et al., 2006). MEMLS was first developed by Wiesmann and Mätzler (1998) to simulate brightness temperatures emitted by a snowpack composed of several layers and was later extended to sea ice (Tonboe et al., 2006). MEMLS uses the information of the properties of the ice and snow layers to simulate the path of microwave radiation from the bottom to the surface of the ice and, if present, snow. It uses the thickness, the temperature, the salinity,

the density, the correlation length (measure for the scatterer size), the wetness, and information about the type of medium (snow, first-year/multiyear ice) of the different sea-ice and snow layers to compute absorption and scattering along the path. This then results in a brightness temperature emitted at the surface of the ice or snow.

Unless otherwise mentioned, we do not take into account the atmosphere in our analysis as its effect is relatively small at 6.9 GHz. The use of the term "brightness temperatures" in the following is therefore equivalent to the use of "brightness temperatures emitted at the surface of the ice and snow column".

B.3.4 General simulation setup

The temperature and salinity profiles produced by SAMSIM are used as input for MEMLS for the simulation of brightness temperatures. Additionally, density profiles are derived from these properties using relationships given by Notz (2005) (see Sec. B.9.1 in Supp. Info.). Next to the temperature, salinity and density profiles, other variables, which are not computed by SAMSIM, have to be provided to MEMLS. These are the correlation length, the incidence angle, the ocean temperature, the incoming brightness temperature from the atmosphere and the ice-ocean reflectivity for vertical polarization. They are set to constants, listed in Tab. B.1.

Additionally, except for snow thickness and temperature, snow properties are neither resolved in SAMSIM nor in MPI-ESM. The main effect of snow on the radiation is its thermal insulation of the ice column and its refractive effect on the radiation induced by the difference in density between ice and snow and snow and atmosphere. The former is taken into account through the use of the SAMSIM snow thickness and snow temperature evolution, and the latter is taken into account through the snow thickness and by using a low density of snow compared to ice. We therefore set all snow properties, except the snow temperature and snow thickness, to constants, also listed in Tab. B.1. In theory, the brightness temperature simulation is affected by the snow wetness if it is above zero. Neither SAMSIM or MPI-ESM resolve the liquid water fraction in the snow. In this study, we set the snow wetness to zero. However, in a possible observation operator resulting from this study, we strongly recommend to not consider periods of melting snow as we do not have the necessary information to simulate plausible brightness temperatures.

Table B.1: MEMLS constant input details and properties of the snow layer.

Incidence angle	55°
Ocean temperature	-1.8 °C
Incoming brightness temperature	0 K
Ice-ocean reflectivity for V-polarization	0.25
Correlation length first-year ice	0.35 mm for depth < 20 cm, 0.25 mm for depth > 20 cm
Correlation length multiyear ice	1.5 mm
Snow thickness	as computed by SAMSIM
Snow density	300 kg/m^3
Snow correlation length	0.15 mm
Snow salinity	0 g/kg
Snow temperature	mean between 2m air temperature from ERA-Interim and temperature at ice-snow interface given by SAMSIM

Our input for the emission model, e.g. salinity, correlation length, brine pocket form, comes with uncertainties. These are mainly caused by a partial or complete lack of in-situ observations and the resulting low understanding of their evolution. We therefore recommend more observations of the ice properties combined with concurrent microwave radiation measurements. A few of such observations exist already, from both laboratory setting and in-situ, but they mainly focus on frequencies higher than 6.9 GHz (e.g. Grenfell et al., 1998; Jezek et al., 1998; Perovich et al., 1998; Hwang et al., 2007). With more combined observations at lower frequencies, we expect that the uncertainty in the brightness temperature simulation can be reduced in the future through further research and better understanding of the components introducing the uncertainty.

For example, a better understanding of sea-ice salinity evolution would be of advantage. The salinity parametrization used in Sec. B.4.3 is based on an "L-shape" of the salinity profile, while it is argued that the sea-ice salinity profile often resembles a "C-shape" (Nakawo and Sinha, 1981; Shokr and Sinha, 2015b). Another parameter of uncertainty is the correlation length. Although it is a variable quite well understood and quantifiable for snow (Mätzler, 2002; Proksch et al., 2015; Lemmetyinen et al., 2018), its quantification in sea ice is not clear and its values not well known. On a similar note, MEMLS makes assumptions about the form of the brine pockets. In our study we assumed spherical brine pockets. However, it is known that the shape depends highly on the ice age and formation. An extensive summary of the brine pocket form can be found in Tonboe et al. (2006).

Finally, the use of MEMLS as a sea-ice emission model is a source of uncertainty as well. Here again, the lack of measurements of the parameters needed for the brightness temperature simulation and of microwave radiation itself has inhibited a comprehensive evaluation of the sea-ice version of MEMLS simulations against reality. Still, it is accepted as one of the main tools for sea-ice brightness temperature simulations and has shown its strength in several previous studies (Tonboe, 2010; Tonboe et al., 2011; Willmes et al., 2014; Lee et al., 2017).

These uncertainties, however, only have a limited impact on the present study. We concentrate on a relative comparison, where we change temperature and salinity in the ice to understand their impact on the brightness temperature, but assumptions about correlation length and the form of brine pockets are the same in our reference and our simplified brightness temperature simulations. The uncertainties will therefore not impact the difference between the two sets of brightness temperatures. Additionally, in regard to the absolute values, Burgard et al. (2019a) show that realistic brightness temperature can be simulated by MEMLS using the above mentioned uncertain assumptions with slight tuning. The effect of the uncertainties therefore remains small when considering large scales.

B.4 The influence of vertical sea-ice properties

B.4.1 Liquid water fraction

Sea-ice brightness temperatures at 6.9 GHz are mainly driven by the distribution of liquid water in the form of brine inside the ice, as absorption plays a larger role than scattering at this frequency. This relationship is clearly visible in the brightness temperatures simulated based on the vertical profiles from SAMSIM output. The brightness temperatures show a strong dependence on the surface liquid water fraction, i.e. the fraction of liquid water contained in the top ice layer of the profiles (Fig. B.3a). If we concentrate the brightness temperature simulation on the ice layers, i.e. using only the ice layers of the snow and ice column as input to MEMLS, the relationship is even clearer (Fig. B.3b).

Especially above a surface liquid water fraction of 0.2, the brightness temperature of bare ice is linearly related to the surface liquid water fraction. This means that no radiation signal from below the surface influences the brightness temperature but only the surface liquid water fraction matters. The brightness temperature transitions roughly linearly between brightness temperatures typical for ice ($\approx$ 260 K) at a surface liquid water fraction of 0.2 and brightness temperatures

typical for open water (≈160 K) at a liquid water fraction of 1. The properties inside the ice do therefore not influence the brightness temperature when the ice surface has a liquid water fraction higher than 0.2. In our SAMSIM profiles, these high surface liquid water fractions occur predominantly in summer, i.e. from April to September. We therefore suggest that a liquid water fraction above 0.2 can be interpreted as a measure for the melt-pond fraction.

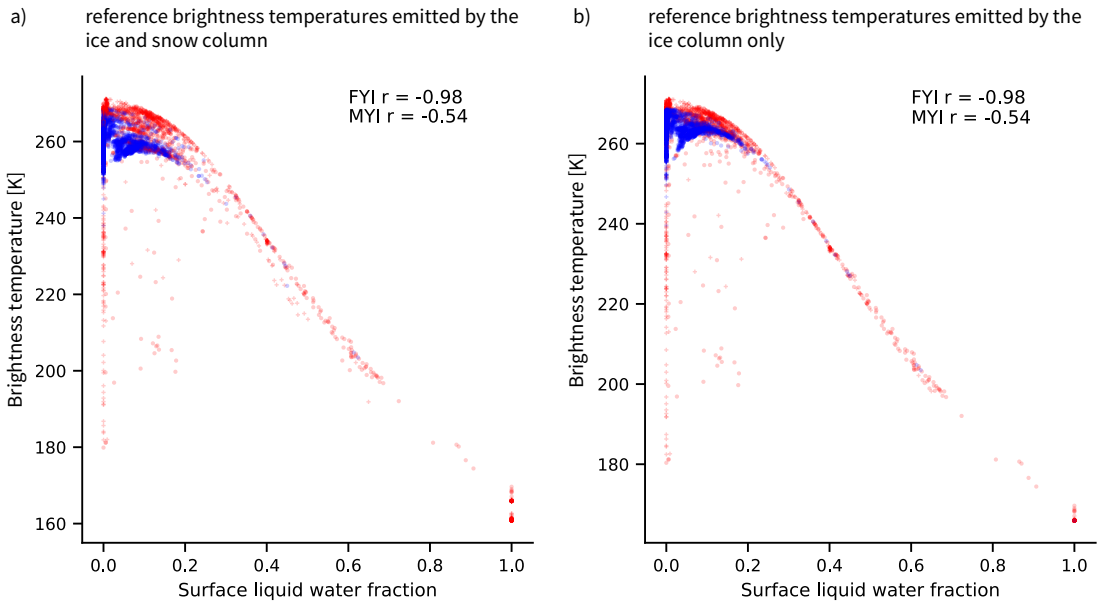

Figure B.3: Reference brightness temperatures at 6.9 GHz, vertical polarization, simulated based on the (a) ice and snow column and on the (b) ice column only as a function of the reference surface liquid water fraction. Circles represent first-year ice (FYI), crosses represent multiyear ice (MYI). Blue is winter (October to March), red is summer (April to September).

For surface liquid water fractions below 0.2, occurring in both winter and summer, the spread between brightness temperatures is 10 to 15 K for similar surface liquid water fractions. In some summer multiyear ice cases, the brightness temperature even drops to ≈180 K. For these surface liquid water fractions, the brightness temperatures are driven by the distribution of liquid water fraction further inside the ice, which is a function of the temperature and salinity distribution. Unfortunately, we could not infer a direct relationship between the brightness temperature and a given layer or a given liquid water fraction inside the ice from our data. We therefore proceed with sensitivity experiments to investigate the effect of simplifications in temperature and salinity profiles, and therefore in liquid water fraction profiles, on the simulated brightness temperature.

These sensitivity experiments demonstrate the effect of the lack of information about the vertical sea-ice profile, as in the sea-ice representation by MPI-ESM. To this end, we compare brightness temperatures simulated based on SAMSIM profiles (in the following our reference) and brightness temperatures simulated based on simplified profiles (in the following our simplification). Our focus lies on the influence of the ice properties on the brightness temperature. We therefore only use the ice layers of the ice and snow column as input for MEMLS. This way, the thermal insulation effect of the snow on the temperature profiles is conserved but the refraction at the snow interface is neglected for the moment. The refraction effect of the snow is discussed in Sec. B.6.

The purpose of the sensitivity experiments is to identify the influence of the different profiles rather than the effect of differences in the vertical resolution, i.e. the number of ice layers. The simplified input profiles are therefore interpolated to the same number of layers as the reference profiles (ranging from 1 to 100 layers, depending on the ice thickness).

B.4.2 Linear Temperature and Constant Salinity

In a first experiment, we investigate the brightness temperature simulated based on information as would be given by MPI-ESM. For the simplified temperature profile, we use the temperature at the interface between ice and snow as simulated by SAMSIM and interpolate linearly to the ice bottom layer, which has a temperature of -1.8 °C. For the salinity profile, MPI-ESM assumes a constant salinity of 5 g/kg. As this is clearly too high for multiyear ice (Ulaby et al., 1986), we assume a constant salinity of 5 g/kg for first-year ice and a constant salinity of 1 g/kg for multiyear ice in our simplified salinity profiles (see dashed lines in Fig. B.4).

The influence of the simplifications is clearly different depending on the season. We therefore divide our results into winter (October to March, see Fig. B.5) and summer (April to September, see Fig. B.6). In winter, the simplified profiles produce brightness temperatures close to reference brightness temperatures for first-year ice, with a mean absolute difference of 2.47±6.37 K (Fig. B.5, first row). For multiyear ice, the spread is higher and there is a tendency of simplified brightness temperatures to underestimate the reference brightness temperatures, with a mean absolute difference of 7.03±4.85 K.

In summer, the mean absolute differences are one order of magnitude higher, with 42.91±44.45 K for first-year ice and 40.65±45.3 K for multiyear ice (Fig. B.6, first row). Simplified and reference brightness temperatures are clearly different most of the

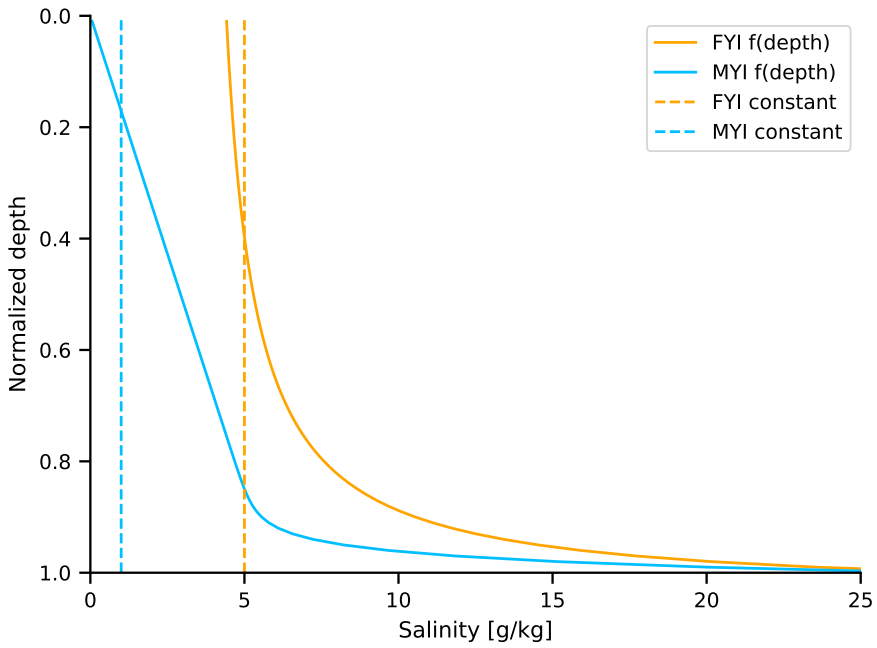

Figure B.4: Salinity profiles used for the simplified profiles. FYI: First-year ice, MYI: Multiyear ice. The dashed lines represent the constant salinity profiles used in Sec. B.4.2 and the full lines represent the salinity profiles as a function of depth used in Sec. B.4.3

time. Especially, the simplified brightness temperature is close or equal to 160 K, i.e. open water brightness temperatures, at most of the time steps. This is because in summer, the physical temperature of the ice surface approaches 0 °C and, the closer it gets to 0 °C, the lower the salinity must be in order for ice to exist. This leads to high surface liquid water fractions at salinities of 5 g/kg and thus to low brightness temperatures. For multiyear ice, the effect of a salinity of 1 g/kg is not visible in the surface liquid water fraction (Fig. B.3) but the low brightness temperatures reaching 180 K suggest that there is an effect deeper inside the ice.

To confirm our findings for summer and understand further our findings for winter, we conduct two additional sensitivity experiments. In the first experiment, the simplified brightness temperature is simulated based on the linear temperature profiles and the reference salinity profiles. In the second experiment, on the contrary, the simplified brightness temperature is simulated based on the reference temperature profiles and the constant salinity profiles. This enables us to separate the effect of the two simplifications. In both seasons, the effect of the constant salinity assumption is the main driver of the spread between the different brightness temperatures (Fig. B.5 and Fig. B.6, third row), while the linear temperature assumption has nearly no effect on the spread in winter brightness

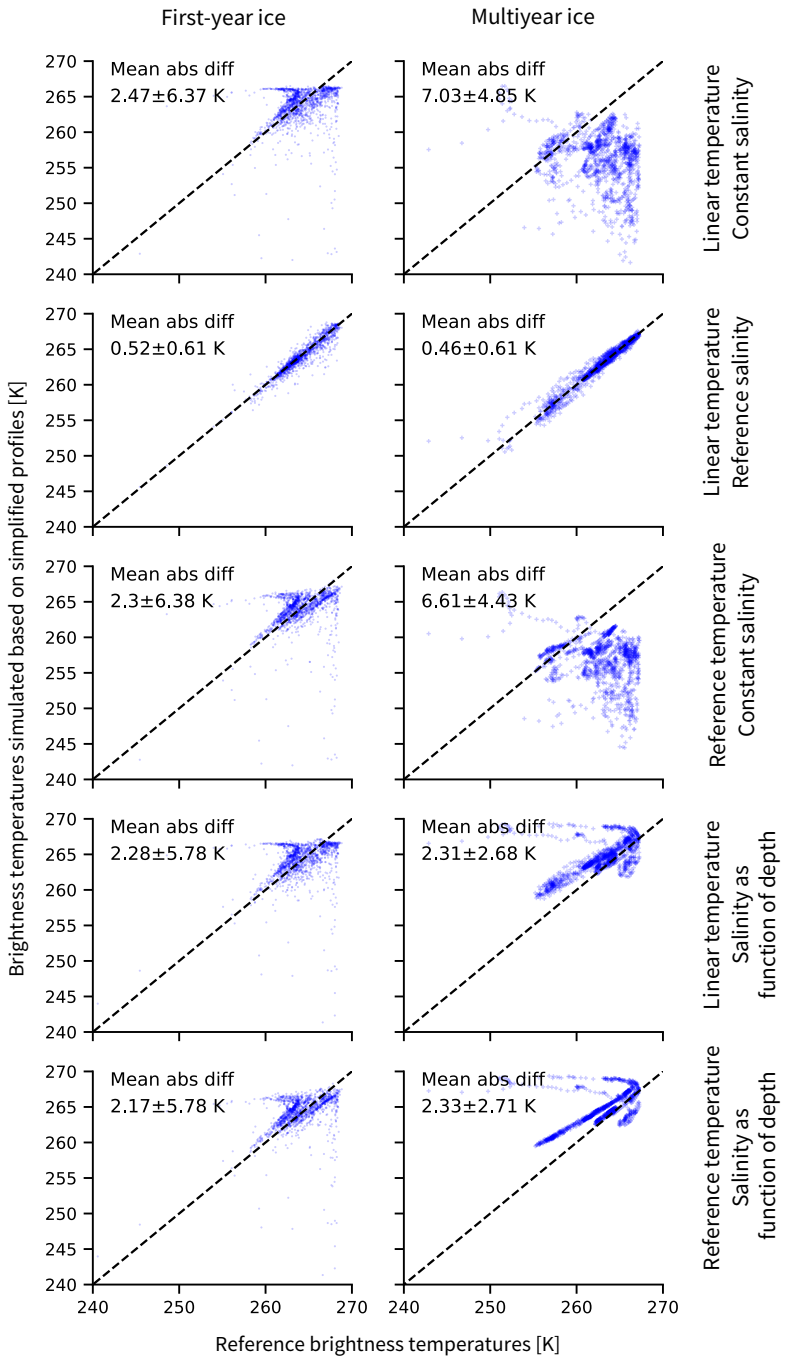

Figure B.5: Brightness temperatures at 6.9 GHz, vertical polarization, simulated based on different simplified profiles as a function of reference brightness temperatures for winter. Left column: first-year ice, right column: multiyear ice. Note that the axes are limited to the range between 240 to 270 K for clarity. The remaining brightness temperatures are scattered between 165 and 240 K and represent around 20% of the simplified data and 8% of the reference data.

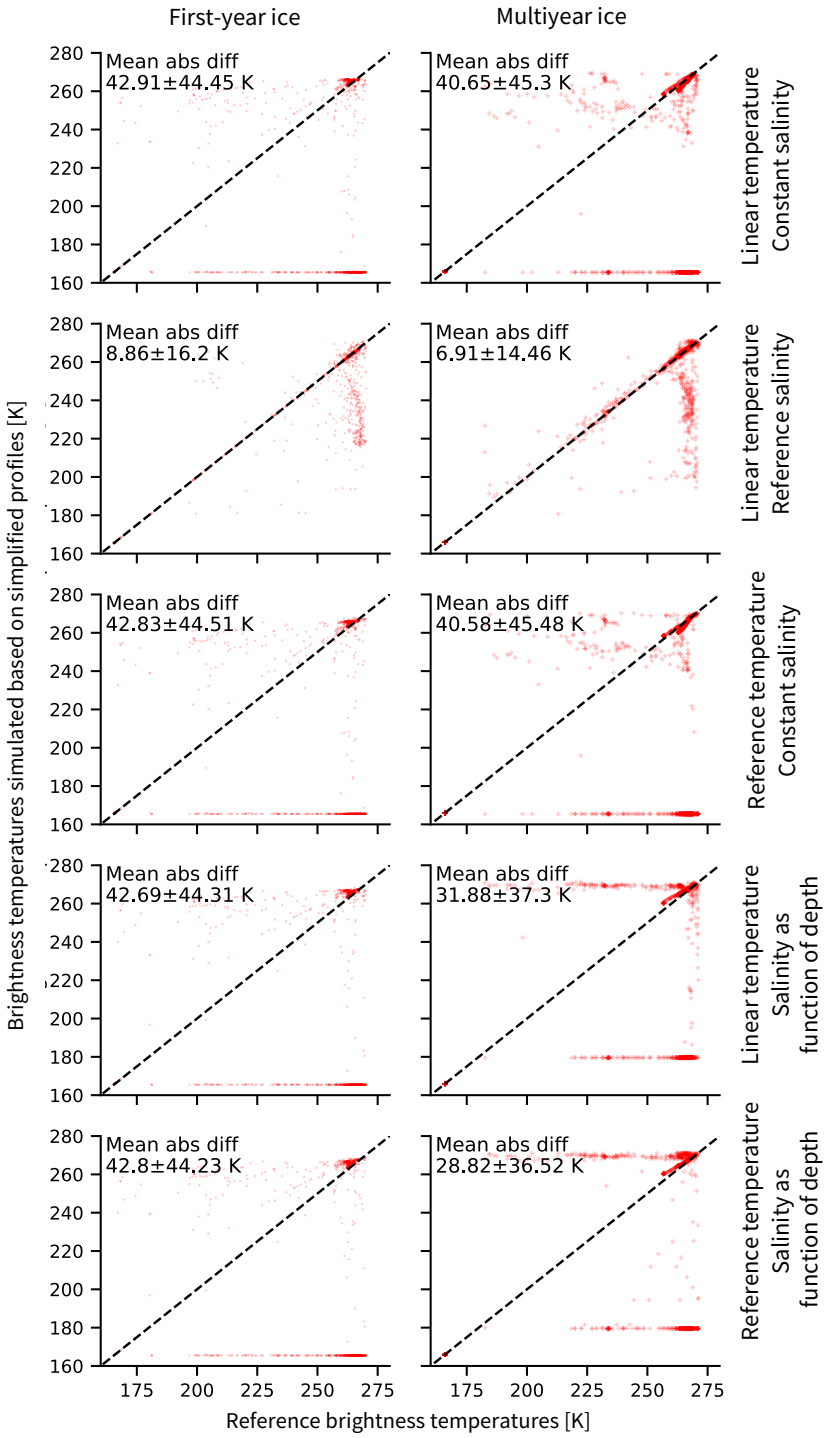

Figure B.6: Brightness temperatures at 6.9 GHz, vertical polarization, simulated based on different simplified profiles as a function of reference brightness temperatures for summer. Left column: first-year ice, right column: multiyear ice.

temperatures and small effects on the spread in summer brightness temperatures (Fig. B.5 and Fig. B.6, second row).

We therefore conclude that the assumption of a linear temperature profile in ice does not introduce large uncertainties in the brightness temperature simulation. The assumption of constant salinity, however, introduces very large uncertainties in summer and smaller but still non-negligible uncertainties for multiyear ice in winter. We therefore explore another simplification approach for salinity profiles in a next step.

B.4.3 Linear Temperature and Salinity as a function of depth

An alternative approach to simplify salinity profiles is a parametrization representing salinity as a function of depth (Griewank and Notz, 2015). This parametrization assumes an L-shaped profile, with low salinity near the surface and a rapidly increasing salinity in the lower ice layers (see Fig. B.4, full lines, and Tab. B.3).

We now simulate the brightness temperature based on the linear temperature profiles and on the salinity profiles as a function of depth (Fig. B.5 and Fig. B.6, fourth row). With a mean absolute difference of 2.28±5.78 K in winter for first-year ice, the uncertainty is comparable to the constant salinity assumption. However, for multiyear ice, the uncertainty is reduced by around two thirds compared to the constant salinity, with a mean absolute difference of 2.31±2.68 K. In summer, the uncertainty is slightly reduced to 31.88±37.30 K for multiyear ice and stays comparable for first-year ice with 42.69±44.31 K. This represents a small improvement but the uncertainty remains too large in summer.

Again, if the brightness temperature is simulated based on reference temperature profiles and on the salinity profiles as a function of depth (Fig. B.5 and Fig. B.6, fifth row), it becomes clear that the assumption in the salinity profiles is the main driver for uncertainties in the brightness temperature simulations. However, using salinity profiles as a function of depth introduces less error than assuming the salinity to be constant throughout depth. We therefore recommend using a linear temperature profile and salinity as a function of depth when simulating brightness temperatures based on GCM output.

The effect of temperature and salinity distribution being clearer now, we turn to another characteristic of GCMs, the limited vertical resolution owing to computational efficiency. Indeed, computing vertical temperature and salinity profiles based on the surface temperature and sea-ice thickness given by a GCM

adds a vertical dimension to a two-dimensional output. This means that the computation time and power needed by an operator applied to a GCM will be much higher than a one-dimensional setup. We therefore investigate the importance of the vertical resolution in a next step.

B.5 THE INFLUENCE OF VERTICAL SPATIAL RESOLUTION

Applying an emission model to a GCM consumes high computation power, as the input profiles must be prepared and the emission model must be applied to many grid cells. In the case of the Arctic Ocean at the MPI-ESM low atmospheric resolution of 1.9°, this would mean for example ≈ 4000 data points per timestep. As ocean components in GCMs often have higher horizontal resolution than the atmosphere, this would mean even more computation power needed when using oceanic variables. Reducing the number of layers for the brightness temperature simulation is a possible aspect to reduce the computation time. This is the issue we explore in the following.

The simplified profiles used for sensitivity experiments in Sec. B.4 are interpolated to the same number of layers as the reference profiles, i.e. a variable number of layers depending on the ice thickness between one and 100 layers. We now run the brightness temperature simulation with the simplified profiles (linear temperature, salinity as a function of depth) interpolated on ten, seven, and three equidistant layers and compare the results to the reference brightness temperatures. We also include the experiment of Sec. B.4 as an indicator for the minimal simplified uncertainty in the comparison. We concentrate on winter months, as we showed that the uncertainty in summer is already very large at high vertical resolution and mainly depends directly on the surface rather than on properties further inside the ice.

Table B.2: Absolute mean difference and standard deviation [K] between simplified brightness temperatures simulated based on profiles interpolated on different number of layers and reference brightness temperatures simulated based on profiles covering 1 to 100 layers, depending on the thickness of the ice. These values only represent winter (October to March).

	3 layers	**7 layers**	**10 layers**	**1 to 100 layers**
First-year ice	2.61±5.82	2.28±5.79	2.26±5.79	2.28±5.78
Multiyear ice	3.04±2.70	2.25±2.69	2.30±2.69	2.31±2.68

We find that there is no substantial difference in uncertainty between the reference simplification between 1 and 100 layers and the interpolation on ten or seven layers, the mean uncertainty varying between 2.26 and 2.28 K for first-year ice and between 2.25 and 2.31 K for multiyear ice (see Tab. B.2). Using three layers, the uncertainty increases slightly by 0.4 K for the former and by 0.7 K for the latter but still remains small. We therefore argue that using as few as seven is as reasonable as 100 layers for the simulation of simplified brightness temperatures.

B.6 The influence of snow and atmosphere

Until now, we concentrated on the influence of sea-ice properties on the simulation of brightness temperatures emitted at the surface of the ice. These simulations included the thermal insulation effect of the snow but did not take into account the refraction effect of the snow cover on the radiation and the path of the radiation through the atmosphere. These are assumed to be small at 6.9 GHz. Nevertheless, it is of interest to quickly investigate the radiative effect of snow cover and atmosphere on the brightness temperature for uncertainty quantification and attribution.

We include the radiative effect of the snow cover in the brightness temperature simulation by using both snow and ice layers of the reference input profiles as input for MEMLS. Except thickness and temperature, all other variables are set to constants (Tab. B.1), as neither SAMSIM nor MPI-ESM compute more details about the snow properties. Especially, we only consider dry snow in this study.

The main driver for the radiative effect of the dry snow cover is its density difference to the ice and atmosphere and its thickness. The density difference between snow and ice on the one hand and between snow and atmosphere on the other hand leads to refraction of the radiation at its boundaries. The snow thickness also has an influence. A linear regression between snow thickness and differences between the simulated brightness temperatures with and without snow layer in winter gives a decrease by 0.13 K for each cm of snow and an intercept of around -1.0 K. This relationship only depends on the snow thickness and the density difference between snow and ice and between snow and atmosphere. It is independent of the snow temperature in our setup. In winter, using both ice and snow layers of the profile leads to a mean effect of -3.15±1.53 K for first-year ice and -4.45±1.28 K for multiyear ice on the brightness temperature compared to only using the ice layers of the profile. Although scattering is limited, the radiative effect of the snow cover hence remains important.

We consider only dry snow here as we do not know anything about the vertical profiles inside the snow from neither MPI-ESM nor SAMSIM. As liquid water and its distribution within the snow strongly affects the brightness temperature, we do not yet have a reliable solution to simulate the sea-ice brightness temperature when covered by wet snow.

We investigate the influence of the atmosphere with a similar approach as the influence of the snow cover. A simple atmospheric radiative transfer model developed by Wentz and Meissner (2000) is applied using the brightness temperatures simulated based on the reference ice and snow input profiles as the lower boundary conditions. The atmospheric effect mainly depends on the columnar liquid and water vapor content, which we again take from the ERA-Interim reanalysis, and on oxygen absorption, included in the radiative transfer model. Assuming a sea-ice concentration of 100%, the absolute mean impact of the atmosphere on the total brightness temperature is between 0.05 and 0.1 K between January and April, around 1 K between May and September and between 0.1 and 0.2 K between October and December.

B.7 Summary and Discussion

B.7.1 Winter brightness temperatures

We showed that in winter, we can reproduce realistic sea-ice surface brightness temperatures using a linear temperature profile and a salinity as a function of depth as input for an emission model. The remaining uncertainty is mainly driven by the assumption made for the salinity distribution inside the ice. These realistic brightness temperatures can be reproduced with similar uncertainty using as few as seven layers. A very high vertical resolution of the ice properties is therefore not needed. The refraction induced by the snow cover affects the brightness temperature, depending on its thickness, by 3 to 5 K. The atmosphere above the ice and snow column is negligible with an effect reaching at most 0.2 K at 100% sea-ice concentration.

This study was motivated by the fact that observational uncertainty could be reduced by the approach of an observational operator. It is however not trivial to evaluate this proposition based on our results. To compare the uncertainty [K] introduced by the brightness temperature simulation to uncertainties [%] introduced by a sea-ice concentration retrieval algorithm, we translate the uncertainty in brightness temperature into uncertainty in sea-ice concentration.

A simple retrieval algorithm to retrieve sea-ice concentration SIC is given by

$$\mathrm{SIC} = \frac{\mathrm{TB} - \mathrm{TB}_w}{\mathrm{TB}_i - \mathrm{TB}_w}, \tag{B.2}$$

with TB the total brightness temperature (ice and open water combined), TB_w a typical open water brightness temperature, and TB_i a typical sea-ice brightness temperature. If we introduce uncertainties ΔSIC and ΔTB in the previous equation, this leads to

$$\mathrm{SIC} + \Delta\mathrm{SIC} = \frac{\mathrm{TB} + \Delta\mathrm{TB} - \mathrm{TB}_w}{\mathrm{TB}_i - \mathrm{TB}_w}, \tag{B.3}$$

resulting in

$$\Delta\mathrm{SIC} = \frac{\Delta\mathrm{TB}}{\mathrm{TB}_i - \mathrm{TB}_w}. \tag{B.4}$$

In our simulated brightness temperatures, TB_i varies around 260 K and TB_w varies around 160 K. An uncertainty of 1 K in brightness temperature therefore approximately translates into 1% of absolute uncertainty in sea-ice concentration. The observational uncertainty of sea-ice concentration in winter is up to 2.5% in consolidated ice and up to 12% for marginal ice zones (Ivanova et al., 2015). The uncertainty of the simulated brightness temperatures translates to a similar range. This might, at first glance, not appear as a solution to drastically reduce the observational uncertainty. However, an observational operator is consistent in time and space and therefore allows a process-understanding of the uncertainties in brightness temperature simulations and, in a possible next step, in retrieval algorithms.

B.7.2 Spring and summer brightness temperatures

In summer, we cannot reproduce realistic sea-ice surface brightness temperatures due to the very high sensitivity of the liquid water fraction to small changes in salinity near 0 °C. We therefore recommend using another approach to simulate summer brightness temperatures. We suggest assuming that the brightness temperature of summer bare ice is similar all over the Arctic, as temperatures are near 0 °C. The surface brightness temperature is a linear combination of the bare ice brightness temperature and the brightness temperature of the melt ponds covering the ice. Therefore, this constant brightness temperature can be combined with open water brightness temperature, weighted by the fraction of melt ponds forming throughout the summer. This approach is simple. We have however not

found any other approach that could come closer to reality as the sensitivities are very high near 0 °C.

Another problematic component when surface temperatures increase in spring and summer is the snow. While the detailed profile of dry snow is not needed as long as its presence is taken into account for the thermal insulation of the ice and for the refraction of the radiation, wet snow has a much higher influence on microwave emission. As in the case of melting snow, very precise information about the snow structure, e.g. wetness distribution, correlation length, and form of snow grains, are needed, we cannot come close to simulate realistic brightness temperatures from GCM output. In our experiments we have ignored this effect by setting the snow wetness to zero at all times. However, for an all-year-round realistic simulation of brightness temperatures, we suggest to exclude data containing melting snow from the brightness temperature simulation.

B.7.3 Outlook

The evaluation framework in this study can be used to explore simulated brightness temperatures at higher frequencies, nearer to the most used operational frequencies. However, snow is a limiting factor in this case. While the radiative effect of the snow cover is small at 6.9 GHz, its impact increases with increasing frequency. It becomes therefore more important to know the snow structure, e.g. snow density, snow temperature, and snow scatterer structure. This information is lacking in GCMs. As the snow structure is more dynamic and changes faster than the ice structure, parametrization for the snow structure do not exist yet to our knowledge. It would be of high interest to explore the evolution of snow on sea ice in more details and perform sensitivity studies to identify possible simplifications. These could eventually lead to realistic brightness temperatures simulated based on GCM output at higher frequencies than 6.9 GHz.

Finally, our analysis focuses on the simulation of brightness temperatures based on output from a GCM which simulates sea ice with a very simple sea-ice model. The use of output from GCMs that simulate sea ice with more complex sea-ice models might yield lower uncertainty in the brightness temperature simulation. However, although these models compute many physical properties inside the ice, they do not necessarily store them for each time step. Using the more complex properties of these models would therefore require one to build the emission model into the model code, instead of applying an "external" operator to already produced model output.

B.8 Conclusions

With the help of a one-dimensional thermodynamic sea-ice model and a one-dimensional emission model, we investigated if realistic sea-ice brightness temperatures can be simulated based on GCM output at a frequency of 6.9 GHz with vertical polarization. We conclude that it is possible to simulate realistic sea-ice brightness temperatures depending on the time of year and the boundary conditions.

We propose the following structure for an observational operator for sea ice at 6.9 GHz, vertical polarization:

- Periods of cold conditions: Use the temperature profile provided by the GCM if existing. Otherwise, use the simulated ice surface temperature to interpolate a linear temperature profile. Use the salinity profile provided by the GCM if existing. Otherwise, interpolate the salinity profile as a function of depth, following the functions given by Griewank and Notz (2015). Apply an emission model, e.g. MEMLS, to these profiles, combined with information about correlation length, sea-ice type, etc. Apply a simple atmospheric radiative transfer model, e.g. Wentz and Meissner (2000), to account for the effect of open water when the sea-ice concentration is below 100% and for the effect of the atmosphere.
- Periods of bare ice near 0 °C: Use a constant brightness temperature for the ice surfaces. Burgard et al. (2019a) derive a summer sea-ice surface brightness temperature of 266.78 from observational estimates. This represents a brightness temperature at the top of the atmosphere of 262.29 K corrected by the mean atmospheric effect of 4.49 K in their simulations. Weight this constant brightness temperature with the melt pond fraction. Apply a simple atmospheric radiative transfer model, e.g. Wentz and Meissner (2000), to account for the effect of open water when the sea-ice concentration is below 100% and for the effect of the atmosphere.
- Periods of melting snow: Ignore these points in the analysis. The GCM output does not provide enough information about the snow properties and wet snow strongly affects the brightness temperature.

The observational operator structure we present here allows us to simulate brightness temperatures from two-dimensional output by a GCM that can be compared with brightness temperatures measured by satellites. This opens new possibilities and perspectives for model-to-observation comparison in the Arctic Ocean.

B.9 Supporting Information to Appendix B

B.9.1 Retrieving sea-ice properties from temperature and salinity

The following formulas were used to compute density and liquid water fraction from temperature and salinity (Notz, 2005)

$$\rho_0 = 916.18 - 0.1403T \tag{B.5}$$

$$S_b = -17.6T - 0.389T^2 - 0.00362T^3 \tag{B.6}$$

$$\rho_w = 1000.3 + 0.78237S_b + 2.8008 \cdot 10^{-4} S_b^2 \tag{B.7}$$

$$\Phi_l = S/S_b \tag{B.8}$$

$$\rho_i = \Phi_l \cdot \rho_w + (1 - \Phi_l) \cdot \rho_0 \tag{B.9}$$

B.9.2 Salinity parametrization as a function of depth

Table B.3: Formulas describing salinity as a function of depth as shown in the full lines in Fig. B.4.

Ice type	**Salinity parametrization as a function of depth z**	**Constants needed**
First-year ice S_{fy}	$\frac{z}{a+bz} + c$	a = 1.0964, b = -1.0552, c = 4.41272
Multiyear ice S_{my}	$\frac{z}{a} + (\frac{z}{b})^{1/c}$	a = 0.17083, b = 0.92762, c = 0.024516
Transition first-year to multiyear ice	$(1-t) * S_{\text{my}}(z) + t * S_{\text{fy}}(z)$	t=0 at start of melt season and t=1 at start of freezing season

C

ARC3O: The Arctic Ocean Observation Operator for 6.9 GHz

Clara Burgard, Dirk Notz, Leif T. Pedersen
and Rasmus T. Tonboe

Abstract

The observational uncertainty in sea-ice-concentration estimates from remotely-sensed passive-microwave brightness temperatures is a challenge for reliable climate model evaluation and initialization. To address this challenge, we introduce a new tool: the Arctic Ocean Observation Operator (ARC3O). ARC3O allows us to simulate brightness temperatures at 6.9 GHz at vertical polarisation from standard output of an Earth System Model. For the evaluation of ARC3O, we simulate brightness temperatures based on three assimilation runs of the MPI Earth System Model (MPI-ESM) assimilated with three different sea-ice concentration products. We then compare these three sets of simulated brightness temperatures to brightness temperatures measured by the Advanced Microwave Scanning Radiometer Earth Observing System (AMSR-E) from space. We find that they differ up to 10 K in the period between October and June, depending on the region and the assimilation run. However, we show that these discrepancies between simulated and observed brightness temperature can be mainly attributed to the underlying observational uncertainty in sea-ice concentration and, to a lesser extent, to the data assimilation process, rather than to biases in ARC3O itself. In summer, the discrepancies between simulated and observed brightness temperatures are larger than in winter and locally reach up to 20 K. This is caused by the very large observational uncertainty in summer sea-ice concentration but also by the melt-pond parametrization in MPI-ESM, which is not necessarily realistic. ARC3O is therefore capable to realistically translate the simulated Arctic Ocean climate state into one observable quantity, which can be used for a more comprehensive climate model evaluation and initialization.

C.1 Introduction

Observational uncertainty in sea-ice concentration affects our understanding of past and future sea-ice evolution as it inhibits reliable climate model evaluation (Notz et al., 2013) and initialization (Bunzel et al., 2016). It also limits our ability to fully exploit relationships between the evolution of sea ice and other climate variables, such as global-mean surface temperature (Niederdrenk and Notz, 2018) and CO_2 emissions (Notz and Stroeve, 2016). To address these issues, we construct an observation operator for the Arctic Ocean at the frequency of 6.9 GHz. This operator opens the possibility for climate model evaluation and initialization directly related to satellite measurements, avoiding the observational uncertainty.

In the case of sea-ice concentration, the observational uncertainty is caused by irreducible physical uncertainty. The brightness temperature measured by passive microwave sensors from satellites is driven by several climate variables. The contribution of the individual drivers cannot be disentangled unambiguously. This leads to uncertainty in the interpretation of the brightness temperature measurements. Nevertheless, a variety of algorithms have been developed to retrieve an estimate of sea-ice concentration from these brightness temperatures, resulting in a range of different sea-ice concentration products, which differ, sometimes substantially (Ivanova et al., 2014). The evaluation of simulated sea-ice concentration in GCMs therefore strongly depends on the choice of the sea-ice concentration product against which a simulation is evaluated (Notz et al., 2013).

Observation operators applied to general circulation model (GCM) output have been suggested as a solution to circumvent observational uncertainty for other climate variables (Flato et al., 2013; Eyring et al., 2019). An observation operator enables us to simulate brightness temperatures based on output from a GCM. This simulated brightness temperature can then be evaluated against the observed brightness temperatures. Uncertainty in the evaluation can therefore only be induced by uncertainties in the observation operator. We argue that the simulated brightness temperature based on a GCM is a more consistent method less prone to uncertainty than the use of retrieval algorithms because the GCM provides an internally consistent climate state over time and space. Additionally, the climate system as a whole can be evaluated with this approach and not only individual variables.

However, the simulation of sea-ice brightness temperatures relies on sea-ice properties not explicitly resolved in MPI-ESM. In particular, brightness temperatures are driven by the vertical liquid water (or brine) distribution inside

the ice and snow, which is driven by temperature and salinity profiles. However, Burgard et al. (2019b) showed in a one-dimensional idealized setup that, using a few simple assumptions, the low complexity of GCM output is sufficient to simulate reasonable sea-ice brightness temperatures at 6.9 GHz at vertical polarization. While we focus on the frequency of 6.9 GHz in this study, the framework proposed here, together with the framework presented in Burgard et al. (2019b), can be extended to investigate the simulation of brightness temperatures at other frequencies in the future as well.

In this study, we first present an Arctic Ocean observation operator that we construct based on the suggestions from Burgard et al. (2019b). We then evaluate the brightness temperatures simulated based on assimilation runs against brightness temperatures observed by satellites and investigate potential uncertainty sources in the brightness temperature simulation.

C.2 The Max Planck Institute Earth System Model

As a baseline for the development of an Arctic Ocean observation operator, we use the Max Planck Institute Earth System Model (MPI-ESM). It is a state-of-the-art Earth System Model that contributed to the Coupled Model Intercomparison Project in its fifth phase (Taylor et al., 2012) and will contribute to its sixth phase (Eyring et al., 2016). We use its low resolution configuration (MPI-ESM-LR).

The atmosphere component, ECHAM6 (Stevens et al., 2013), has a horizontal resolution of T63 (~1.9° x 1.9°) and a vertical division into 47 levels between surface and 0.01 hPa. The ocean component, MPIOM (Jungclaus et al., 2013), is based on a curvilinear grid with two poles located in South Greenland and Antarctica. The horizontal resolution ranges from 15 km near Greenland to 185 km in the tropical Pacific. Vertically, the ocean is divided into 40 levels between surface and bottom. The sea ice is simulated within MPIOM by a dynamic/thermodynamic sea-ice model based on Hibler (1979). In this simple setup, the sea-ice salinity is kept constant at 5 g/kg, and the ice bottom temperature is kept constant at -1.8 °C. There is no explicit simulation of the ice thickness distribution. Still, the simulation of the mean state and variability of Arctic sea ice is realistic (Notz et al., 2013).

For our observation operator, we use output from the atmosphere component ECHAM6. The sea-ice properties, like sea-ice concentration, sea-ice thickness and snow thickness, are computed within the ocean component and communicated to the atmosphere component through coupling on a daily frequency (Jungclaus et al., 2013). Based on these properties, ECHAM6 computes the snow cover fraction

and the melt pond coverage (Giorgetta et al., 2013), which are needed for a comprehensive assessment of the radiative properties of the surface. Additionally, ECHAM6 provides the atmospheric water and ice content, which are needed for the calculation of the radiation path through the atmosphere (see Sec. C.3.2). ECHAM6 therefore provides all variables needed for the simulation of Arctic Ocean brightness temperatures.

C.3 The Arctic Ocean Observation Operator ARC3O

The purpose of the ARCtic Ocean Observation Operator for 6.9 GHz (ARC3O) is to simulate Arctic Ocean brightness temperatures as could be seen at the top of the atmosphere by a theoretical satellite flying around the model. This brightness temperature is a result of radiation emitted by the surface, upwelling atmospheric radiation, reflected downwelling atmospheric radiation, atmospheric transmission, and reflected space radiation (Swift and Cavalieri, 1985).

As a consequence, ARC3O is based on two parts. In the first part, an emission model computes the sea-ice surface brightness temperature (see Sec. C.3.1). In the second part, an atmospheric radiative transfer model combines the sea-ice surface emission with ocean emission and atmospheric emission and transmission (see Sec. C.3.2). The workflow of ARC3O follows five steps (see Fig. C.1), which we explain in the following.

C.3.1 The contribution of the sea-ice surface to the brightness temperature

The brightness temperature emitted at the sea-ice surface at 6.9 GHz, vertical polarization, is mainly driven by the vertical distribution of the brine volume fraction inside the ice, which principally depends on the temperature and salinity profile. However, MPI-ESM does not provide temperature and salinity profiles. To circumvent this lack of information, we follow the suggestion of Burgard et al. (2019b) to simplify the sea-ice properties, based on the climatic boundary conditions.

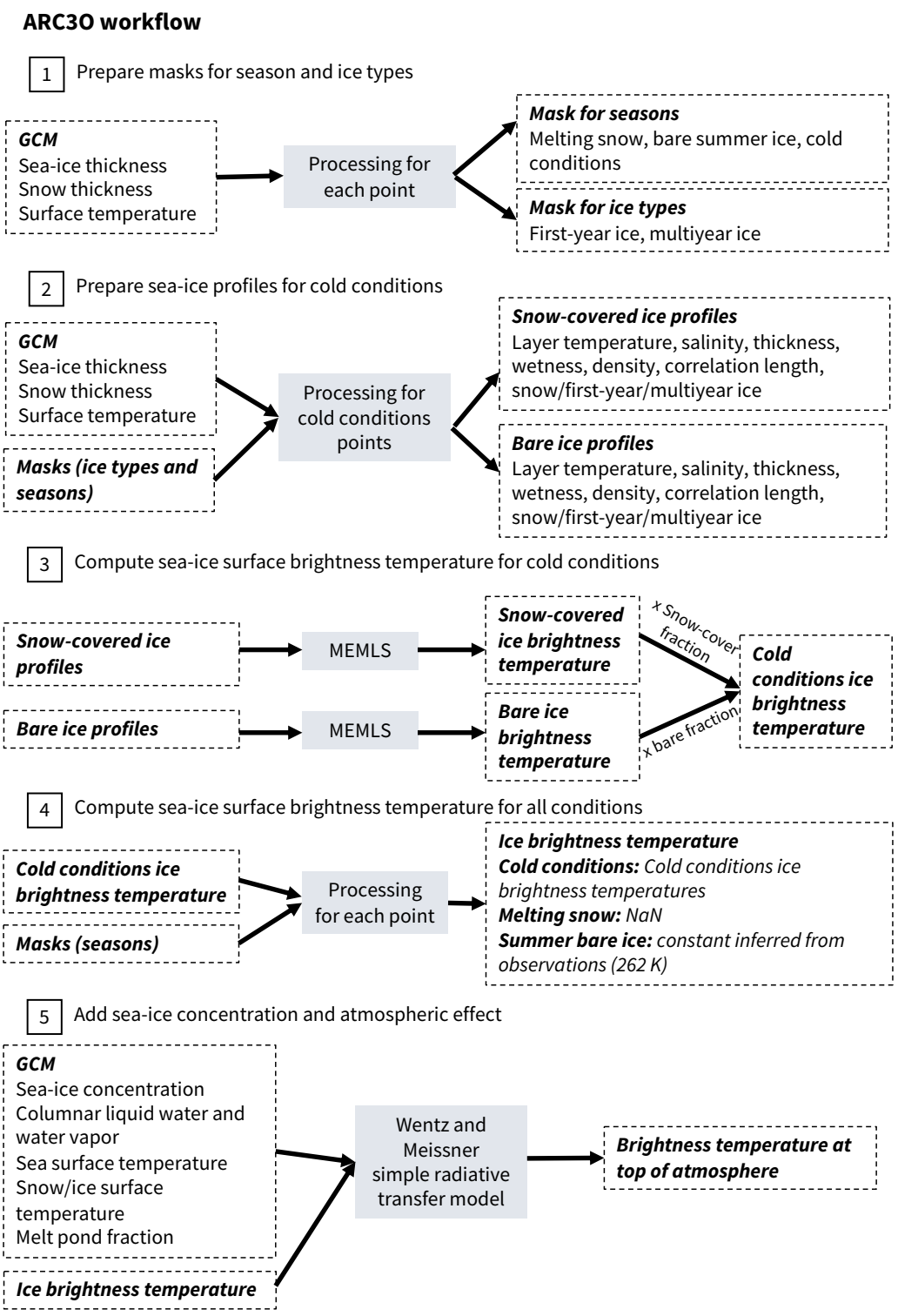

Figure C.1: Workflow of the Arctic Ocean Observation Operator ARC3O.

C.3.1.1 IDENTIFYING DIFFERENT PERIODS AND ICE TYPES

Burgard et al. (2019b) showed that the simulation of sea-ice surface brightness temperatures relies on different assumptions, depending on the conditions of the ice. A year can be divided into three type of periods: periods of cold conditions, periods of melting snow, and periods of bare ice near 0 °C. Additionally, sea-ice brightness temperatures depend on the ice type, i.e whether the ice is first-year or multiyear ice.

We therefore flag the different type of periods and different ice types based on the sea-ice properties given by the MPI-ESM output (Step 1 in Fig C.1) . Grid cells containing melting snow are flagged as "melting snow periods", grid cells containing bare ice in July, August and September are flagged as "bare ice near 0°C", and the remaining grid cells are flagged as "cold conditions". To flag the different grid cells as "first-year ice", "multiyear ice" and "open water only", we consider the ice thickness evolution. If the ice thickness is zero, the ice type is set to "open water only", if the ice thickness is larger than zero but there has been at least one "open water only" timestep in the year preceding the timestep evaluated, the ice type is set to "first-year ice". If none of the two before apply, the ice type is set to "multiyear ice".

C.3.1.2 COLD CONDITIONS

In periods of cold conditions, Burgard et al. (2019b) showed that the sea-ice surface brightness temperature can be simulated with low uncertainty using a linear vertical temperature profile and a function of depth for the salinity interpolated to less than ten layers. We therefore construct profiles (Step 2 in Fig C.1), divided into eleven layers, namely ten layers of ice and one layer of snow. The ice layers are equidistant, based on the ice thickness given by MPI-ESM, and the snow layer thickness is equal to the snow thickness given by MPI-ESM.

We construct temperature profiles based on the ice surface temperature given by MPI-ESM, which represents the temperature at the top of the snow and ice column. For each grid cell, we construct two sets of profiles. One set of profiles interprets the surface temperature as the snow surface temperature. This profile is a combination of two linear profiles, one in the snow, defined by the snow thermal conductivity, and one in the ice, defined by the ice thermal conductivity (see formula in Sec. C.6.1 of the Supp. Info.). The other set of profiles interprets the surface temperature as the ice surface temperature and is a linear profile between surface and bottom temperature. The ice bottom temperature is taken as constant at -1.8 °C in both cases.

The salinity is taken as a function of depth, as formulated by Griewank and Notz (2015). The salinity is defined as follows for first-year ice:

$$S_{fy}(z) = \frac{z}{a + b\,z} + c \tag{C.1}$$

with a = 1.0964, b = -1.0552 and c = 4.41272
and as follows for multiyear ice:

$$S_{my}(z) = \frac{z}{a} + (\frac{z}{b})^{1/c} \tag{C.2}$$

with a = 0.17083, b = 0.92762 and c = 0.024516.
We set the snow salinity to zero. Note, however, that the validity of this assumption is slightly uncertain as the lowest layer of the snow can be saline, especially above first-year ice (Barber et al., 1998; Shokr and Sinha, 2015a), enabling the presence of liquid water at the base of the snow.

The vertical profile of the ice density ρ_i is computed based on the temperature and salinity profiles, with the following formula (Notz, 2005):

$$\rho_i = \Phi_l \cdot \rho_w + (1 - \Phi_l) \cdot \rho_0 \tag{C.3}$$

with the pure ice density $\rho_0 = 916.18 - 0.1403T$, the brine salinity $S_b = -17.6T - 0.389T^2 - 0.00362T^3$, the density of seawater $\rho_w = 1000.3 + 0.78237S_b + 2.8008 \cdot 10^{-4} S_b^2$, and the liquid water fraction $\Phi_l = S/S_b$. The snow density is set to 300 kg/m^3 (Giorgetta et al., 2013).

The vertical profile of the correlation length, a measure for the scatterer size (snow particles, brine inclusions, air bubbles), depends on the ice type. The correlation length is set to 0.35 mm in the upper 20 cm of first-year ice and to 0.25 mm in the lower layers (Tonboe, 2010). For multi-year ice, it is set to 1.5 mm (Burgard et al., 2019b). The correlation length of snow is set to 0.15 mm (Tonboe, 2010).

The sea-ice surface brightness temperature is simulated based on the temperature, salinity, density, thickness, and correlation length profiles described above. A slightly modified version of the Microwave Emission Model for Layered Snowpacks (MEMLS, Wiesmann and Mätzler, 1998) extended for sea ice (Tonboe et al., 2006) is used for the brightness temperature simulation. It relates the snow and ice properties to emission, absorption and scattering of the microwave radiation in each layer. Hence, MEMLS simulates the path of the radiation through the ice and snow from bottom to top, resulting in a brightness temperature emitted at the surface.

To take the snow cover fraction at the surface into account, two sea-ice surface brightness temperatures are simulated for each grid cell. One set of brightness temperatures is simulated using the temperature profiles divided between snow and ice, and the other set using the temperature profiles linear between surface and bottom temperature (Step 3 in Fig C.1). These surface brightness temperatures are then weighted by the snow cover fraction given by MPI-ESM, to result in a mean sea-ice surface brightness temperature.

C.3.1.3 Melting snow

In spring, temperatures increase across the Arctic Ocean, leading to the melting of the snow covering the sea ice. Wet snow strongly affects the emitted microwave radiation. This effect mainly depends on the water content of the snow, on the density and on the size and form of the snow particles (Chang and Gloersen, 1975; Ulaby et al., 1986; Shokr and Sinha, 2015a). Due to the high wetness, the melting snow brightness temperature can decrease towards the brightness temperature of open water. However, it also leads to a warming of the layer emitting the radiation, hence leading to an increase in brightness temperature. The net effect of the snow wetness on the microwave brightness temperature is therefore not necessarily clear (Shokr and Sinha, 2015a) and needs precise information to be simulated accurately. As we do not have the necessary information about the snow properties in MPI-ESM, we cannot simulate the sea-ice surface brightness temperature reliably in this period and mask out these grid cells.

C.3.1.4 Summer bare ice near 0 °C

In summer, after the snow has fully melted away, the salinity profile inside the ice cannot necessarily be represented by a simple function of depth. As surface temperatures are close to 0°C, the liquid water fraction at the ice surface increases and melt ponds form. Above a surface liquid water fraction of 0.2 on, the brightness temperature is proportional to the surface liquid water fraction (Burgard et al., 2019b). We suggest that liquid water fractions above 0.2 can be interpreted as a measure for the melt-pond fraction. For these warm conditions, Burgard et al. (2019b) showed that we do not currently have a valid simplification for temperature and salinity profiles. They therefore suggest a very simple approach: at these temperatures, the ice surface which is not covered by melt ponds is assumed to have a similar surface temperature and composition over the whole Arctic, resulting in a similar surface brightness temperature.

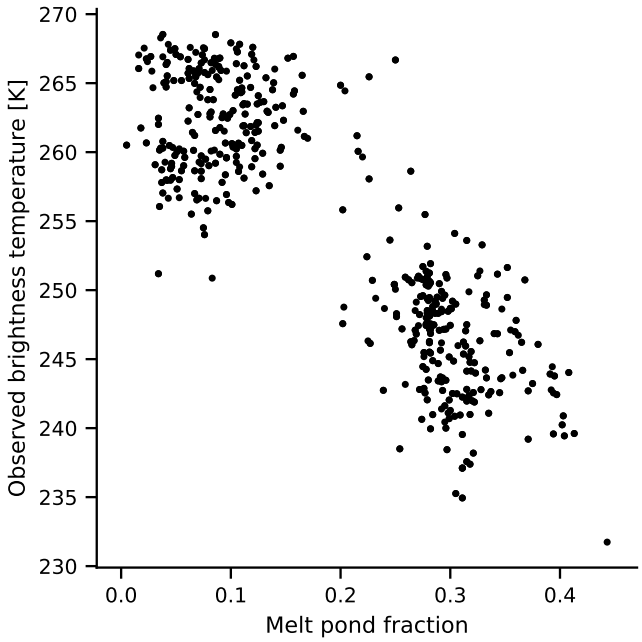

Figure C.2: Brightness temperatures measured from AMSR2 against melt pond fraction for different points represented in the Round Robin Data Package from May to mid-August 2011.

To find a surface brightness temperature representing the sea-ice surface in summer, we use the observational dataset Round Robin Data Package (RRDP, Pedersen et al., 2018) developed as part of the European Space Agency (ESA) sea-ice Climate Change Initiative (SICCI). These data cover the period from May to mid-August 2011. The RRDP contains sea-ice data measured in-situ by plane and ice-mass buoys. These in-situ measurements are collocated with microwave brightness temperatures between 6 and 89 GHz measured by the Advanced Microwave Scanning Radiometer 2 (AMSR2) and with the melt-pond fraction product by Istomina et al. (2015b). Using the combination of the melt-pond fraction and the observed brightness temperatures, we can infer the summer brightness temperature of melt-pond-free sea ice (Fig. C.2). We do so by taking the mean brightness temperature for melt-pond fractions between zero and 0.2, as Burgard et al. (2019b) showed that below a liquid water fraction of 0.2, the brightness temperature is not driven only by the surface properties of the ice. This method results in a summer brightness temperature of 262.29±3.56 K.

As this is the brightness temperature measured at the top of the atmosphere, we add an atmospheric correction of 4.49 K. We run ARC3O once on the MPI-ESM output presented in Sec. C.4.2 to infer this correction, which is the mean atmospheric effect in regions covered by 99% of ice or more in summer. Adding the

atmospheric correction, we therefore use a constant brightness temperature of 266.78 K as a constant brightness temperature representing the radiation emitted at the summer bare ice surface. This bare ice surface is then combined with open water brightness temperatures, weighted by the melt-pond fraction, to obtain the comprehensive summer sea-ice brightness temperature (see Sec. C.3.2).

C.3.2 The contribution of ocean and atmosphere to the brightness temperature

The sea-ice surface brightness temperature is set for each grid cell depending on the three periods presented above (Step 4 in Fig. C.1). As the Arctic Ocean is not covered by 100% of sea ice, the brightness temperature of the surface also depends on the open water surface brightness temperature. Additionally, to simulate the radiation reaching the top of the atmosphere, the atmospheric contribution has to be added to the surface brightness temperature. We use a geophysical model developed by Wentz and Meissner (2000) to take into account the oceanic and atmospheric contributions (Step 5 in Fig. C.1).

The total brightness temperature of an Arctic Ocean grid cell is computed with this model as a combination of the upwelling atmosphere emission, the upwelling surface emission by ocean, sea ice, and melt ponds, the atmospheric transmittance, the atmospheric emission reflected by the different types of surface, and the reflected background radiation from space. The ocean surface brightness temperature is computed as a function of surface temperature, surface salinity, and wind speed. The melt-pond brightness temperature is computed similarly to the ocean brightness temperature, but setting salinity and wind speed to zero. Finally, as the atmosphere is mostly transparent to radiation in the low microwave range, the radiative transfer through the atmosphere is computed based only on the columnar water vapor and columnar cloud liquid water.

C.4 Evaluation of ARC3O

The approach we use to construct ARC3O was proposed by Burgard et al. (2019b), based on an idealized one-dimensional setup that did not involve actual observations. In the following, we evaluate our simulated Arctic Ocean brightness temperatures against brightness temperatures measured by satellites.

We do so by comparing brightness temperatures simulated by ARC3O based on MPI-ESM output from assimilation experiments, i.e. experiments where the model is regularly nudged towards observations. Hence, we expect the simulated climate system to be close to reality and the simulated brightness temperature to be close to the observed brightness temperature.

However, the observations used in the data assimilation are reanalysis data for the atmosphere and ocean and retrieved sea-ice concentration products for the sea ice. They are therefore not direct observations but already-processed products prone to differences to reality. Additionally, in the assimilation process, MPI-ESM is nudged towards observations but some characteristic features inherent to the mean model state might remain. The uncertainty of the observed brightness temperature itself is considered to be small and thus neglected here. Hence, differences between observed and simulated brightness temperature can arise from three sources: (1) the difference between real and retrieved climate state due to the difference between retrieval algorithms or reanalysis and the real climate state, (2) the difference between the assimilated climate state and the retrieved or reanalysis product, and (3) biases in ARC3O (Fig. C.3). In the following, we try to quantify how the first two uncertainty sources contribute to differences between the simulated and observed brightness temperatures. Any remaining biases can then be attributed to biases of ARC3O itself.

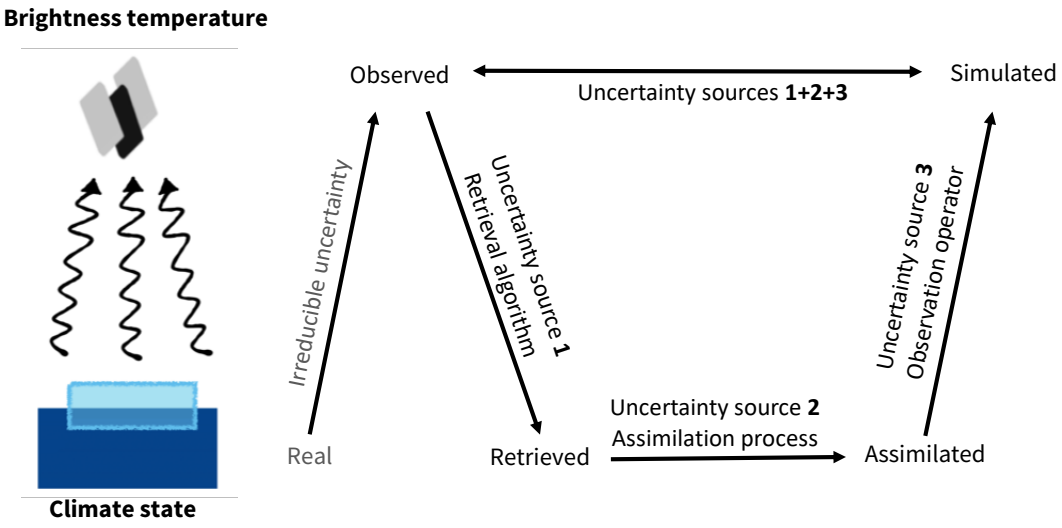

Figure C.3: Uncertainty sources possibly introducing differences between simulated and observed brightness temperature.

C.4.1 Observation data

As observed brightness temperatures, we use Calibrated Passive Microwave Daily EASE-Grid 2.0 (CETB) brightness temperatures processed as part of the NASA Making Earth System Data Records for Use in Research Environments (MEaSUREs) program (Brodzik et al., 2016, Updated 2018). They are an improved, enhanced-resolution, gridded passive microwave Earth System Data Record (ESDR) for monitoring cryospheric and hydrologic time series from the measurement devices Scanning Multi-channel Microwave Radiometer (SMMR), Special Sensor Microwave Imager/Sounder (SSM/I-SSMIS) and Advanced Microwave Scanning Radiometer - Earth Observing System (AMSR-E). These data cover the period between 1978 and 2017 and are provided on a 25 km x 25 km grid. For the comparison with MPI-ESM data, we focus on the period from 2002 to 2008 and interpolate the observations bilinearly to the model grid. Again, we concentrate on the frequency of 6.9 GHz, vertical polarization. At this frequency and this time period, the observations stem from AMSR-E.

C.4.2 Model data

We use model data from assimilation runs, as they are nudged towards the observed climate state and are therefore expected to be a reasonable estimate of the real climate state in the model. Differences between simulated and observed brightness temperatures should therefore be small and can be attributed to the three uncertainty sources presented before. To examine the impact of the choice in retrieval product, we use three assimilation runs based on three different sea-ice concentration products. The atmosphere and the ocean component are assimilated in the same way in all three cases.

The assimilation experiments cover the period from 2002 to 2008 and were conducted by Bunzel et al. (2016). The assimilation technique used was Newtonian relaxation, also called nudging. Atmospheric, oceanic and sea-ice properties were nudged into the model using full-field data assimilation in all atmospheric and oceanic levels. In the atmosphere, vorticity, divergence, temperature, and surface pressure were nudged into the model with a relaxation time of one day, while salinity and temperature in the ocean were nudged with a relaxation time of ten days. For the assimilation of atmospheric quantities, the ERA-Interim dataset (Dee et al., 2011) was used, while the ocean was nudged toward Ocean Reanalysis System 4 data (Balmaseda et al., 2013).

For sea ice, only sea-ice concentration was assimilated. The three different sea-ice concentration products are the ESA SICCI Version 2 (SICCI2) dataset (Lavergne et al., 2019) as a 50-km-gridded product, the NASA Team dataset (Cavalieri et al., 1996) and the Bootstrap dataset (Comiso, 2000), both as 25-km-gridded products. We choose these datasets because SICCI2 is a new algorithm combining several existing algorithms with the goal of improving the retrieved sea-ice concentration product, Bootstrap sea-ice concentrations are in the upper range of retrieved sea-ice concentrations, and NASA Team sea-ice concentrations are in the lower range (Ivanova et al., 2014). The data were interpolated bilinearly to the model grid before assimilation. In grid boxes containing missing values, e.g. the polar observation hole, no assimilation was applied. The sea ice was then exclusively calculated by the model. The relaxation time was 20 days. Relaxation times differ among the model components to account for the different response times of the components. In order to allow for a realistic relation between ice concentration and thickness, sea-ice thickness was updated in the model proportionally to ice concentration nudging (Tietsche et al., 2013).

C.4.3 Cold seasons (JFM, AMJ, OND)

C.4.3.1 Comparison between simulated and observed brightness temperatures

The first comparison between simulated and brightness temperatures clearly showed a positive bias over the whole Arctic Ocean in the simulated brightness temperatures (Fig. C.10, left, in Supp. Info.). The brightness temperature is defined as the product of the emissivity and the physical temperature of the emitting part of the ice (Ulaby et al., 1986). A comparison of the simulated emissivities with emissivities derived from observational data from the RRDP showed that ARC3O systematically overestimates the emissivity. It is however not straightforward to find where the bias is produced in the emission model. We therefore chose to correct the bias by multiplying the inherent sea-ice emissivity by a tuning coefficient at the end of step 3 of the ARC3O workflow (see Fig. C.1). The coefficient which yields the best agreement with observations is 0.968 (Fig. C.10, right, in Supp. Info.). More information about the tuning process is found in Supp. Info. C.6.2. In the following, we discuss brightness temperatures simulated with this tuning procedure.

The three different sets of simulated brightness temperatures show largely similar behaviours in the cold seasons winter (January/February/March, JFM), spring

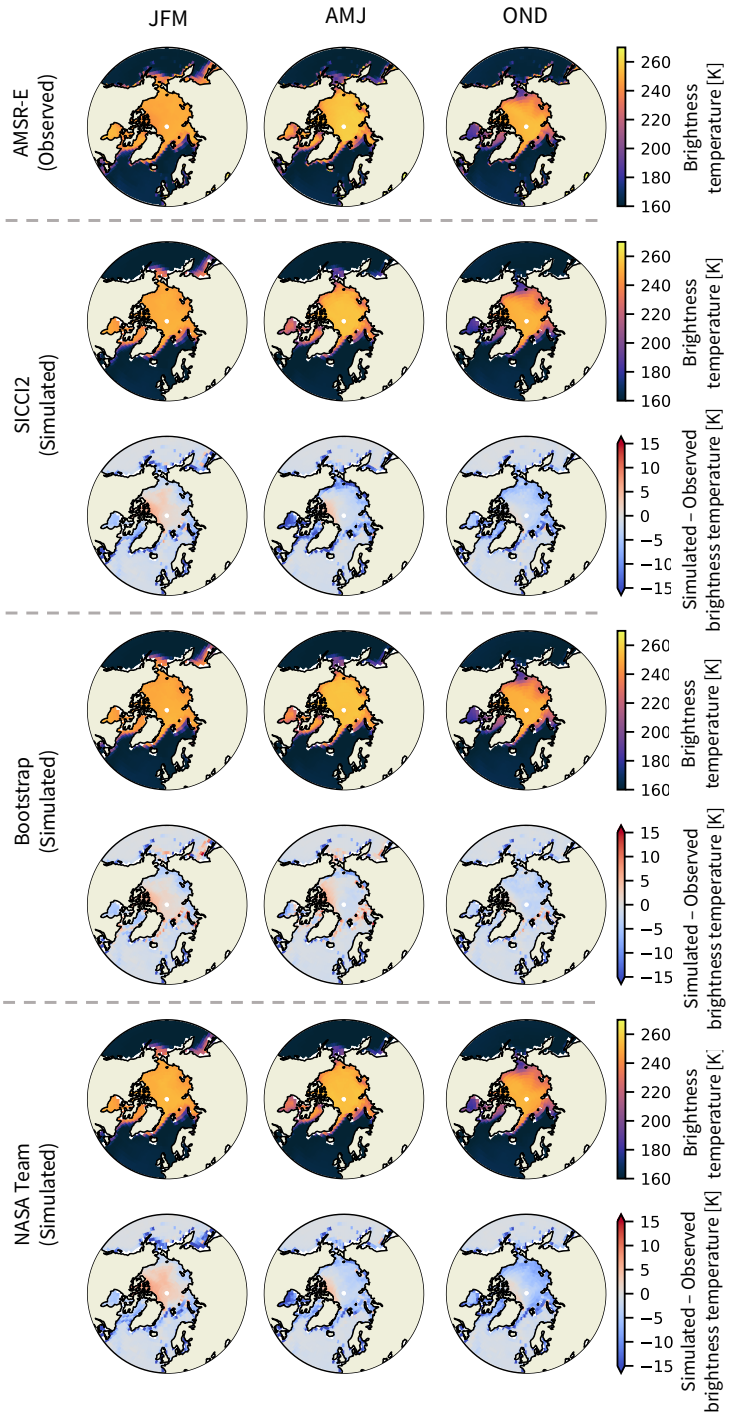

Figure C.4: Observed brightness temperatures by AMSR-E (1st row). Brightness temperatures simulated with ARC3O from MPI-ESM output assimilated with SICCI2 (2nd row), Bootstrap (4th row) and NASA Team (6th row) sea-ice concentration and difference to observations (3rd, 5th and 7th row respectively). The columns stand for the three cold seasons: JFM, AMJ, OND. Summer (JAS) is discussed in Sec. C.4.4.

(April/May/June, AMJ), and autumn (October/November/December, OND) (Fig. C.4). Overall, differences between simulated and observed brightness temperatures are very small and are generally lower than 10 K. The pattern of differences appears to be similar across seasons. The simulated brightness temperatures are slightly higher than the observed ones in regions of high sea-ice concentration and thickness, e.g. north of the Canadian Archipelago and the Central Arctic in winter. In contrast, they are lower than the observed ones in regions of low sea-ice concentration and thickness, e.g. in the marginal zones such as the Barents Sea, the Pacific sector, and the Hudson Bay.

The overestimation on the order of 2 to 4 K in the Central Arctic in winter has a similar pattern in all three sets of simulated brightness temperatures. Otherwise, brightness temperatures based on the Bootstrap assimilation run are very close to the observed ones, with differences to the observations of usually less than 3 K. Only a few individual points in the Atlantic sector show larger biases. Brightness temperatures based on the NASA Team and SICCI2 assimilation run show stronger differences to observations. The simulated brightness temperatures are up to 10 K lower than the observations in the North Pacific in winter and up to 15 K lower than the observations in the Hudson Bay in spring. In the Central Arctic and the Atlantic Sector, the NASA Team brightness temperatures are 2 to 5 K lower than observations in spring and 5 to 10 K lower than observations in autumn. The pattern of differences between SICCI2 brightness temperatures and observations is similar to the pattern of differences between NASA Team brightness temperatures and observations but the SICCI2 brightness temperatures are about 2 K higher than the NASA Team brightness temperatures.

C.4.3.2 Investigating uncertainty sources

The total difference Δ_{tot} between simulated and observed brightness temperatures is a consequence of the difference between real and retrieved climate state Δ_{retriev}, of the difference between retrieved and simulated climate state Δ_{assim}, and of biases in the brightness temperature simulation by ARC3O Δ_{ARC3O} (Fig. C.3):

$$\Delta_{\text{tot}} = \Delta_{\text{retriev}} + \Delta_{\text{assim}} + \Delta_{\text{ARC3O}} \tag{C.4}$$

We set out to investigate Δ_{assim} and Δ_{retriev} to gain an estimate of Δ_{ARC3O}.

In a first step, we investigate the influence to which drivers the brightness temperature is particularly sensitive. In the cold seasons, the most important

drivers are the sea-ice concentration, sea-ice thickness, snow thickness, and surface temperature.

We examine the sensitivity for the month of October, representing the beginning of the freezing period, and for the month of March, representing the end of the freezing period. We use only one of the assimilation runs, the SICCI2 run, as we assume that the physical relationships linking the different variables are the same in all three assimilation runs. For both October and March, we compute, for each grid cell and each variable, the anomaly to the time mean. By taking the standard deviation of these anomalies, we have a representation of the variability of the given variable in the grid cell (Fig. C.11 in Supp. Info.).

Table C.1: Sensitivity of the simulated brightness temperature to different input variables. We show the 5th and 95th percentile of the difference between modulated and reference brightness temperature and the 5th and 95th percentile of the modulating variable. The latter range is computed as the standard deviation of the anomaly to the time mean in each grid cell. Straight font represents the sensitivity to the increase in the variable, italic font represents the sensitivity to the decrease.

	Range of difference in brightness temperature	**Range of variability**
March		
Snow thickness	0.02 to 0.98 K *-1.39 to -0.04 K*	±0.7 to 11 cm
Sea-ice thickness	-0.88 to -0.09 K *-0.13±1.02 K*	±7 to 43 cm
Sea-ice concentration	0.33 to 17.84 K *-18.65 to -0.56 K*	±0.05 to 26 %
Surface temperature	0.14 to 3.24 K *-3.38±-0.16 K*	±3.31 to 7.97 K
October		
Snow thickness	0.06 to 0.43 K *-0.66 to 0.10 K*	±0.1 to 7 cm
Sea-ice thickness	-0.49 to -0.12 K *-0.12±0.54 K*	±8 to 52 cm
Sea-ice concentration	1.14 to 16.51 K *-25.98 to -1.34 K*	±1 to 36 %
Surface temperature	0.80 to 2.00 K *-2.03±-0.87 K*	±2.84 to 6.38 K

With these variability fields, we conduct sensitivity studies for each variable of interest. For both October and March, we conduct two sets of experiments per variable of interest, one in which we add the variability field and one in which we

subtract the variability field. The main message emerging from the results is that the sea-ice concentration variability is the main driver for variations in the brightness temperature (Tab. C.1) changing it by up to ≈ 25 K, while the variability in other variables affects the brightness temperature only up to ≈ 3 K. Spatially, the sea-ice concentration is the main driver for variability in regions not completely covered by ice (Fig. C.5). In regions covered by near to 100% of ice, the surface temperature has the highest effect on the brightness temperature. Sea-ice thickness and snow thickness do not play an important role for uncertainties in the total brightness temperature of a grid cell as their mean absolute contribution to the brightness temperature variability is on the order of 1 K. To understand the total uncertainty Δ_{tot}, we therefore need to focus on two variables: the sea-ice concentration and the surface temperature.

In a next step, we investigate the influence of Δ_{assim} on Δ_{tot}. The goal of a data assimilation is to reach a simulated climate state close to reality. During the data assimilation process, the model is nudged towards three distinct observational datasets: an ocean reanalysis, an atmosphere reanalysis, and a sea-ice concentration product, which are not necessarily consistent with each other. Hence, discrepancies can arise between the variables before and after the assimilation. This is the case for example when a non-zero sea-ice concentration is assimilated at one point but the ocean temperature is too warm to sustain the ice at that point and the ice directly melts away.

As the sea-ice concentration is the main driver for uncertainties in the brightness temperature simulation, we here focus on the effect of the data assimilation on the sea-ice concentration in the three different assimilation runs. This effect is mostly visible in the marginal regions (Fig. C.6) and is of similar magnitude for all three sea-ice concentration datasets. At the ice edge, the differences are highest, on the order of 5 %. As a rule of thumb, differences of 1% in sea-ice concentration are equivalent to differences of 1 K in brightness temperatures (see Burgard et al., 2019b), so the differences in sea-ice concentration are roughly equivalent to resulting differences in brightness temperature of around 5 K. Δ_{assim} can therefore account for a large part of the total difference between simulated and observed brightness temperature Δ_{tot} in the ice edge region (see Fig. C.4).

Unfortunately, the difference between real and retrieved sea-ice concentration Δ_{retriev} cannot be as robustly quantified as Δ_{assim}. In-situ observations for a robust evaluation of the retrieved sea-ice concentration products are largely lacking. This inhibits the evaluation of the products against reality. The effect of Δ_{retriev} and Δ_{ARC3O} can therefore not clearly be disentangled.

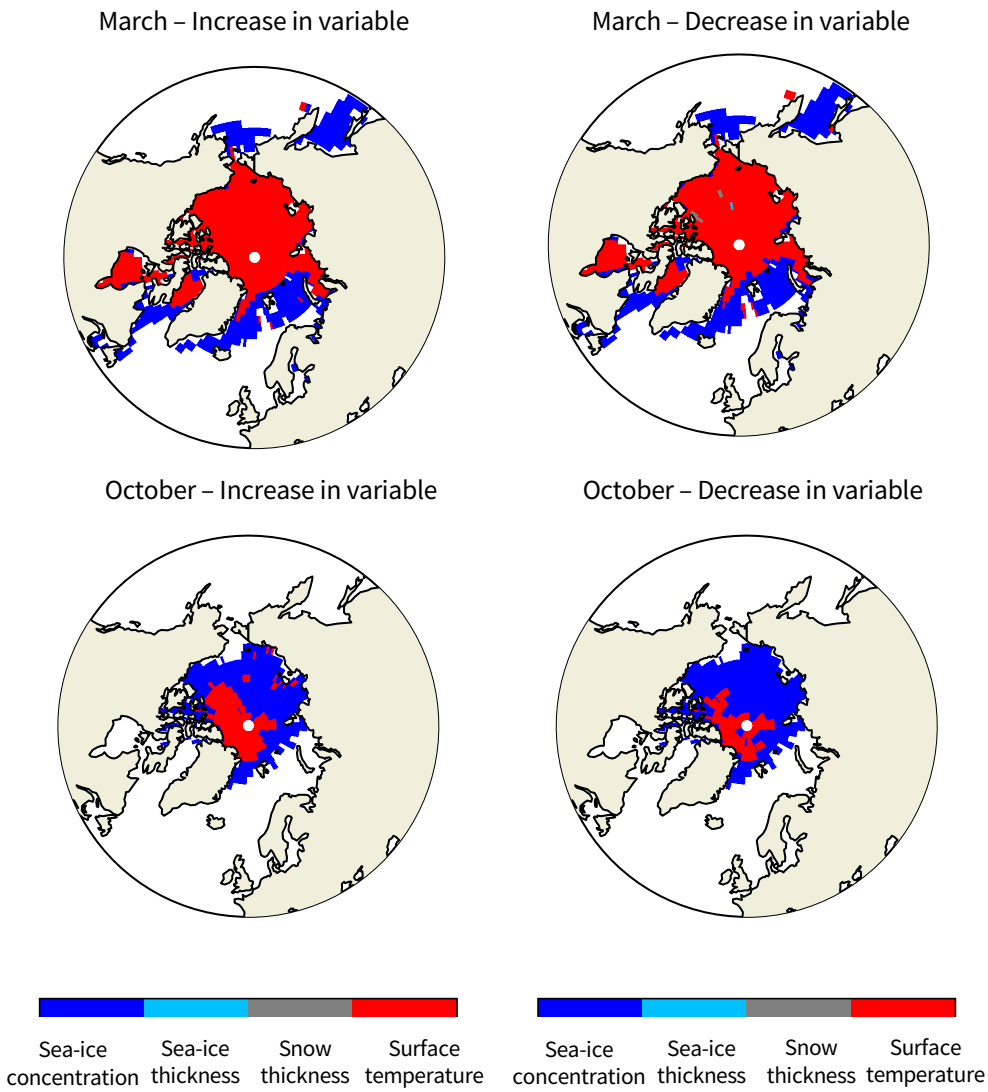

Figure C.5: Variable which has the highest absolute mean effect on the brightness temperature in March (top) and October (bottom) when their variability field is added to (left) and subtracted from (right) the input variable. Inspired from Fig. 5 in Richter et al. (2018)

Still, we can give an estimated range for Δ_{ARC3O} by assuming that the real sea-ice concentration lies between the Bootstrap dataset, which is in the higher range of sea-ice area estimates and NASA Team, which is in the lower range (Fig. C.7 and Ivanova et al., 2014)). To estimate Δ_{ARC3O} based on this assumption, we first subtract Δ_{assim} from the simulated brightness temperature. Δ_{tot} is now only a sum of $\Delta_{\mathrm{retriev}}$ and Δ_{ARC3O}. Second, for each grid cell and each time step, we evaluate if the observed brightness temperature is located within the range of the brightness temperatures simulated based on the three different sea-ice concentration

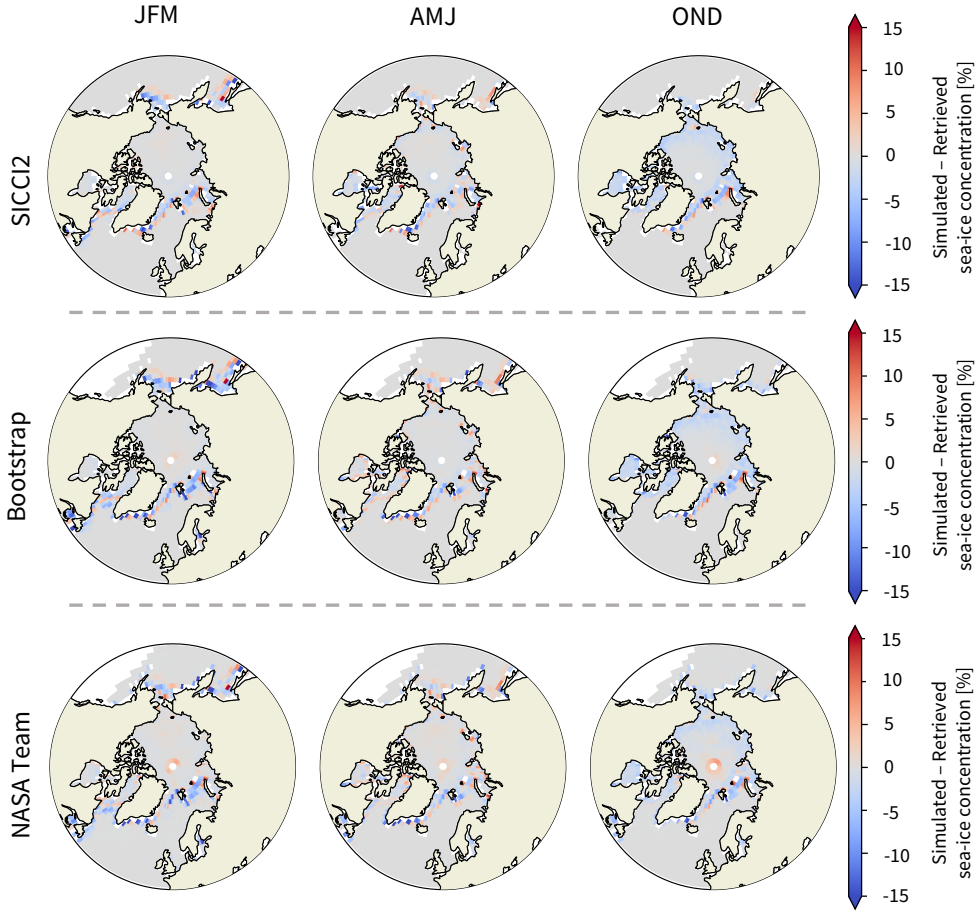

Figure C.6: Difference between retrieved and simulated sea-ice concentration for the three assimilation runs.

products. If yes, differences are not necessarily a bias induced by ARC3O. If not, it is likely that ARC3O induces a bias. In this case, the simulated brightness temperature with the lowest absolute distance from the observed brightness temperature represents the smallest plausible estimate of Δ_{ARC3O} (Fig. C.8, 2nd row). The largest absolute difference between simulated and observed brightness temperatures in contrast gives an estimate of the largest plausible value of Δ_{ARC3O} (Fig. C.8, 3rd row). If the observed brightness temperature is within the range obtained for the different retrieved sea-ice concentration estimates, the estimate of Δ_{ARC3O} is set to zero.

The resulting mean estimates of Δ_{ARC3O} are both very small, as the minimal estimates are well below 5 K and the maximal estimates are 5 K or below, except in the Hudson Bay. Additionally, the comparison of the Δ_{ARC3O} estimates to the spread

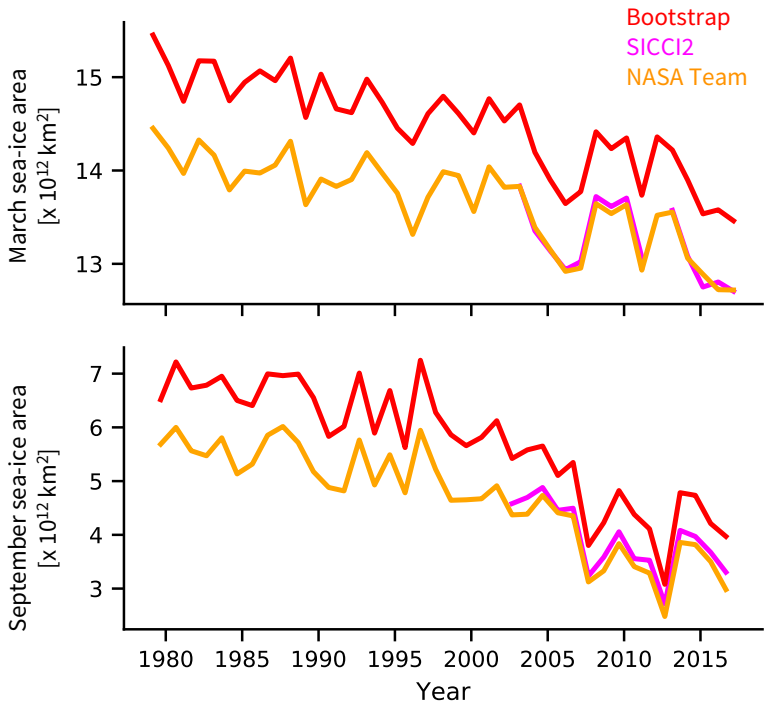

Figure C.7: March (top) and September (bottom) sea-ice area for the three observational datasets used in the three assimilation runs used.

in sea-ice concentration between Bootstrap and NASA Team (Fig. C.8, 4th row) shows that biases in ARC3O, i.e. Δ_{ARC3O}, are small compared to the uncertainty in retrievals, i.e. Δ_{retriev}.

The remaining uncertainty contained in Δ_{ARC3O} can have several sources: ARC3O itself, further biases in the simulated climate state, or wrong assumptions. Biases in ARC3O itself can arise from wrong assumptions in the emission model MEMLS, but also from the definition of first-year and multiyear ice. The definition we use does not take into account the dynamics of the ice. As a consequence, if a grid cell is located in a region where sea-ice circulates horizontally and this grid cell therefore contains ice for more than a year, the ice in this grid cell will be defined as multiyear ice. This is the case even if the ice transported through the grid cell is not the same physical ice floe throughout this time period but a different first-year ice floe every day for example.

We currently cannot explore the additional impact of model biases in simulated surface temperature, sea-ice thickness, and snow thickness, as sufficiently robust in-situ observation data sets of these variables are lacking. Notwithstanding this fact, we expect small biases for the simulated surface temperature, because the

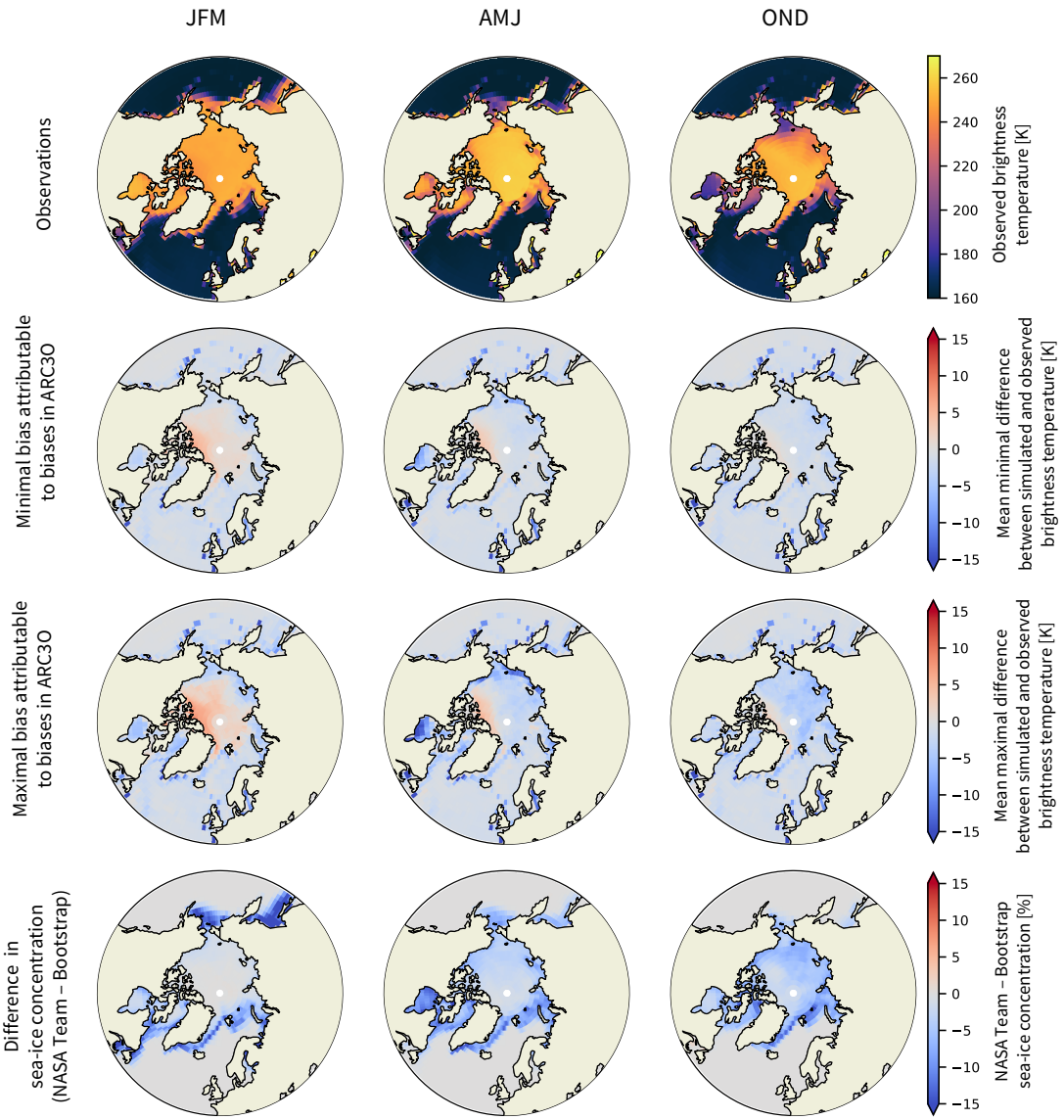

Figure C.8: Observed brightness temperatures (1st row), mean minimal (2nd row) and mean maximal (3rd row) estimates of Δ_{ARC3O} and differences in sea-ice concentration (4th row) between the NASA Team and Bootstrap assimilation runs, i.e. maximal estimates of $\Delta_{\mathrm{retriev}}$.

ERA-Interim reanalysis compares well to the few available in-situ observations (Lindsay et al., 2014). Observational estimates for sea-ice and snow thickness are mainly based on retrieval algorithms, similar to sea-ice concentration estimates. Possible biases may therefore remain in these variables compared to reality. For example, the sea-ice thickness in our assimilation runs is on the order of 2 m at its thickest north of the Canadian Archipelago (not shown). Observational estimates

show thicknesses of rather 4 m or more. This is much more than we varied in our sensitivity study and points to a possible stronger influence of sea-ice thickness on the difference between simulated and observed brightness temperature than estimated from the sensitivity study.

Finally, we assumed that the real sea-ice concentration lies in the range between the Bootstrap and the NASA Team estimates. As only limited evaluation against reality is possible, the uncertainty between real and retrieved sea-ice concentration might be different to our assumption.

As a conclusion, we showed in the consistent model setup that the sea-ice concentration is the main driver for large variations in the brightness temperature in regions that are not fully ice-covered. In regions where the sea-ice concentration is very high and does not vary much, such as the Central Arctic in winter, the surface temperature is the main driver of variations in the brightness temperature. Simulated and observed brightness temperatures are generally in good agreement. Most differences are likely driven by the uncertainty brought by the sea-ice concentration products compared to reality. Remaining differences attributable to biases in ARC3O remain below 5 K.

The lack of evaluation possibilities for the observation operator is an indicator for how little is actually known about the real Arctic climate state, in particular the real sea-ice concentration and the surface temperature. Extending this observation operator to lower and higher frequencies would be of advantage to fill this gap. Brightness temperatures at different frequencies and polarizations are sensitive to different particular parameters. The combination of different brightness temperatures could enable a comprehensive assessment of the Arctic Ocean surface and atmosphere, and a comprehensive evaluation of the individual observation operators. For example, using an observation operator applied to reanalysis data, Richter et al. (2018) simulated brightness temperatures at the frequency of 1.4 GHz. They found that sea-ice concentration and surface temperature are the main drivers for variations in the brightness temperature in the Central Arctic but that, in regions of thin ice, the ice thickness is the dominating driver at this frequency. Combining frequencies in this case would then enable a climate model evaluation encompassing different perspectives.

C.4.4 Melting season (JAS)

Like in winter, the simulation of summer brightness temperatures heavily relies on the underlying sea-ice concentration. Melt ponds are then the main challenge for

sea-ice retrieval algorithms, as their passive microwave signature is undistinguishable from open water. This leads to large uncertainties and potential underestimation of the sea-ice concentration in summer (Meier and Notz, 2010; Cavalieri et al., 1990; Comiso and Kwok, 1996; Fetterer and Untersteiner, 1998; Rösel et al., 2012b; Kern et al., 2016). The difference between observed and simulated brightness temperature (Fig. C.9, left) and the difference between observational sea-ice concentration products is therefore much larger in summer than in winter (Ivanova et al., 2015; Kern et al., 2016).

In summer, the simulation of brightness temperatures in ARC3O is only based on the combination of a constant bare ice brightness temperature and melt-pond brightness temperature, weighted by the melt-pond fraction. We derived the constant brightness temperature from direct observations and it is representative for summer bare ice on the order of ±3.56 K (see Sec. C.3.1.4). We therefore assume that the uncertainty between simulated and observed brightness temperatures in summer is mainly driven by two parameters: the difference between real and retrieved sea-ice concentration and the difference between real and simulated melt-pond fraction.

In the following, we can therefore evaluate the sea-ice concentration products in summer and their relationship to the melt pond fraction. To do so, we distinguish between two types of sea-ice concentration: the total sea-ice concentration and the pond-free sea-ice concentration. The pond-free sea-ice concentration is the concentration of sea ice visible by the satellite, assuming that melt ponds are open water. In MPI-ESM, we know both the total sea-ice concentration and the pond-free sea-ice concentration as melt ponds are represented through a melt-pond parametrization, which is a function of the surface energy budget and water drainage to the ocean (Roeckner et al., 2012). In the SICCI2 algorithm, melt ponds are not explicitly accounted for. However, the dynamic tie-points are based on observed brightness temperatures in areas of high sea-ice concentration, which are covered by melt ponds in summer. The retrieved sea-ice concentration will therefore implicitly be influenced by the melt-pond fraction of the tie-points (Kern et al., 2016; Lavergne et al., 2019). In the Bootstrap algorithm, a correction is applied to sea-ice concentration to account for the effect of melt ponds by synthetically increasing the sea-ice concentration, while in the NASA Team algorithm, no correction is applied (Bunzel et al., 2016). By switching on and off the melt-pond parametrization in MPI-ESM, we can evaluate the ability of observational products to produce a reasonable pond-free and total sea-ice concentration.

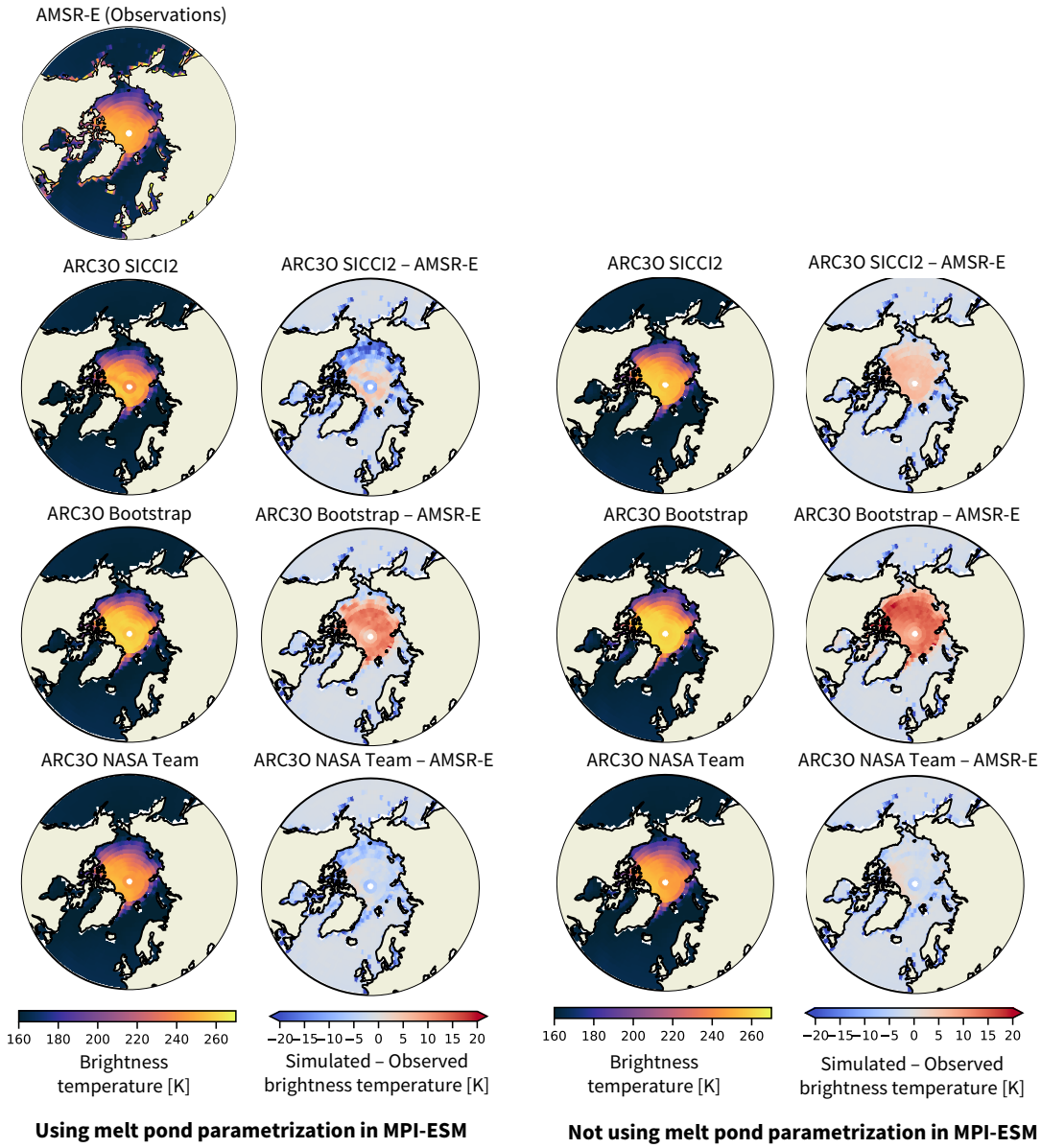

Figure C.9: Experiment to compare brightness temperatures in summer (July/August/September) simulated based on assimilation runs assimilated with different sea-ice concentration products (SICCI2, Bootstrap, NASA Team) to brightness temperatures measured by AMSR-E. In the left column, the assimilated sea-ice concentration is used in combination with a melt-pond parametrization in MPI-ESM. In the right column, the melt-pond fraction is set to zero at all times.

In this experiment, we run ARC3O on the three MPI-ESM assimilation runs setting the melt-pond fraction to zero everywhere. We then compare this set of simulated brightness temperatures to observed brightness temperatures (Fig. C.9, right panel) and to the set of brightness temperatures simulated taking into account the

melt-pond distribution simulated by MPI-ESM (Fig. C.9, left panel). The results give different insights depending on the sea-ice concentration product used for the assimilation.

For the SICCI2 product, the simulated brightness temperature of the pond-free sea ice is higher than the observed brightness temperature in the Central Arctic. Melt ponds cover the whole ice-covered Arctic Ocean (Rösel et al., 2012a; Istomina et al., 2015a). Adding their effect in the brightness temperature simulation could therefore reduce the difference between simulated and observed brightness temperature. However, while the melt-pond parametrization in MPI-ESM reduces the overall brightness temperature, the reduction is very heterogeneous so that the brightness temperature is now largely underestimated in the Pacific sector but still overestimated in most of the Central Arctic. This means that the dynamic tie-point approach of the SICCI2 algorithm seems to take into account the effect of melt ponds in a reasonable way, therefore yielding a too high pond-free sea-ice concentration. The brightness temperatures simulated using the melt-pond parametrization suggest that SICCI2 does not represent well the total sea-ice concentration. However, the melt-pond distribution in MPI-ESM seems to be too heterogeneous and therefore unrealistic in some regions, as most simulated melt ponds concentrate in the Pacific sector and not many can be found over the Central Arctic (Roeckner et al., 2012). If, on the contrary, melt ponds were distributed homogeneously across the sea-ice cover as suggested by previous studies (Rösel et al., 2012a; Istomina et al., 2015a), the brightness temperature would be reduced more homogeneously over the whole basin and therefore approach the observed one. As a consequence, it seems that the total sea-ice concentration might be well represented in the SICCI2 dataset but we cannot robustly confirm this assumption with our setup due to the apparently somewhat unrealistic melt-pond parametrization provided by MPI-ESM.

For the Bootstrap product, if the ice is assumed to be pond-free the simulated brightness temperature is more than 10 K higher than the observed brightness temperature over the whole Central Arctic. Due to this large difference, adding melt ponds on top of the ice is not sufficient to counteract this overestimation of the brightness temperature, which remains on the order of 10 K. This means that Bootstrap tends to overestimate both the pond-free and total sea-ice concentration in summer.

For the NASA Team product, the simulated brightness temperature of the pond-free ice is very close to the observed brightness temperature. As a consequence, the addition of melt ponds leads mainly to a negative bias compared to observations. This means that the NASA Team dataset represents well the

pond-free sea-ice concentration, in agreement with previous results by Ivanova et al. (2015) but that it tends to underestimate the total sea-ice concentration in summer.

The main conclusions show that the main driver for differences between simulated and observed summer brightness temperatures are again the differences between retrieved and real sea-ice concentration. However, the melt-pond parametrization used in MPI-ESM is too heterogeneous and unrealistic and therefore contributes to the difference between simulated and observed brightness temperatures as well. For further analysis, the melt-pond parametrization could however be replaced by a climatology using observational melt-pond estimates, such as Rösel et al. (2012a) or Istomina et al. (2015a). This could reduce the uncertainty induced by the melt-pond parametrization.

C.5 Conclusions

In this study, we present the first observational operator for the Arctic Ocean that is applied to GCM output, following suggestions from Burgard et al. (2019b). It allows us to simulate brightness temperatures at a frequency of 6.9 GHz, vertical polarization, for the whole Arctic Ocean.

Simulated and observed brightness temperatures compare well. In winter, differences between observed and simulated brightness temperatures attributable to biases in ARC3O are well below 5 K. In comparison, the total difference between observed and simulated brightness temperatures ranges from well below 5 K up to 10 K. The large differences can be attributed to possible differences between real and retrieved climate state, especially in sea-ice concentration, and, to a lower extent, to the process of data assimilation into the model. In summer, the difference between simulated and observed brightness temperatures locally reach more than 15 K. This difference can be attributed to high uncertainties in the underlying sea-ice concentration products and potential biases arising from the melt-pond parametrization in the climate model.

The low difference between simulated and observed brightness temperatures showed that it is possible to simulate realistic brightness temperatures based on simple output of a GCM. This is a necessary step to open the way for similar observation operators for different frequencies and polarizations and, as a consequence, for new climate model evaluation and model initialization techniques in a hindcast or unconstrained model run. Additionally, ARC3O can be

used to evaluate observation products against satellite measurements by using assimilation runs.

An observation operator translates a consistent climate state into one observable quantity. In climate model evaluation, the full simulated Arctic climate state can therefore be evaluated against one observed quantity instead of several different retrieved quantities, which all carry uncertainties with them, especially in the Arctic region (Jakobson et al., 2012; Lindsay et al., 2014; Ivanova et al., 2015; Boisvert et al., 2018). With one observation operator at one single frequency, not all effects can be disentangled clearly, e.g. in this case the influence of sea-ice concentration and surface temperature in the Central Arctic are comparable. Further development of observational operators for different frequencies is essential to use this approach to its fullest. A multi-frequency framework would allow us to investigate this consistent climate state from different perspectives, as different variables affect different frequencies differently.

The possibility of comparing the climate state of a climate model in only one observable quantity is also very beneficial to model initialization through data assimilation. The first-guess procedure used in data assimilation methods, such as variational data assimilation (Talagrand and Courtier, 1987; Andersson et al., 1994) or ensemble Kalman filters (Evensen, 1994; Hunt et al., 2007), would then be based on a consistent climate state and be conducted in observation space, independent of retrieval algorithms (Richter et al., 2018). This is already done and has led to improvements in weather prediction systems for other regions than the Arctic (e.g. Terasaki and Miyoshi, 2017).

The observational uncertainty of the sea-ice concentration is very large in summer. We showed here that, if we are able to reduce the uncertainty in the melt-pond representation of the model, we can relate differences between observed and simulated brightness temperatures directly to differences between retrieved and real total sea-ice concentration. This is a promising perspective as melt ponds are a strong challenge for the retrieval of summer sea-ice concentrations.

Finally, ARC3O is a simple observation operator as it is based on variables simulated by all GCMs, can be applied to output from any kind of GCM simulation, and does not require extensive computational power. It is therefore a powerful tool which has the potential to uncover model biases and improve model initialization by providing a new perspective on the Arctic climate system.

C.6 Supporting Information to Appendix C

C.6.1 Temperature profile in snow and ice

The temperature at the interface between ice and snow is computed as follows:

$$T_{\text{ice,surf}} = \frac{T_{\text{snow,surf}} \cdot \frac{k_s}{h_s} + T_{\text{bottom}} \cdot \frac{k_i}{h_i}}{\frac{k_s}{h_s} + \frac{k_i}{h_i}} \tag{C.5}$$

with k_s the thermal conductivity of snow (= 0.31 W/Km), k_i the thermal conductivity of ice (= 2.17 W/Km), h_s the snow thickness, h_i the ice thickness, $T_{\text{snow,surf}}$ the temperature at the surface of the snow, T_{bottom} the temperature at the bottom of the ice, set to -1.8 °C.

C.6.2 Tuning of the temperature profiles

The brightness temperatures initially produced by ARC3O were clearly to bright (Fig. C.10, left). A comparison of the simulated emissivities with emissivities derived from observational data from the RRDP showed that ARC3O systematically overestimates the emissivity. The brightness temperature is defined as the product of the emissivity and the physical temperature of the emitting part of the ice (Ulaby et al., 1986). As it is not straightforward to find where the bias is produced in the emission model, we chose to multiply the inherent sea-ice emissivity with a tuning coefficient to counteract the systematic bias. To do so, we selected all points with a sea-ice concentration of 99.7% or more to avoid influence from open water, in the year 2004. We then multiplied the sea-ice surface brightness temperature by a range of coefficients between 0.96 and 0.975. We found the best agreement between simulated and observed brightness temperatures for a coefficient of 0.963 in the months January, February, and March and for a coefficient of 0.973 in the months October, November, December. As a consensus, we therefore chose a coefficient of 0.968 to apply to the sea-ice brightness temperatures, which yields a more reasonable distribution of brightness temperatures (Fig. C.10, right).

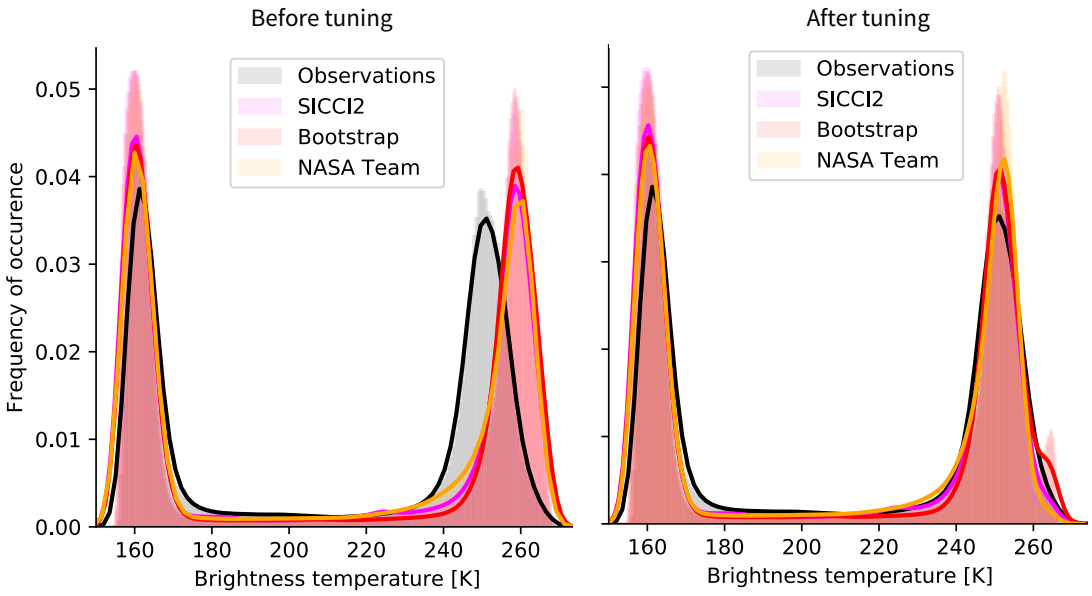

Figure C.10: Density distribution of the brightness temperatures in the three simulated cases and in observations in the untuned (left) and tuned (right) version for the years 2005 to 2008.

C.6.3 VARIABILITY IN CLIMATE PARAMETERS

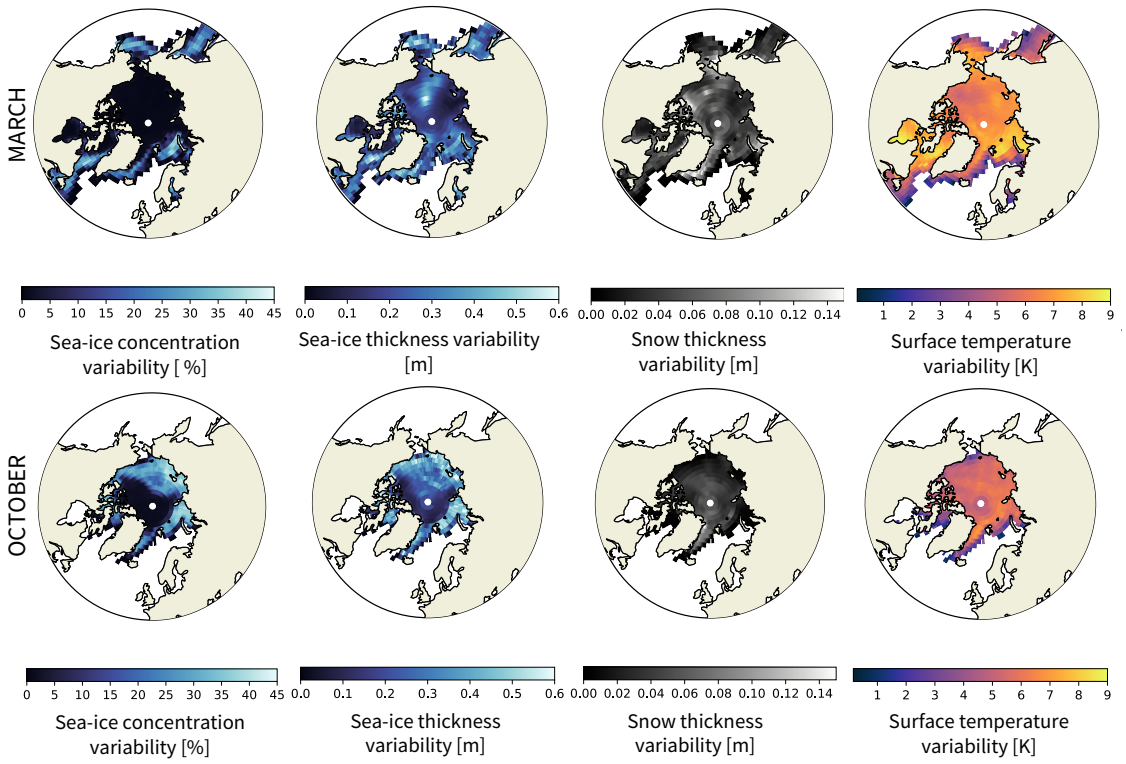

Figure C.11: Standard deviation of the anomaly with regard to the time mean for each grid cell. This is the parameter used to modulate the input variables in the sensitivity studies of Sec. C.4.3.2

EPILOGUE

"Science is not finished until it's communicated."
Sir Mark Walport

While this PhD thesis summarizes well the time I spent on scientific research, it would not be complete without a small contribution about science communication. In my slightly more than three years of being a doctoral researcher, I have enjoyed sitting in my office face to face with my computer some of the time but I cannot imagine what this thesis would have become without communication. Communication is important on all levels: within the office, in group meetings, in scientific workshops and conferences, and in interactions with non-scientific audiences. Having had the chance to get a glimpse in several of these levels, I found all of these enriching and motivating, but unfortunately rated differently by my scientific peers. In the following, I briefly discuss why I think that scientific communication to the non-scientific audience is essential and should be valued as a solid part of a scientific career instead of being dismissed as a nice soft skill.

The currently most-valued type of communication in the scientific environment is the communication of our research results to peers through presentations and scientific papers. The current method for climbing the ladder of a scientific career is to publish many papers, preferentially in high-impact journals. As the number of early-career scientists rapidly increases, the pressure to get as many publications as possible increases as well, sometimes at the cost of clarity and quality. Remaining time for other engagements is not necessarily available because the first priority is to secure funding.

Much less pressure is exerted from within the scientific community to communicate our results to a larger audience than our direct peers. Most scientists are reluctant, some even afraid, to engage with a non-scientific audience. I do not want to believe that arrogance is the main reason for this attitude and I rather think that our training as a scientist makes us over-cautious, so that we do not want to communicate anything which is not sure to 100% to the "outside world". The problem is: very often, there is no way to get this high level of certainty about the overall validity of our results.

While we scientists hide in our bubble, other people fill the void space of scientific communication and information. These people do not necessarily follow the same

ethics. They propagate fake news, exaggerate scientific and non-scientific findings arbitrarily, and are sometimes following personal interest. These are the facts that reach a large audience, especially nowadays, where social media supports the rapid propagation of information, verified or not.

I argue that the time has come for scientists to reclaim their position in the public space by engaging more in scientific communication to a non-scientific audience. To do so, the individual scientists need support from their institutions, from their peers, and from communication experts outside the field. Translating scientific findings into non-scientific language is not straightforward and is time-demanding. If scientists spend time and effort on science communication, it should be valued and not be seen as a "nice" extra on the side.

The benefits of supporting scientists to engage with the non-scientific community are numerous. It provides alternative paths for a scientific career and enlarges the definition of what is a "good" scientist. Communicating science effectively outside the institute promotes the image of the institution. Working on communicating our science to larger audiences is a good training for communication with peers. Finally, the non-scientific community would be better informed and would have a more realistic image of what it means to do science and relate to the scientists on a more personal level. This could motivate people to engage into science on a day-to-day basis and to think more critically.

Personally, I am passionate about science communication as I like the variety of channels it can go through, e.g. social media, blogging, board games, art. Also, I like that it makes me think about climate research from a different perspective. It is always refreshing to change the point of view on our priorities and has helped me overcome some large motivation gaps and moments of frustration. From experience, I know I am not the only (climate) scientist with this opinion. Science deniers are currently reaching an increasing number of people. I strongly hope that the academic system is ready to counteract this trend and to back the scientists who are willing to spend some of their working time to keep the scientific voice present in the public space.

BIBLIOGRAPHY

Aagaard, K., J. Swift, and E. Carmack (1985): "Thermohaline circulation in the Arctic Mediterranean seas". *J. Geophys. Res. Oceans (1978–2012)*, 90(C3), 4833–4846.

Ådlandsvik, B. and H. Loeng (1991): "A study of the climatic system in the Barents Sea". *Polar Res.*, 10(1), 45–49, doi:10.3402/polar.v10i1.6726.

Andersson, E., J. Pailleux, J.-N. Thépaut, J. Eyre, A. McNally, G. Kelly, and P. Courtier (1994): "Use of cloud-cleared radiances in three/four-dimensional variational data assimilation". *Q. J. Roy. Meteor. Soc.*, 120, 627–653, doi:10.1002/qj.49712051707.

Armour, K., J. Marshall, J. Scott, A. Donohoe, and E. Newson (2016): "Southern Ocean warming delayed by circumpolar upwelling and equatorward transport". *Nat. Geosci.*, 9, 549–555, doi:10.1038/ngeo2731.

Årthun, M., T. Eldevik, L. Smedsrud, Ø. Skagseth, and R. Ingvaldsen (2012): "Quantifying the Influence of Atlantic Heat on Barents Sea Ice Variability and Retreat". *J. Clim.*, 25, 4736–4743, doi:10.1175/JCLI-D-11-00466.1.

Bailey, D., A. DuVivier, M. Holland, E. Hunke, B. Lipscomb, B. Briegleb, C. Bitz, and J. Schramm (2018): "CESM CICE5 Users Guide", Tech. rep.

Balmaseda, M., K. Mogensen, and A. Weaver (2013): "Evaluation of the ECMWF ocean reanalysis system ORAS4". *Q. J. Roy. Meteor. Soc.*, 139, 1132–1161, doi:10.1002/qj.2063.

Barber, D., K. Dethloff, S. Gerland, J. Inoue, C. Lee, B. Loose, A. Makshtas, W. Maslowski, M. Nicolaus, D. Notz, I. Peeken, D. K. Perovich, O. Persson, J. Schmale, M. Shupe, M. Tjernström, T. Vihma, and J. Zhao (2016): "MOSAiC Science Plan", Tech. rep., International Arctic Science Committee.

Barber, D., A. Fung, T. Grenfell, S. Nghiem, R. Onstott, V. Lytle, D. Perovich, and A. Gow (1998): "The role of snow on microwave emission and scattering over first-year sea ice". *IEEE T. Geosci. Remote*, 36, 1750–1763, doi:10.1109/36.718643.

Bathiany, S., D. Notz, T. Mauritsen, G. Raedel, and V. Brovkin (2016): "On the Potential for Abrupt Arctic Winter Sea Ice Loss". *J. Clim.*, 29, 2703–2719, doi:10.1175/JCLI-D-15-0466.1.

Bitz, C. M., P. R. Gent, R. A. Woodgate, M. M. Holland, and R. Lindsay (2006): "The influence of sea ice on ocean heat uptake in response to increasing CO2". *J. Clim.*, 19(11), 2437–2450, doi:10.1175/JCLI3756.1.

Bjerknes, J. (1964): "Atlantic Air-Sea Interaction". *Adv. Geophys.*, 10, 1–82, doi:10.1016/S0065-2687(08)60005-9.

Boisvert, L., M. Webster, A. Petty, T. Markus, D. Bromwich, and R. Cullather (2018): "Intercomparison of Precipitation Estimates over the Arctic Ocean and

Its Peripheral Seas from Reanalyses". *J. Climate*, 31, 8441–8462, doi:10.1175/JCLI-D-18-0125.1.

Brodzik, M., D. Long, M. Hardman, A. Paget, and R. Armstrong (2016, Updated 2018): "MEaSUREs Calibrated Enhanced-Resolution Passive Microwave Daily EASE-Grid 2.0 Brightness Temperature ESDR, Version 1", doi:10.5067/MEASURES/CRYOSPHERE/NSIDC-0630.001, [Accessed in October 2018].

Bunzel, F., D. Notz, J. Baehr, W. Müller, and K. Fröhlich (2016): "Seasonal climate forecasts significantly affected by observational uncertainty of Arctic sea ice concentration". *Geophys. Res. Lett.*, 43(2), 852–859, doi:10.1002/2015GL066928.

Bunzel, F., D. Notz, and L. Pedersen (2018): "Retrievals of Arctic Sea-Ice Volume and Its Trend Significantly Affected by Interannual Snow Variability". *Geophys. Res. Lett.*, 45, 11751–11759, doi:10.1029/2018GL078867.

Burgard, C., D. Notz, L. Pedersen, and R. Tonboe (2019a): "ARC3O: The Arctic Ocean Observation Operator for 6.9 GHz". *To be submitted to The Cryosphere*.

Burgard, C., D. Notz, L. Pedersen, and R. Tonboe (2019b): "How to obtain sea-ice brightness temperatures at 6.9 GHz from climate model output". *To be submitted to The Cryosphere*.

Cavalieri, D., B. Burns, and R. Onstott (1990): "Investigation of the effects of summer melt on the calculation of sea ice concentration using active and passive microwave data". *J. Geophys. Res-Oceans*, 95, 5359–5369, doi:10.1029/JC095iC04p05359.

Cavalieri, D. J., C. Parkinson, P. Gloersen, and H. Zwally (1996): "Sea ice concentrations from Nimbus-7 SMMR and DMSP SSM/I-SSMIS passive microwave data, version 1", doi:10.5067/8GQ8LZQVL0VL, [Accessed in August 2014, updated yearly].

Chang, T. and P. Gloersen (1975): "Microwave Emission from dry and wet snow", in: A. Rango (ed.), "Operational Applications of Satellite Snowcover Observations", chap. 27, pp. 399–407, NASA.

Comiso, J. (2000): "Bootstrap sea ice concentrations from Nimbus-7 SMMR and DMSP SSM/I-SSMIS, version 2", doi:10.5067/J6JQLS9EJ5HU, [Accessed in August 2014, updated yearly].

Comiso, J. and R. Kwok (1996): "Surface and radiative characteristics of the summer Arctic sea ice cover from multisensor satellite observations". *J. Geophys. Res-Oceans*, 101, 28397–28416, doi:10.1029/96JC02816.

Dee, D., S. Uppala, A. Simmons, P. Berrisford, P. Poli, S. Kobayashi, U. Andrae, M. Balmaseda, G. Balsamo, P. Bauer, P. Bechtold, A. Beljaars, L. van de Berg, J. Bidlot, N. Bormann, C. Delsol, R. Dragani, M. Fuentes, A. Geer, L. Haimberger, S. Healy, H. Hersbach, E. Holm, L. Isaksen, P. Kållberg, M. Köhler, M. Matricardi, A. McNally, B. Monge-Sanz, J.-J. Morcrette, B.-K. Park, C. Peubey, P. de Rosnay, C. Tavolato, J.-N. Thébaut, and F. Vitart (2011): "The ERA-Interim reanalysis:

configuration and performance of the data assimilation system". *Q. J. Roy. Meteor. Soc.*, 137, 553–597, doi:10.1002/qj.828.

Edwards, P. (2011): "History of climate modeling: History of climate modeling". *WiRes Clim Change*, 2, 128–139, doi:10.1002/wcc.95.

Evensen, G. (1994): "Sequential data assimilation with a nonlinear quasi-geostrophic model using Monte Carlo methods to forecast error statistics". *J. Geophys. Res-Oceans*, 99, 10143–10162, doi:10.1029/94JC00572.

Eyring, V., S. Bony, G. Meehl, C. Senior, B. Stevens, R. Stouffer, and K. Taylor (2016): "Overview of the Coupled Model Intercomparison Project Phase 6 (CMIP6) experimental design and organization". *Geosci. Model Dev.*, 9, 1937–1958, doi:10.5194/gmd-9-1937-2016.

Eyring, V., P. Cox, G. Flato, P. Gleckler, G. Abramowitz, P. Caldwell, W. Collins, B. Gier, A. Hall, F. Hoffman, G. Hurtt, A. Jahn, C. Jones, S. Klein, J. Krasting, L. Kwiatkowski, R. Lorenz, E. Maloney, G. Meehl, A. Pendergrass, R. Pincus, A. Ruane, J. Russell, B. Sanderson, B. Santer, S. Sherwood, I. Simpson, R. Stouffer, and M. Williamson (2019): "Taking climate model evaluation to the next level". *Nat. Clim. Change*, doi:10.1038/s41558-018-0355-y.

Fetterer, F. and N. Untersteiner (1998): "Observations of melt ponds on Arctic sea ice". *J. Geophys. Res-Oceans*, 103, 24821–24835, doi:10.1029/98JC02034.

Flato, G., J. Marotzke, B. Abiodun, P. Braconnot, S. Chou, W. Collins, P. Cox, F. Driouech, S. Emori, V. Eyring, C. Forest, P. Gleckler, E. Guilyardi, C. Jakob, V. Kattsov, C. Reason, and M. Rummukainen (2013): *Evaluation of Climate Models*, book section 9, pp. 741–866, Cambridge University Press, Cambridge, United Kingdom and New York, NY, USA, doi:10.1017/CBO9781107415324.020.

Gabarro, C., A. Turiel, P. Elosegui, J. Pla-Resina, and M. Portabella (2017): "New methodology to estimate Arctic sea ice concentration from SMOS combining brightness temperature differences in a maximum-likelihood estimator". *Cryosphere*, 11, 1987–2002, doi:10.5194/tc-11-1987-2017.

Giorgetta, M., E. Roeckner, T. Mauritsen, J. Bader, T. Crueger, M. Esch, S. Rast, L. Kornblueh, H. Schmidt, S. Kinne, C. Hohenegger, B. Möbis, T. Krismer, K. Wieners, and B. Stevens (2013): "The atmospheric general circulation model ECHAM6: Model description", Tech. Rep. Reports on Earth System Science, 135/2013, Max Planck Institute for Meteorology.

Gould, J., D. Roemmich, S. Wijffels, H. Freeland, M. Ignaszewsky, X. Jianping, S. Pouliquen, Y. Desaubies, U. Send, K. Radhakrishnan, K. Takeuchi, K. Kim, M. Danchenkov, P. Sutton, B. King, B. Owens, and S. Riser (2004): "Argo profiling floats bring new era of in situ ocean observations". *Eos, Transactions American Geophysical Union*, 85, 190–191, doi:10.1029/2004EO190002.

Gregory, J., P. Stott, D. Cresswell, N. Rayner, C. Gordon, and D. Sexton (2002): "Recent and future changes in Arctic sea ice simulated by the HadCM3 AOGCM". *Geophys.*

Res. Lett., 29, 28–1–28–4, doi:10.1029/2001GL014575.

Grenfell, T., D. Barber, A. Fung, A. Gow, K. Jezek, E. Knapp, S. Nghiem, R. Onstott, D. Perovich, C. Roesler, C. Swift, and F. Tanis (1998): "Evolution of electromagnetic signatures of sea ice from initial formation to the establishment of thick first-year ice". *IEEE T. Geosci. Remote*, 36, 1642–1654, doi:10.1109/36.718636.

Griewank, P. and D. Notz (2013): "Insights into brine dynamics and sea ice desalination from a 1-D model study of gravity drainage". *J. Geophys. Res-Oceans*, 118, 3370–3386, doi:10.1002/jgrc.20247.

Griewank, P. and D. Notz (2015): "A 1-D modelling study of Arctic sea-ice salinity". *Cryosphere*, 9, 305–329, doi:10.5194/tc-9-305-2015.

Hallikainen, M. and D. Winebrenner (1992): "The Physical Basis for Sea Ice Remote Sensing", in: F. Carsey (ed.), "Microwave Remote Sensing of Sea Ice", chap. 4, pp. 29–46, American Geophysical Union.

Hawkins, E., P. Ortega, E. Suckling, A. Schurer, G. Hegerl, P. Jones, T. Joshi, M. Osborn, V. Masson-Delmotte, J. Mignot, P. Thorne, and G. van Oldenborgh (2017): "Estimating Changes in Global Temperature since the Preindustrial Period". *B. Am. Meteorol. Soc.*, 98, 1841–1856, doi:10.1175/BAMS-D-16-0007.1.

Hibler, W. (1979): "A Dynamic Thermodynamic Sea Ice Model". *J. Phys. Oceanogr.*, 9, 815–846.

Holland, M. and C. Bitz (2003): "Polar amplification of climate change in coupled models". *Clim. Dyn.*, 21, 221–232, doi:10.1007/s00382-003-0332-6.

Hunt, B., E. Kostelich, and I. Szunyogh (2007): "Efficient data assimilation for spatiotemporal chaos: A local ensemble transform Kalman filter". *Physica D*, 230, 112–126, doi:10.1016/j.physd.2006.11.008.

Huwald, H., L.-B. Tremblay, and H. Blatter (2005): "Reconciling different observational data sets from Surface Heat Budget of the Arctic Ocean (SHEBA) for model validation purposes". *J. Geophys. Res. Oceans*, 110(C5), doi:10.1029/2003JC002221, c05009.

Hwang, B., J. Ehn, D. Barber, R. Galley, and T. Grenfell (2007): "Investigations of newly formed sea ice in the Cape Bathurst polynya: 2. Microwave emission". *J. Geophys. Res-Oceans*, 112, C05003, doi:10.1029/2006JC003703.

Ikeda, M. (1990): "Decadal oscillations of the air-ice-ocean system in the Northern Hemisphere". *Atmos. Ocean*, 28(1), 106–139, doi:10.1080/07055900.1990.9649369.

IPCC (2013): *Climate Change 2013: The Physical Science Basis. Contribution of Working Group I to the Fifth Assessment Report of the Intergovernmental Panel on Climate Change*, Cambridge University Press, Cambridge, United Kingdom and New York, NY, USA, 1535 pp.

Istomina, L., G. Heygster, M. Huntemann, H. Marks, C. Melsheimer, E. Zege, A. Malinka, A. Prikhach, and I. Katsev (2015a): "Melt pond fraction and spectral sea ice albedo retrieval from MERIS data - Part 2: Case studies and trends of sea

ice albedo and melt ponds in the Arctic for years 2002-2011". *Cryosphere*, 9, 1567–1578, doi:10.5194/tc-9-1551-2015.

Istomina, L., G. Heygster, M. Huntemann, P. Schwarz, G. Birnbaum, P. Scharien, C. Polashenski, D. Perovich, E. Zege, A. Malinka, A. Prikhach, and I. Katsev (2015b): "Melt pond fraction and spectral sea ice albedo retrieval from MERIS data - Part 1: Validation against in situ, aerial, and ship cruise data". *Cryosphere*, 9, 1551–1566, doi:10.5194/tc-9-1551-2015.

Ivanova, N., O. M. Johannessen, L. T. Pedersen, and R. T. Tonboe (2014): "Retrieval of Arctic Sea Ice Parameters by Satellite Passive Microwave Sensors: A Comparison of Eleven Sea Ice Concentration Algorithms". *IEEE T. Geosci. Remote*, 52(11), 7233–7246, doi:10.1109/TGRS.2014.2310136.

Ivanova, N., L. Pedersen, S. Kern, G. Heygster, T. Lavergne, A. Sørensen, R. Saldo, G. Dybkjaer, L. Brucker, and M. Shokr (2015): "Inter-comparison and evaluation of sea ice algorithms: towards further identification of challenges and optimal approach using passive microwave observations". *Cryosphere*, 9, 1797–1817, doi:10.5194/tc-9-1797-2015.

Jakobson, E., T. Vihma, H. Keernik, and J. Jaagus (2012): "Validation of atmospheric reanalyses over the central Arctic Ocean". *Geophys. Res. Lett.*, 39, doi:10.1029/2012GL051591.

Jezek, K., D. Perovich, K. Golden, C. Luther, D. Barber, P. Gogineni, T. Grenfell, A. Jordan, C. Mobley, S. Nghiem, and R. Onstott (1998): "A broad spectral, interdisciplinary investigation of the electromagnetic properties of sea ice". *IEEE T. Geosci. Remote*, 36, 1633–1641, doi:10.1109/36.718635.

Jungclaus, J., N. Fischer, H. Haak, K. Lohmann, J. Marotzke, D. Matei, U. Mikolajewicz, D. Notz, and J. von Storch (2013): "Characteristics of the ocean simulations in the Max Planck Institute Ocean Model (MPIOM) the ocean component of the MPI-Earth system model". *J. Adv. Model Earth Sy.*, 5, 422–446, doi:10.1002/jame.20023.

Jungclaus, J. and T. Koenigk (2010): "Low-frequency variability of the arctic climate: the role of oceanic and atmospheric heat transport variations". *Clim. Dyn.*, 34, 265–279, doi:10.1007/s00382-009-0569-9.

Kern, S., A. Rösel, L. Pedersen, N. Ivanova, R. Saldo, and R. Tonboe (2016): "The impact of melt ponds on summertime microwave brightness temperatures and sea-ice concentrations". *Cryosphere*, 10, 2217–2239, doi:10.5194/tc-10-2217-2016.

Knutti, R., D. Masson, and A. Gettelmann (2013): "Climate model genealogy: Generation CMIP5 and how we got there". *Geophys. Res. Lett.*, 40, 1194 – 1199.

Koenigk, T. and L. Brodeau (2013): "Ocean heat transport into the Arctic in the twentieth and twenty-first century in EC-Earth". *Clim. Dyn.*, 42, 3101–3120, doi:10.1007/s00382-013-1821-x.

Laîné, A., M. Yoshimori, and A. Abe-Ouchi (2016): "Surface Arctic Amplification Factors in CMIP5 Models: Land and Oceanic Surfaces and Seasonality". *J. Clim.*, 29, 3297–3316, doi:10.1175/JCLI-D-15-0497.1.

Lavergne, T., A. Macdonald Sørensen, S. Kern, R. Tonboe, D. Notz, S. Aaboe, L. Bell, Dybkjær, S. Eastwood, C. Gabarro, G. Heygster, M. Killie, M. Brandt Kreiner, J. Lavelle, R. Saldo, S. Sandven, and L. Pedersen (2019): "Version 2 of the EUMETSAT OSI SAF and ESA CCI sea-ice concentration climate data records". *Cryosphere*, 13, 49–78, doi:10.5194/tc-13-49-2019.

Lee, S.-M., B.-J. Sohn, and S.-J. Kim (2017): "Differentiating between first-year and multiyear sea ice in the Arctic using microwave-retrieved ice emissivities". *J. Geophys. Res-Atm*, 122, 5097–5112, doi:10.1002/2016JD026275.

Lemmetyinen, J., C. Derksen, H. Rott, G. Macelloni, J. King, M. Schneebeli, A. Wiesmann, L. Leppännen, A. Kontu, and J. Pulliainen (2018): "Retrieval of Effective Correlation Length and Snow Water Equivalent from Radar and Passive Microwave Measurements". *Remote Sensing*, 10, 170, doi:10.3390/rs10020170.

Li, C., D. Notz, S. Tietsche, and J. Marotzke (2013): "The Transient versus the Equilibrium Response of Sea Ice to Global Warming". *J. Climate*, 26, 5624–5636, doi:10.1175/JCLI-D-12-00492.1.

Lindsay, R., M. Wensnahan, A. Schweiger, and J. Zhang (2014): "Evaluation of Seven Different Atmospheric Reanalysis Products in the Arctic". *J. Climate*, 27, 2588–2606, doi:10.1175/JCLI-D-13-00014.1.

Mahlstein, I. and R. Knutti (2011): "Ocean heat transport as a cause for model uncertainty in projected Arctic warming". *J. Climate*, 24(5), 1451–1460, doi:10.1175/2010JCLI3713.1.

Mahlstein, I. and R. Knutti (2012): "September Arctic sea ice predicted to disappear near 2°C global warming above present". *J. Geophys. Res-Atm*, 117, doi:10.1029/2011JD016709.

Marshall, J., K. Armour, J. Scott, Y. Kostov, U. Hausmann, D. Ferreira, T. Shepherd, and C. Bitz (2014): "The ocean's role in polar climate change: asymmetric Arctic and Antarctic responses to greenhouse gas and ozone forcing". *Phil. Trans. R. Soc. A*, 372, doi:10.1098/rsta.2013.0040.

Marshall, J., J. Scott, K. Armour, J.-M. Campin, M. Kelley, and A. Romanou (2015): "The ocean's role in the transient response of climate to abrupt greenhouse gas forcing". *Clim. Dyn.*, 44, 2287–2299, doi:10.1007/s00382-014-2308-0.

Mätzler, C. (2002): "Relation between grain size and correlation length of snow". *J. Glaciol.*, 48, 461–466, doi:10.3189/172756502781831287.

Mayer, M., L. Haimberger, M. Pietschnig, and A. Storto (2016): "Facets of Arctic energy accumulation based on observations and reanalyses 2000-2015: Recent trends in Arctic energy budget". *Geophys. Res. Lett.*, ISSN 00948276, doi:10.1002/2016GL070557.

Meehl, G., C. Covey, T. Delworth, M. Latif, B. McAvaney, J. Mitchell, R. Stouffer, and K. Taylor (2007): "THE WCRP CMIP3 Multimodel Dataset: A New Era in Climate Change Research". *B. Am. Meteorol. Soc.*, 88, 1383–1394, doi:10.1175/BAMS-88-9-1383.

Meier, W. and D. Notz (2010): "A note on the accuracy and reliability of satellite-derived passive microwave estimates of sea-ice extent". *CliC Arctic sea ice working group consensus document, World Climate Research Program*.

Nakamura, N. and A. Oort (1988): "Atmospheric heat budgets of the polar regions". *J. Geophys. Res-Atm*, 93, 9510–9524, doi:10.1029/JD093iD08p09510.

Nakawo, M. and N. Sinha (1981): "Growth Rate and Salinity Profile of First-Year Sea Ice in the High Arctic". *J. Glaciol.*, 27, 315–330, doi:10.3189/S0022143000015409.

Nansen, F. (1911): *Nebelheim: Entdeckung und Erforschung der nördlichen Länder und Meere. Band I und II*, Brockhaus, F.A., Leipzig.

Nghiem, S., R. Kwok, S. Yueh, and M. Drinkwater (1995): "Polarimetric signatures of sea ice: 2. Experimental observations". *J. Geophys. Res.-Oceans*, 100, 13681–13698, doi:10.1029/95JC00938.

Niederdrenk, A. and D. Notz (2018): "Arctic sea ice in a 1.5°C warmer world". *Geophys. Res. Lett.*, 45(4), doi:10.1002/2017GL076159.

Notz, D. (2005): *Thermodynamic and Fluid-Dynamical Processes in Sea Ice*, Ph.D. thesis, University of Cambridge.

Notz, D. (2014): "Sea-ice extent and its trend provide limited metrics of model performance". *Cryosphere*, 8, 229–243, doi:10.5194/tc-8-229-2014.

Notz, D., A. Haumann, H. Haak, and J. Marotzke (2013): "Arctic sea-ice evolution as modeled by Max Planck Institute for Meteorology's Earth system model". *J. Adv. Model Earth Sy.*, 5, 173–194, doi:10.1002/jame.20016.

Notz, D. and J. Stroeve (2016): "Observed Arctic sea-ice loss directly follows anthropogenic CO_2 emission". *Science*, doi:10.1126/science.aag2345.

Nummelin, A., C. Li, and P. Hezel (2017): "Connecting ocean heat transport changes from the mid-latitudes to the Arctic Ocean". *Geophys. Res. Lett.*, accepted online, doi:10.1002/2016GL071333.

Onarheim, I., T. Eldevik, M. Årthun, R. Ingvaldsen, and L. Smedsrud (2015): "Skillful prediction of Barents Sea ice cover". *Geophys. Res. Lett.*, 42, 5364–5371, doi:10.1002/2015GL064359.

Overland, J. and M. Wang (2013): "When will the summer Arctic be nearly sea ice free?" *Geophys. Res. Lett.*, 40, 2097–2101.

Pedersen, L., R. Saldo, N. Ivanova, S. Kern, G. Heygster, R. Tonboe, M. Huntemann, B. Ozsoy, F. Ardhuin, and L. Kaleschke (2018): "Reference dataset for sea ice concentration", doi:10.6084/m9.figshare.6626549.v6, URL `https://figshare.com/articles/Reference_dataset_for_sea_ice_concentration/6626549/3`.

Perovich, D., J. Longacre, D. Barber, R. Maffione, G. Cota, C. Mobley, A. Gow, R. Onstott, T. Grenfell, W. Pegau, M. Landry, and C. Roesler (1998): "Field observations of the electromagnetic properties of first-year sea ice". *IEEE T. Geosci. Remote*, 36, 1705–1715, doi:10.1109/36.718639.

Polyakov, I., L. Timokhov, V. Alexeev, S. Bacon, I. Dmitrenko, L. Fortier, I. Frolov, G. J.-C., E. Hansen, V. Ivanov, S. Laxon, C. Mauritzen, D. Perovich, K. Shimada, H. Simmons, V. Sokolov, M. Steele, and J. Toole (2010): "Arctic Ocean Warming Contributes to Reduced Polar Ice Cap". *J. Phys. Oceanogr.*, 40, 2743–2756, doi: 10.1175/2010JPO4339.1.

Proksch, M., H. Löwe, and M. Schneebeli (2015): "Density, specific surface area, and correlation length of snow measured by high-resolution penetrometry". *J. Geophys. Res-Earth*, 120, 346–362, doi:10.1002/2014JF003266.

Richter, F., M. Drusch, L. Kaleschke, N. Maaß, X. Tian-Kunze, and S. Mecklenburg (2018): "Arctic sea ice signatures: L-band brightness temperature sensitivity comparison using two radiation transfer models". *Cryosphere*, 12, 921–933, doi: 10.5194/tc-12-921-2018.

Ridley, J., J. Lowe, and H. Hewitt (2012): "How reversible is sea ice loss?" *Cryosphere*, 6, 193–198, doi:10.5194/tc-6-193-2012.

Roeckner, E., T. Mauritsen, M. Esch, and R. Brokopf (2012): "Impact of melt ponds on Arctic sea ice in past and future climates as simulated by MPI-ESM". *J. Adv. Model Earth Sy.*, 4, doi:10.1029/2012MS000157.

Rösel, A., L. Kaleschke, and G. Birnbaum (2012a): "Melt ponds on Arctic sea ice determined from MODIS satellite data using an artificial neural network". *Cryosphere*, 6, 431–446, doi:10.5194/tc-6-431-2012.

Rösel, A., L. Kaleschke, and S. Kern (2012b): "Influence of melt ponds on microwave sensors' sea ice concentration retrieval algorithms". *2012 IEEE International Geoscience and Remote Sensing Symposium*, pp. 3261–3264, doi:10.1109/IGARSS.2012.6350608.

Rosenblum, E. and I. Eisenman (2017): "Sea Ice Trends in Climate Models Only Accurate in Runs with Biased Global Warming". *J. Climate*, 30, 6265–6278, doi: 10.1175/JCLI-D-16-0455.1.

Schauer, U., E. Fahrbach, S. Osterhus, and G. Rohardt (2004): "Arctic warming through the Fram Strait: Oceanic heat transport from 3 years of measurements". *J. Geophys. Res-Oceans (1978–2012)*, 109(C6), doi:10.1029/2003JC001823.

Serreze, M., A. Barrett, A. Slater, M. Steele, J. Zhang, and K. Trenberth (2007a): "The large-scale energy budget of the Arctic". *J. Geophys. Res. Atmos (1984–2012)*, 112(D11), doi:10.1029/2006JD008230.

Serreze, M. and R. Barry (2011): "Processes and impacts of Arctic amplification: A research synthesis". *Global Planet. Change*, 77(1), 85–96.

Serreze, M., M. Holland, and J. Stroeve (2007b): "Perspectives on the Arctic's Shrinking Sea-Ice Cover". *Science*, 315(5818), doi:10.1126/science.1139426.

Shokr, M. and N. Sinha (2015a): "Remote Sensing Principles Relevant to Sea Ice", in: A. G. Union (ed.), "Sea Ice: Physics and Remote Sensing, Geophysical Monograph 209, First Edition", chap. 7, pp. 271–335, John Wiley & Sons, Inc.

Shokr, M. and N. Sinha (2015b): "Sea ice Properties: Data and Derivations", in: A. G. Union (ed.), "Sea Ice: Physics and Remote Sensing, Geophysical Monograph 209, First Edition", chap. 3, pp. 99–137, John Wiley & Sons, Inc.

Smedsrud, L., I. Esau, R. Ingvaldsen, T. Eldevik, P. Haugan, C. Li, V. Lien, A. Olsen, A. Omar, O. Otterå, B. Risebrobakken, A. Sandø, V. Semenov, and S. Sorokina (2013): "The role of the Barents Sea in the Arctic climate system". *Rev. Geophys.*, 51(3), 415–449, ISSN 87551209, doi:10.1002/rog.20017.

Sorteberg, A., V. Kattsov, J. Walsh, and T. Pavlova (2007): "The Arctic surface energy budget as simulated with the IPCC AR4 AOGCMs". *Clim. Dynam.*, 29, 131–156, doi:10.1007/s00382-006-0222-9.

Spielhagen, R., K. Werner, S. Sørensen, K. Zamelczyk, E. Kandiano, G. Budeus, K. Husum, T. Marchitto, and M. Hald (2011): "Enhanced Modern Heat Transfer to the Arctic by Warm Atlantic Water". *Science*, 331, 450–453, doi:10.1126/science.1197397.

Steele, M., W. Ermold, and J. Zhang (2008): "Arctic Ocean surface warming trends over the past 100 years". *Geophys. Res. Lett.*, 35(L02614), doi:10.1029/2007GL031651.

Stevens, B., M. Giorgetta, M. Esch, T. Mauritsen, T. Crueger, S. Rast, M. Salzmann, H. Schmidt, J. Bader, K. Block, R. Brokopf, I. Fast, S. Kinne, L. Kornblueh, U. Lohmann, R. Pincus, T. Reichler, and E. Roeckner (2013): "Atmospheric component of the MPI-M Earth System Model: ECHAM6". *J. Adv. Model Earth Sy.*, 5, 146–172, doi:10.1002/jame.20015.

Stroeve, J., M. Holland, W. Meier, T. Scambos, and M. Serreze (2007): "Arctic sea ice decline: Faster than forecast". *Geophys. Res. Lett.*, 34(L09501), doi:10.1029/2007GL029703.

Stroeve, J., V. Kattsov, A. Barrett, M. Serreze, T. Pavlova, M. Holland, and W. Meier (2012): "Trends in Arctic sea ice extent from CMIP5, CMIP3 and observations". *Geophys. Res. Lett.*, 39(16), doi:10.1029/2012GL052676.

Stroeve, J. and D. Notz (2015): "Insights on past and future sea-ice evolution from combining observations and models". *Global Planet. Change*, 135, 119–132, doi:10.1016/j.gloplacha.2015.10.011.

Swart, N., J. Fyfe, E. Hawkins, J. Kay, and A. Jahn (2015): "Influence of internal variability on Arctic sea-ice trends". *Nat. Clim. Change*, 5, 86–89, doi:10.1038/nclimate2483.

Swift, C. and D. Cavalieri (1985): "Passive microwave remote sensing for sea ice research". *Eos, Transactions American Geophysical Union*, 66, 1210–1212, doi: 10.1029/EO066i049p01210.

Talagrand, O. and P. Courtier (1987): "Variational Assimilation of Meteorological Observations With the Adjoint Vorticity Equation. I: Theory". *Q. J. Roy. Meteor. Soc.*, 113, 1311–1328, doi:10.1002/qj.49711347812.

Taylor, K., R. Stouffer, and G. Meehl (2012): "An Overview of CMIP5 and the Experiment Design". *Bull. Amer. Meteor. Soc.*, 93, 485–498.

Terasaki, K. and T. Miyoshi (2017): "Assimilating AMSU-A Radiances with the NICAM-LETKF". *J. Meteorol. Soc. Jpn. Ser. II*, 95, 433–446, doi:10.2151/jmsj. 2017-028.

Tietsche, S., D. Notz, J. Jungclaus, and J. Marotzke (2013): "Assimilation of sea-ice concentration in a global climate model - physical and statistical aspects". *Ocean Sci.*, 9, 19–36, doi:10.5194/os-9-19-2013.

Tonboe, R. (2010): "The simulated sea ice thermal microwave emission at window and sounding frequencies". *Tellus*, 62A, 333–344, doi:10.1111/j.1600-0870.2010. 00434.x.

Tonboe, R., S. Andersen, L. Toudal, and G. Heygster (2006): "Sea ice emission modelling", in: C. Mätzler, P. Rosenkranz, A. Battaglia, and J. Wigneron (eds.), "Thermal Microwave Radiation - Applications for Remote Sensing", pp. 382–400, IET Electromagnetic Waves Series 52.

Tonboe, R., G. Dybkjaer, and J. Højer (2011): "Simulations of the snow covered sea ice surface temperature and microwave effective temperature". *Tellus*, 63A, 1028–1037, doi:10.1111/j.1600-0870.2011.00530.x.

Tonboe, R., S. Eastwood, T. Lavergne, A. Sørensen, N. Rathmann, G. Dybkjær, L. Pedersen, J. Høyer, and S. Kern (2016): "The EUMETSAT sea ice concentration climate data record". *Cryosphere*, 10, 2275–2290, doi:10.5194/tc-10-2275-2016.

Ulaby, F., R. Moore, and A. Fung (1986): "Passive microwave sensing of the ocean", in: "Microwave Remote Sensing, Active and Passive Volume III, From Theory to Applications", chap. 18, pp. 1412–1521, Artech House, Inc.

Untersteiner, N. (1980): "AIDJEX review", in: R. Pritchard (ed.), "Sea Ice Processes and Models", pp. 3–11, University of Washington, Seattle.

Uttal, T., J. Curry, M. McPhee, D. Perovich, R. Moritz, J. Maslanik, P. Guest, H. Stern, J. Moore, R. Turenne, A. Heiberg, M. Serreze, D. Wylie, O. Persson, C. Paulson, C. Halle, J. Morison, P. Wheeler, A. Makshtas, H. Welch, M. Shupe, J. Intrieri, K. Stamnes, R. Lindsey, R. Pinkel, W. Pegau, T. Stanton, and T. Grenfeld (2002): "Surface Heat Budget of the Arctic Ocean". *Bull. Amer. Meteor. Soc.*, 83, 255?276, doi:10.1175/1520-0477(2002)083<0255:SHBOTA>2.3.CO;2.

Van der Swaluw, E., S. Drijfhout, and W. Hazeleger (2007): "Bjerknes Compensation at High Northern Latitudes: The Ocean Forcing the Atmosphere". *J. Clim.*, 20,

6023–6032, doi:10.1175/2007JCLI1562.1.

Vancoppenolle, M., T. Fichefet, H. Goosse, S. Bouillon, G. Madec, and M. Morales Maqueda (2009): "Simulating the mass balance and salinity of Arctic and Antarctic sea ice. 1. Model description and validation". *Ocean Model.*, 27, 33–53, doi:10.1016/j.oceamod.2008.10.005.

Vavrus, S., M. Holland, A. Jahn, D. Bailey, and B. Blazey (2011): "Twenty-First-Century Arctic Climate Change in CCSM4". *J. Clim.*, 25, doi:10.1175/JCLI-D-11-00220.1.

Weeks, W. (2010): *On Sea Ice*, University of Alaska Press, ISBN 9781602231016.

Wentz, F. and T. Meissner (2000): "Algorithm theoretical basis document (atbd), version 2", Tech. Rep. AMSR Ocean Algorithm, RSS Tech. Proposal 121599A-1, Remote Sensing Systems, Santa Rosa, CA.

Wetzel, P., H. Haak, J. Jungclaus, and E. Maier-Reimer (2012): "The Max-Planck-Institute Global Ocean/Sea-Ice Model MPI-OM", Tech. rep., Max Planck Institute for Meteorology.

Wiesmann, A. and C. Mätzler (1998): "Microwave emission model of layered snowpacks". *Remote Sens. Environ.*, 70, 307–316.

Willmes, S., M. Nicolaus, and C. Haas (2014): "The microwave emissivity variability of snow covered first-year sea ice from late winter to early summer: a model study". *Cryosphere*, 8, 891–904, doi:10.5194/tc-8-891-2014.

Winebrenner, D., J. Bredow, A. Fung, M. Drinkwater, S. Nghiem, A. Gow, D. Perovich, T. Grenfell, H. Han, J. Kong, J. Lee, S. Mudaliar, R. Onstott, L. Tsang, and R. West (1992): "Microwave Sea Ice Signature Modeling", in: F. Carsey (ed.), "Microwave Remote Sensing of Sea Ice", chap. 8, pp. 137–175, American Geophysical Union.

Winton, M. (2011): "Do Climate Models Underestimate the Sensitivity of Northern Hemisphere Sea Ice Cover?" *J. Climate*, 24, 3924–3934, doi:10.1175/2011JCLI4146.1.

Zhang, J. (2005): "Warming of the Arctic ice-ocean system is faster than the global average since the 1960s". *Geophys. Res. Lett.*, 32(L19602), doi:10.1029/2005GL024216.

ACKNOWLEDGMENTS

These past years have been eventful and there were a lot of highs and lows. I would like to thank all of you who made the highs even higher and the lows less low.
First and foremost I thank Dirk Notz who gave me the opportunity to conduct my PhD research at the MPI for Meteorology, a great climate research environment. Thanks for your patience, believing in me, even in the most frustrating moments, and teaching me so many things. I also thank Lars Kaleschke, Leif T. Pedersen, and Rasmus Tonboe who were my personal sea-ice remote sensing experts and gave me helpful support throughout the time. Finally, many thanks go to Johanna Baehr, for the helpful advices and discussions in the stressful time before submission.
I thank the sea-ice group, especially my office mates, Dirk Olonscheck and Laura Niederdrenk, for the fruitful discussions and breaks.
Special thanks go to the three strong women who make the life of the IMPRS doctoral researchers much easier than it would be otherwise: Antje, Cornelia and Michaela, you're the best!
Everyday life at the institute and the lunch breaks would have been quite boring without my fellow IMPRS students. Especially, I thank Laura Suarez-Gutierrez, who has stood by my side since the first day of my Master's program. I really enjoyed sharing this long way with you and I hope we'll share it even further!
Science communication has been a big and fun part of my life in the past years. In this regard, I thank the EGU Cryosphere blog team, especially Sophie Berger, Violaine Coulon, and Emma Smith for the good time! Also, I thank Dörte and the whole Twitter team for the exciting experience!
In my first year, I had the slightly crazy idea of making a "Climate Model Calendar". Two years later, I had finally convinced enough people to pose for the pictures and I still cannot believe we sold 100 copies of it! Thank you so much to the models and photographers: Leo, Andreas, Katherine, Hauke, Benji, Alex, Veit, Nele, Laura, Sabine, Anke, Sebastian, Aaron, and Olga! Thanks also to Lydi, Lukas and Rafaela who I could not convince to actively take part in the calendar but I still enjoyed spending time with throughout the years :)
I would not be writing these lines without the support of my family, especially my parents and my sister. You gave me curiosity, creativity and a bit of craziness, just what I needed to conduct a PhD research. Thank you for being there for me and letting me try new opportunities whenever I felt like it.
And of course, finally, my deepest thanks go to Tobias, my partner. Thanks for being in my life, believing in me, and bravely fighting my bad mood moments!

Versicherung an Eides statt

Hiermit versichere ich an Eides statt, dass ich die vorliegende Dissertation mit dem Titel: "Rethinking the relationship between the observed, simulated and real Arctic sea-ice evolution" selbstständig verfasst und keine anderen als die angegebenen Hilfsmittel - insbesondere keine im Quellenverzeichnis nicht benannten Internet-Quellen - benutzt habe. Alle Stellen, die wörtlich oder sinngemäß aus Veröffentlichungen entnommen wurden, sind als solche kenntlich gemacht. Ich versichere weiterhin, dass ich die Dissertation oder Teile davon vorher weder im In- noch im Ausland in einem anderen Prüfungsverfahren eingereicht habe und die eingereichte schriftliche Fassung der auf dem elektronischen Speichermedium entspricht.

Hamburg, den

_____

Clara Burgard

Hinweis / Reference

Die gesamten Veröffentlichungen in der Publikationsreihe des MPI-M
„Berichte zur Erdsystemforschung / Reports on Earth System Science“,
ISSN 1614-1199

sind über die Internetseiten des Max-Planck-Instituts für Meteorologie erhältlich:
http://www.mpimet.mpg.de/wissenschaft/publikationen.html

All the publications in the series of the MPI -M
„Berichte zur Erdsystemforschung / Reports on Earth System Science“,
ISSN 1614-1199

are available on the website of the Max Planck Institute for Meteorology:
http://www.mpimet.mpg.de/wissenschaft/publikationen.html